

DTIC FILE COPY

AD-A190 439

**THERMAL RESPONSE OF M55 ROCKETS
TO POOL FIRES DURING TRANSIT**

by
Donald E. Ketchum
Charles E. Anderson, Jr.

FINAL REPORT
SwRI 8461 / 005

DTIC
ELECTED
JAN 06 1988
S D

April 1985

DISTRIBUTION UNLIMITED / APPROVED FOR PUBLIC RELEASE

Prepared for

U.S. ARMY TOXIC AND HAZARDOUS MATERIALS AGENCY
ABERDEEN PROVING GROUND, MARYLAND 21010-5401

DISCLAIMER

The findings in this report are not to be construed as an official Department of the Army position unless so designated by other authorizing documents.

TABLE OF CONTENTS

	<u>Page</u>
LIST OF FIGURES	v
LIST OF TABLES	vii
I. BACKGROUND	1
II. SCENARIO DEFINITION	5
A. Description of Pool Fire	5
B. Thermal Loads on the Rocket	6
1. Thermal Response of the Carrier	6
a. Convective Heat Transfer Coefficient	6
b. Carrier Modeling	10
2. Shielding by the Pallet and Other Rockets	15
III. ROCKET RESPONSE TO THERMAL LOADS	24
A. Rocket Description	24
B. Boundary Conditions	24
1. Truck	26
2. Railcar	27
3. CAMPACT	27
C. Axial Heating	27
D. Thermal Response of Rocket Sections	30
1. Propellant	32
2. Igniter	38
3. Agent	44
4. Burster	44
E. Comparison of Cross-Sectional Thermal Responses	52
F. Failure Temperatures and Expected Times to Failure	62
IV. CONCLUSIONS	65
V. REFERENCES	67
APPENDIX A - LIST OF COMPUTER RUNS	A1
APPENDIX B - ANALYTICAL TOOLS	B1
APPENDIX C - ANALYSIS OF CONVECTION WITHIN THE CARRIER	C1
APPENDIX D - ANALYSIS OF RADIATION WITHIN THE CARRIER	D1
APPENDIX E - NATURAL CONVECTION WITHIN THE SHIPPING TUBE	E1
APPENDIX F - AGENT BURST ANALYSIS	F1
APPENDIX G - THERMAL PROPERTY DATA (Figures p1 - p6)	G1

LIST OF FIGURES

<u>Figure No.</u>		<u>Page</u>
1	Pallet of M55 Missiles	3
2	Correlation of Natural Convection Data for Vertical Surfaces	9
3	Carrier Geometries for Computer Analysis	12
4	Transient Convective Heat Transfer Coefficient Inside the Boxcar	16
5	Transient Boxcar Wall (inner surface) Temperature	17
6	Transient Gas Temperature Inside the Boxcar	18
7	Temperature Contours Within the CAMPACT	19
8	Configuration Factor Geometries with Rockets and Pallet	21
9	Configuration Factors as a Function of Angular Position	23
10	Rocket, 115mm, GB, M55	25
11	One Dimensional Representations of Rocket Ends	28
12	Node Locations for Two-Dimensional Computer Analysis of Propellant Section	34
13	Node Locations for Two-Dimensional Computer Analysis of Propellant Section after Fiberglass Melt	35
14	Temperature-Time History of Propellant for Truck	36
15	Temperature-Time History of Propellant for Railcar	37
16	Node Locations for Two-Dimensional Computer Analysis of Igniter Section	40
17	Node Locations for Two-Dimensional Computer Analysis of Igniter Section	41
18	Temperature-Time History of Igniter for Truck	42
19	Temperature-Time History of Igniter for Railcar	43
20	Node Locations for Two-Dimensional Computer Analysis of Agent Section	46
21	Node Locations for Two-Dimensional Computer Analysis of Agent Section	47
22	Temperature-Time Histories of Agent for Truck	48
23	Temperature-Time Histories of Agent for Railcar	49
24	Node Locations for Two-Dimensional Computer Analysis of Burster Section	51
25	Node Locations for Two-Dimensional Computer Analysis of Burster Section	53
26	Temperature-Time History of Burster for Truck	54
27	Temperature-Time Histories of Burster for Railcar	55
28	Comparison of Truck versus Railcar Thermal Response for Burster, Propellant and Igniter	56
29	Comparison of Truck versus Railcar Thermal Response for Agent Section	57
30	Comparison of Thermal Histories for the Energetic Materials - Shielded Rockets in Truck	58
31	Comparison of Thermal Histories for the Energetic Materials - Shielded Rockets in Railcar	59
32	Temperature Contours After 12 Minutes Heating (Railcar)	61

LIST OF TABLES

<u>Table No.</u>		<u>Page</u>
1	Constants to be used in Equation (3) for Natural Convection in Air	8
2	Convective Heat Transfer Coefficient as a Function of Temperature Differential	11
3	Carrier Properties	13
4	Material Properties for Axial Heating Analysis	29
5	Transient Flux Ratios, Carrier Vs. Rocket Response	31
6	Propellant Properties	33
7	Igniter Properties	39
8	Agent Properties	45
9	Burster Properties	50
10	Time to Failure	63

ACKNOWLEDGEMENTS

The authors wish to thank Dr. William R. Rhyne of H&R Technical Associates, Mr. Tom Ashwood and Dr. Chris Stoddard of Oak Ridge National Laboratory for their assistance throughout the course of this study. Thanks also go to Ms. Norma Sandoval and Ms. Patricia Bowles of SwRI for their able assistance in executing the computer codes used in the program. Finally, we would like to thank Mrs. Janet Banda for typing and preparing this report.

I. BACKGROUND

Demilitarization of aging, stockpiled chemical munitions, in particular the M55 rocket, has a high priority within the Department of Defense. A facility is being constructed on Johnson Atoll in the Pacific for demilitarization of the chemical munitions stockpiled on Johnson Island. Considerable attention is being paid to potential hazards and safety considerations during the "demil" operation [1,2,3,4]. The US Army has undertaken studies for demilitarization of chemical munitions stockpiled in the continental United States, and a number of options exist. One option is to build demil facilities at the locations where the munitions are stockpiled. This option requires the construction of several facilities. An alternate approach is to transport the stored munitions to a central facility which necessitates transporting the weapons by some cargo carrier such as train or truck. Transportation is complicated by the increased probability of some sort of catastrophic accident during the transport of the munition. Different studies are being conducted to assess which option is the most viable from cost and hazard considerations.

A number of different accident scenarios can be envisioned in the transport of the chemical munitions; the type of accident, and the probability of an accident type depend upon whether the carrier is by air, rail, or highway. Typically, a risk assessment is made where the probabilities of a catastrophic occurrence (in this case, the release of agent from a M55 rocket) are computed for the various accident scenarios (such as outlined in "Severities of Transportation Accidents" [5,6]) , and a determination is made whether the risk (probability of occurrence) is sufficiently high to warrant concern. One type of accident scenario is the case where the carrier vehicle is exposed to a hydrocarbon fuel fire. A realistic analysis of the thermal response of the M55 rocket to a fire environment is needed to assess the risk of shipping these weapons. Recent risk analyses on the transport of these weapons by rail or highway [7] have identified some uncertainty of the thermal response of an M55 rocket when exposed to a fuel fire. Preliminary calculations of rocket heating were made, but these calculations are subject to criticism because of the conservatisms inherent in the approximations used. There is a need for a more precise estimate of the thermal response of

a M55 rocket in a fuel fire during transit to clarify the magnitude of the risks of transporting these chemical weapons.

This report documents the thermal response of an M55 rocket to a hydrocarbon fuel fire for three different modes of transportation: trailer truck, boxcar, and a CAMPACT shipping container (which would reside on a flatbed railcar). A pallet of M55 missiles, contained in their launch tubes, is shown in Figure 1. Depending on the carrier, various numbers of pallets can be transported simultaneously. The transient temperatures of the energetic materials in the rocket (propellant, igniter, burster, and agent) are determined for the three different carrier configurations when exposed to a hydrocarbon fuel fire. The carrier configurations affect the thermal response of the rocket by the differences in thermal protection provided by the differing geometries (thicknesses and materials) of the carriers.

The report is divided into two main sections: scenario definition and thermal response of the M55 rocket. To compute the thermal response of the rocket, the thermal environment, i.e., the boundary conditions, must be described. The geometry and materials of the rocket are independent of the carrier; once they are described, they are the same for every scenario. What differs in each problem is the thermal environment to which the rocket is subjected. Mathematically, this thermal environment is described by defining, as a function of time, the heat flux at the outside boundary of the rocket. These boundary conditions must take into account differences in the protection provided by the different transport carriers, which are assumed to be immersed in a hydrocarbon fuel fire. The relative location of a rocket in a pallet must be considered since rockets can be shielded from thermal radiation by the pallet and other rockets. Thus, the purpose of the scenario definition is to define the heat flux incident, as a function of time and position, on a M55 rocket for each scenario and rocket location analyzed. Once the boundary conditions are specified for the differing scenarios, the thermal responses of the rocket are computed.

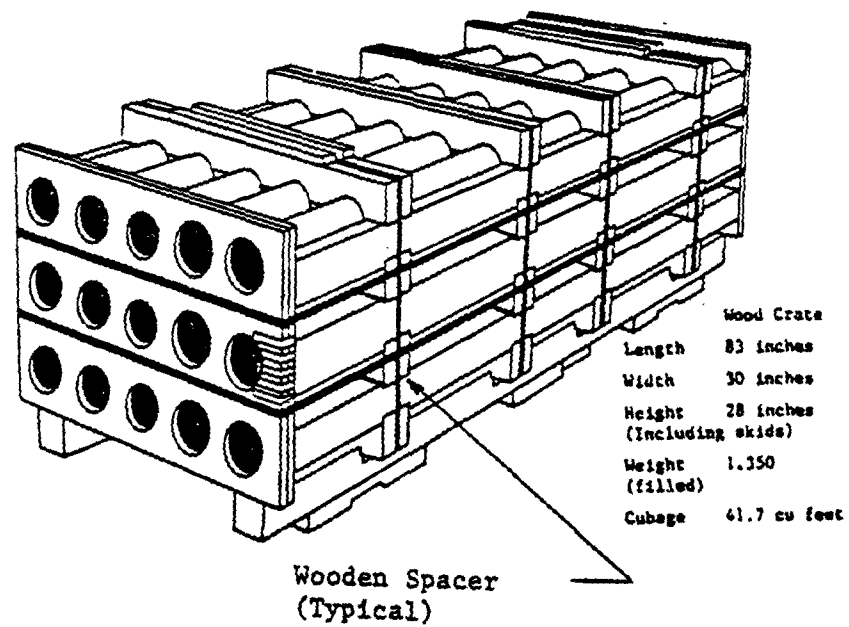


Figure 1. Pallet of M55 Missiles (in Launch Tubes)

Thirty-three computer runs, Appendix A, were made to determine the thermal response of the M55 rockets as a function of time. Both one and two dimensional computer programs, ONEDIM [8] and SINDA [9], were used for the computer calculations; the following sections discuss the modeling assumptions and the applicability of using one or two dimensional calculations. Brief descriptions of the two computer programs are given in Appendix B.

II. SCENARIO DEFINITION

A. Description of Pool Fire

The hydrocarbon pool fire is assumed to totally engulf the transport vehicle. In an accident simulation code described in Reference 5, hydrocarbon pool fires caused by truck/tanker collisions are assumed to spread to an average size of 200 ft² (16 feet diameter). Railroad accidents involving tank cars produce spills of about 700 ft² (30 feet diameter) [6]. The height of fuel fires may be estimated [10] by

$$\frac{H}{D} = -2 \left(\frac{\dot{m}}{\rho_a g D} \right)^{.61} \quad (1)$$

where H is the fire height, D is the diameter of the fire, ρ_a is the density of air, g is the acceleration due to gravity, and \dot{m} is the hydrocarbon fuel burn rate (= 0.65 lb/ft³ min). Expected heights of the truck and railcar fires are approximately 31 and 48 feet, respectively. As the sizes of the fires greatly exceed the carrier dimensions, the truck and railcar are considered entirely engulfed in flames. According to Reference 6, a fire of thickness four feet will effectively transmit blackbody radiation. That same reference reports the average temperature of a hydrocarbon fuel fire as 1850°F. Convective heat transfer from flames to an engulfed container is about a factor of 10 times lower than the radiative heat transfer [6]. For this reason, convective heat transfer to the walls of the carriers (truck, railcar, or COMPACT) is neglected, as recommended in Reference 6. It has been found that the assumption that fire acts as a blackbody radiator (emissivity of 1.0) tends to compensate for neglecting free convection. Thus, the carriers are assumed to be totally engulfed in a blackbody fire of 1850°F.

The fire will be taken to last for no more than four hours. Reports on truck and railroad fires [5,6] show that the vast majority of recorded accidental fires have an even shorter duration. The accident scenarios considered in this analysis were examined for four hours or until the energetic materials significantly surpassed expected "cookoff" temperatures (whichever is shorter).

B. Thermal Loads on the Rocket

1. Thermal Loads on the Rocket

In establishing the thermal load imposed on the M55 rockets during a pool fire, the response of the walls of the truck, railcar, or CAMPACT positioned between the fire and the weapons must first be evaluated. The fire acting on these walls causes heat to diffuse into the solid material, heating and possibly melting away the protective barrier. As the backfaces of the carrier walls heat, convective currents circulate within the carrier, transferring heat to the rockets. Thermal radiation will also be emitted from the walls. Initially, convective heat transfer is the dominant transport mechanism, but as the walls heat, the backface wall temperature increases and radiative transport becomes an important heat transfer mechanism. Thus, the heat load on the rockets is transient, and both convective and radiative processes must be considered.

The thermal responses of the carriers are considered as a one-dimensional problem (edge effects and differences between the sides, ends, and roof are neglected). The following paragraphs document the procedure whereby an estimate of the convective and radiative fluxes to a rocket are determined. The convective heat transfer coefficient to the rocket is assumed to be independent of rocket location, but the exchange of radiation between the carrier walls and the rocket is a function of rocket position because of shielding by the curvature of the rocket, shielding by other rockets, and shielding by the pallet. Both the convective heat transfer coefficient and radiant heat flux are functions of time because the temperature gradients and wall temperatures are functions of time.

a. Convective Heat Transfer Coefficient

The overall procedure is to compute the thermal response of the carrier wall to the fire. The temperature of the back surface of the carrier wall as a function of time is the result of heat being conducted through the wall from the fire, heat losses to the interior air because of natural convection, and radiant exchange of the wall with the rockets. The convective

heat transfer coefficient between the back surface of the wall and the air is a function of the Grashof, Gr, and Prandtl, Pr, numbers:

$$Nu = f(Gr, Pr) \quad (2)$$

where:

$$\begin{aligned} Nu &= hL/k \\ Gr &= \beta g \Delta T L^3 / \nu^2 \\ Pr &= \nu / \alpha \end{aligned}$$

where Nu is the Nusselt number, h is the convective heat transfer coefficient, k is the thermal conductivity of the air, L is a typical wall dimension, β is the coefficient of thermal expansion of air, g is the gravitational constant, ν is the kinematic viscosity of air, α is the thermal diffusivity of air, and ΔT is the temperature difference between the wall and the interior air. The convective heat transfer coefficient depends on whether the wall is horizontal or vertical in orientation; if the wall is horizontal, the functional relationship between the Nusselt number and Gr and Pr depends on whether the hot wall is facing up or facing down with respect to the gas. Finally, for a vertical wall, the functional relationship changes depending on whether the boundary layer is laminar or turbulent.

Investigators performing numerous experiments have determined the functional relationships for the Nusselt number, and these can be found in many heat transfer texts. A simplification can be made for the particular problem being considered here since the fluid involved in the convective processes is air at atmospheric pressure. The more general expressions can be modified to apply specifically to air and a simplified expression for the heat transfer coefficient can be written in the form [11]:

$$h = a(\Delta T/L)^b \quad (3)$$

where a and b are constants, depending on geometry and flow conditions, and L is the characteristic length, also a function of geometry and flow. Table 1 lists the constants to be used in Equation (3) for natural convection in

Table 1. Constants to be used in Equation (3) for Natural Convection in Air. From McAdams, Heat Transmission, 3rd ed. (New York: McGraw-Hill, 1954) referenced from Ref [11]

<u>Geometry</u>	<u>Applicable range</u>	<u>a</u>	<u>b</u>	<u>L</u>
Vertical surfaces (planes and cylinders)	$10^4 < Gr_L Pr < 10^9$	0.29	1/4	height
	$10^9 < Gr_L Pr < 10^{12}$	0.19	1/3	1
Horizontal plane cold plates facing up or hot plates facing down	$3 \times 10^5 < Gr_L Pr < 3 \times 10^{10}$	0.12	1/4	length of side

air. Note that two expressions exist for vertical surfaces depending on the value of the Rayleigh number Ra ($Ra = Gr \cdot Pr$), which describes the transition from laminar to turbulent flow. Figure 2 depicts the correlation of Nusselt and Rayleigh numbers for vertical surfaces. Note that for computational purposes, the heat transfer coefficient is always given by the maximum of the laminar and turbulent expressions.

An average heat transfer coefficient has been computed which averages h over the different surfaces of the carrier:

$$\bar{h} = [2h_v(H \cdot D) + 2h_v(H \cdot W) + h_h(D \cdot W)] / [2(H \cdot D) + 2(H \cdot W) + D \cdot W] \quad (4)$$

where D , W , and H are the depth (length), width, and height of the carrier, respectively, and the subscripts v and h refer to the use of the vertical and horizontal expressions from Table 1. The assumption is that, to a first approximation, the roof, ends, and sides of the carrier are essentially the same construction and the fire is sufficiently large for total engulfment of the carrier such that all wall temperatures are approximately equal. The floor of the carrier, because of its close proximity to the ground, and its much "beefier" construction, does not heat sufficiently to contribute to heat transfer from the fire to the interior. Equations (3) and (4) can now be used to determine the average convective heat transfer coefficient. A computer program was written to generate the heat transfer coefficient as a function of ΔT for the various geometries subject to the conditions in Table 1. A

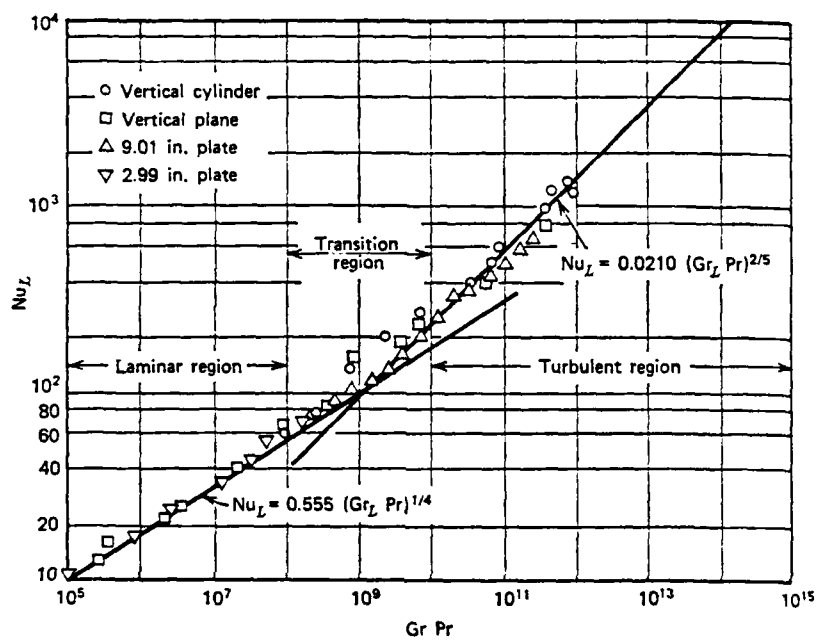


Figure 2. Correlation of Natural Convection Data for Vertical Surfaces (From E.R.G. Eckert and T. W. Jackson, NACA RFM 50 D25, July 1950.)
 From Reference [11]

listing of this program is given in Appendix C. Table 2 lists the average heat transfer coefficient as a function of ΔT for the three different carriers being considered.

b. Thermal Environment of Carriers

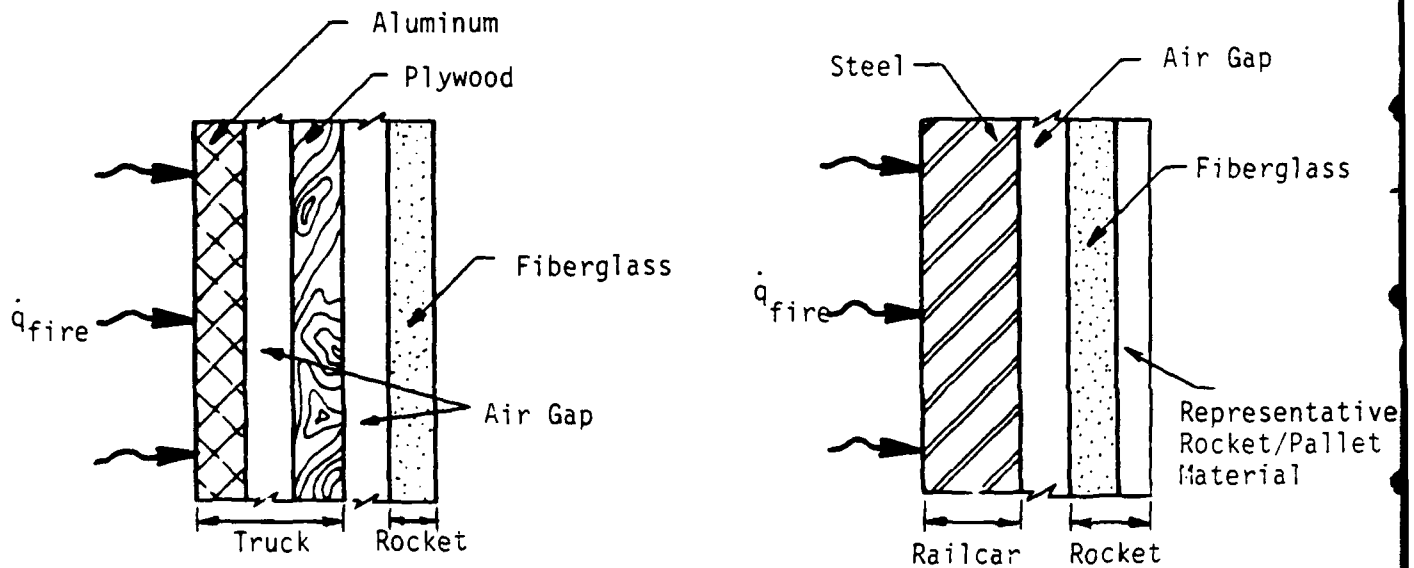
The computer code ONEDIM [8] was used to compute the transient thermal response of the carrier's walls with the fire. The external carrier walls receive radiation from a constant temperature, blackbody fire. The various materials comprising the thickness of the walls are divided into zones. The back surface of the wall is bounded by an air gap which permits the transmission of convective and radiant energy to the rocket shipping case. The pallet and rockets are represented in this one-dimensional model by two material layers; the first layer is fiberglass having the thickness of the shipping tubes, and a second layer which is modeled to have an effective heat capacity of the contents (thickness equal to cube root of the pallet volume, and average pallet density). Three parameters are required as a function of time in order to prescribe the heat flux boundary conditions on the rockets: the convective heat transfer coefficient, the interior gas temperature T_g , and the backface wall temperature T_b . Figure 3 depicts the general geometry of the carrier wall and its interaction with the fire and the carrier interior as analyzed by ONEDIM. Table 3 lists the dimensions and materials of the carrier wall for the different carriers considered in this study.

Heat leaves the carrier wall via convection and radiation. Since the assumption is that all walls and the ceiling of the carrier are at the same temperature, then all heat exchange between the carrier and its interior is with the interior gas and the rockets. For the purpose of defining the parameters of interest (h , T_g , T_b) as a function of time, the thermal response of the interior of the rocket is not of interest, only the heat absorbed by the rocket case, pallet, and floor (all assumed to have approximately the same average thermal properties). The detailed computations of the rocket response requires a two-dimensional computation; the present procedures define the environment to which the rocket is exposed.

Table 2. Convective Heat Transfer Coefficient
as a Function of Temperature Differential

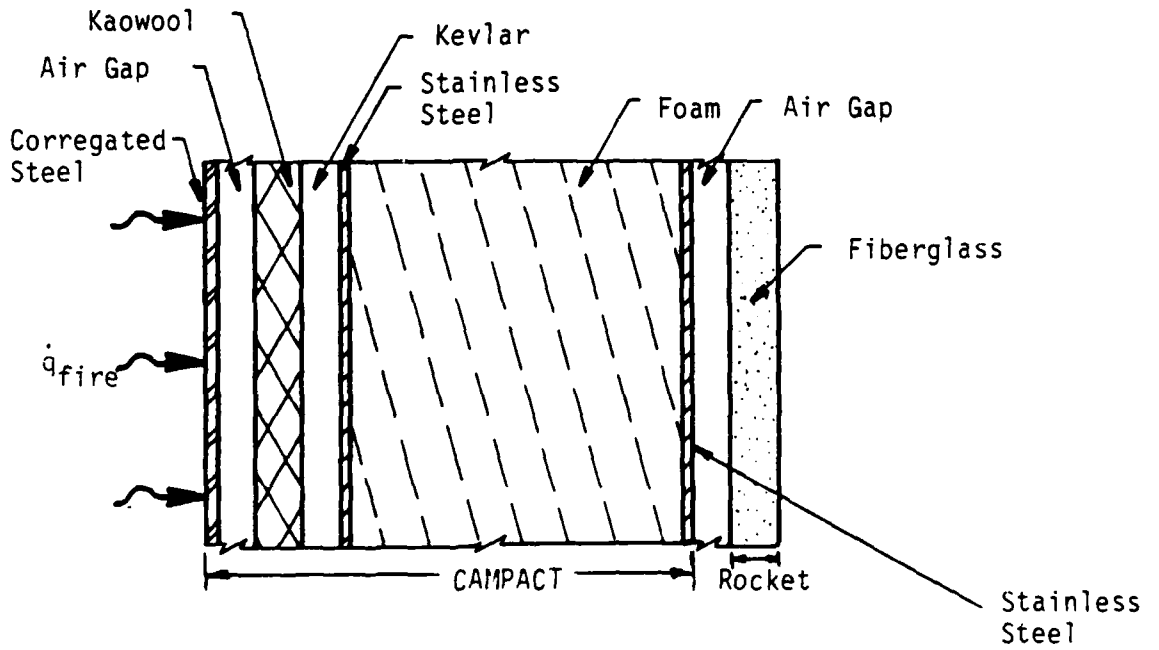
CONVECTIVE HEAT TRANSFER COEFFICIENT (BTU/HR SQ FT F)

DIMENSIONS: Length Width Height (FT)			
Truck	48.0	7.7	8.5
Railcar	50.5	9.5	10.7
Campact	19.2	6.2	7.2
Delta Temp (deg F)	Truck	Railcar	Campact
0.0000E+00	0.0000E+00	0.0000E+00	0.0000E+00
0.1000E+03	0.3157E+00	0.2980E+00	0.3454E+00
0.2000E+03	0.3754E+00	0.3544E+00	0.4107E+00
0.3000E+03	0.4155E+00	0.3922E+00	0.4545E+00
0.4000E+03	0.4465E+00	0.4215E+00	0.4884E+00
0.5000E+03	0.4721E+00	0.4456E+00	0.5164E+00
0.6000E+03	0.4941E+00	0.4664E+00	0.5405E+00
0.7000E+03	0.5135E+00	0.4847E+00	0.5618E+00
0.8000E+03	0.5309E+00	0.5012E+00	0.5808E+00
0.9000E+03	0.5468E+00	0.5162E+00	0.5982E+00
0.1000E+04	0.5614E+00	0.5300E+00	0.6142E+00
0.1100E+04	0.5749E+00	0.5427E+00	0.6290E+00
0.1200E+04	0.5876E+00	0.5547E+00	0.6447E+00
0.1300E+04	0.5995E+00	0.5659E+00	0.6617E+00
0.1400E+04	0.6120E+00	0.5765E+00	0.6778E+00
0.1500E+04	0.6258E+00	0.5865E+00	0.6932E+00
0.1600E+04	0.6391E+00	0.5960E+00	0.7079E+00
0.1700E+04	0.6518E+00	0.6051E+00	0.7220E+00
0.1800E+04	0.6640E+00	0.6161E+00	0.7355E+00
0.1900E+04	0.6758E+00	0.6270E+00	0.7486E+00
0.2000E+04	0.6872E+00	0.6375E+00	0.7611E+00



A. Aluminum Wall of Truck

B. Steel Wall of Railcar



C. Composite Wall of CAMPACT

Figure 3. Carrier Geometries for Computer Analysis

Table 3. Carrier Properties

Carrier	Material	Thickness (in)	Thermal Conductivity k (BTU/ft hr °F)	Specific Heat Cp (BTU/lb °F)	Density ρ (lb/ft ³)	Heat of Transition h _{sf} (BTU/lb)	Transition Temperature T _m (°F)
Railcar	steel (ø 680F) [15][13]	.120	25	See Eq (p4)	487		
	aluminum (ø 680F) [15][13]	.04	93	See Eq (p3)	164	5.3 x 10 ⁻⁵	1218
Truck	air [15]	1.375					
	for 800F		.01516	.2402	.0735		
	350		.02142	.2438	.0489		
	620		.02692	.2520	.0367		
	890		.03183	.2593	.0294		
	plywood (fir) [15]	.375	.08	.65	26		550*
Campact	301 corrugated [15] stainless steel	.012	See Eq (p1)	.11	488		
	air [15]	1.0					
	for 800F		.01516	.2402	.0735		
	350		.02142	.2438	.0489		
	620		.02692	.2520	.0294		
	kaowool [7]	1.0	See Fig P6	See Eq (p2)	6.0		
	kevlar 29 [7]	.843	See Fig P3	See Fig P4-5	90.0		
	301 stainless steel [7]	.150	See Eq (p1)	.11	488		
	FR-9606 Foam [7]	7.5	See Fig P1	See Fig P2	6		
	304 stainless steel [7]	.188	See Eq (p1)	.11	488		

*Auto ignition temperature (Ref. 19)

Material Property Equations

(p1) For stainless steel, $k = 8.6 + .00045T$ (T in °F, k in BTU/ft hr °F)

(p2) For kaowool, $C_p = 0.2227 + 1.79 \times 10^{-5}T$ (T in °F, Cp in BTU/lb °F)

(p3) For aluminum, molar specific heat, $C_p = 4.94 + 2.96 T/1000$ (T in °K, Cp in cal/gmole °K). Divide by 26.9 to get cal/g °K = BTU/lb °F.

(p4) For steel, molar specific heat, $C_p = 3.37 + 7.1 T/1000 + .43 \times 10^{-5}T^2$ (T in °K, Cp in cal/gmole °K). Divide by 55.8 to get cal/g °K = BTU/lb °F.

The truck walls present a special problem in having an air gap between the aluminum skin and plywood. Natural convection and radiation are accounted for in ONEDIM in considering the transfer from the aluminum side to the plywood. At the melt-through of the aluminum outer covering, the heat flux from the fire is applied directly on the plywood. When the plywood reaches auto ignition temperature (550°F) it will burn at 0.16 lb/ft² min for the first 30 minutes (linear decrease from 0.24 to 0.09 lb/ft² min) and 0.09 lb/ft² min thereafter [6]. Rockets are exposed to thermal radiation directly from the fire following burn-through of the plywood.

The gas temperature is approximated as the average of the back surface wall temperature T_b , and the rocket wall temperature T_r :

$$T_g = (T_b + T_r)/2 \quad (5)$$

Different schemes were considered for estimating the interior gas temperature as a function of time, but all schemes had certain inherent assumptions necessary to make the problem tractable; the more "elaborate" schemes did not necessarily make them any more accurate than the one chosen. Also, the scheme chosen has the advantage of simplicity, with the knowledge that the gas temperature must be somewhere between the backwall temperature and the wall temperature of the rockets, and that an average of those two temperatures is an adequate first approximation.

(1) Truck Thermal Environment

The aluminum wall of the truck heated to its melt temperature within 62 seconds. At this point the computer program was stopped and the aluminum layer was removed from the computational grid. The computer program was then restarted. After another twenty seconds, the outer surface of the plywood reached auto ignition temperature. Burnthrough of the plywood took 5.1 minutes; thus the truck wall was removed completely from the problem after 6.5 minutes. During that time, the strong thermal resistance of the plywood prevented the backface of the carrier from heating significantly, so the environment of the rockets inside the truck was treated as direct exposure

to the fire (1850°F wall and gas temperatures) following a 6.5 minute time shift.

(2) Railcar Thermal Environment

The thermal environment created within the boxcar is shown in Figures 4 through 6. Unlike the truck, the boxcar walls permit heat transfer to the rockets as soon as the fire begins. Also, the boxcar's walls remain intact (do not melt and burn away) throughout the duration of the fire. Figure 4 illustrates the change in convective heat transfer coefficient (assumed uniform throughout the enclosure) with time. The transient backface surface temperature of the boxcar walls is shown in Figure 5. The effective gas temperature increases with time as shown in Figure 6.

(3) CAMPACT Thermal Environment

The CAMPACT effectively resists the thermal load from the fire. Temperature profiles across the thickness of the CAMPACT are shown in Figure 7. At one hour into the heating, the stainless steel outer liner and the surface of the kaowool have risen to near the fire temperature, while temperatures half-way through the foam remain at ambient. The kaowool, kevlar, and foam layers resist the heat flow into the CAMPACT so well that the inner liner of stainless steel rises less than five degrees in 4 hours. This indicates that rockets housed within the CAMPACT remain near ambient temperatures even after 4 hours of fire exposure. Note that in this analysis it has been assumed the CAMPACT has not been punctured or damaged in any way prior to fire exposure. A puncture through the kaowool and kevlar could provide a path for oxygen flow, allowing the foam to burn or smoulder.

2. Shielding by the Pallet and Other Rockets

The fraction of thermal radiation emitted by the hot walls of the container and striking the rockets is limited by the geometry of the rockets and pallets, and the surfaces radiating heat to them. The fraction of the total thermal radiation leaving one surface that strikes another is termed the configuration factor. This factor is related to the distance between heat

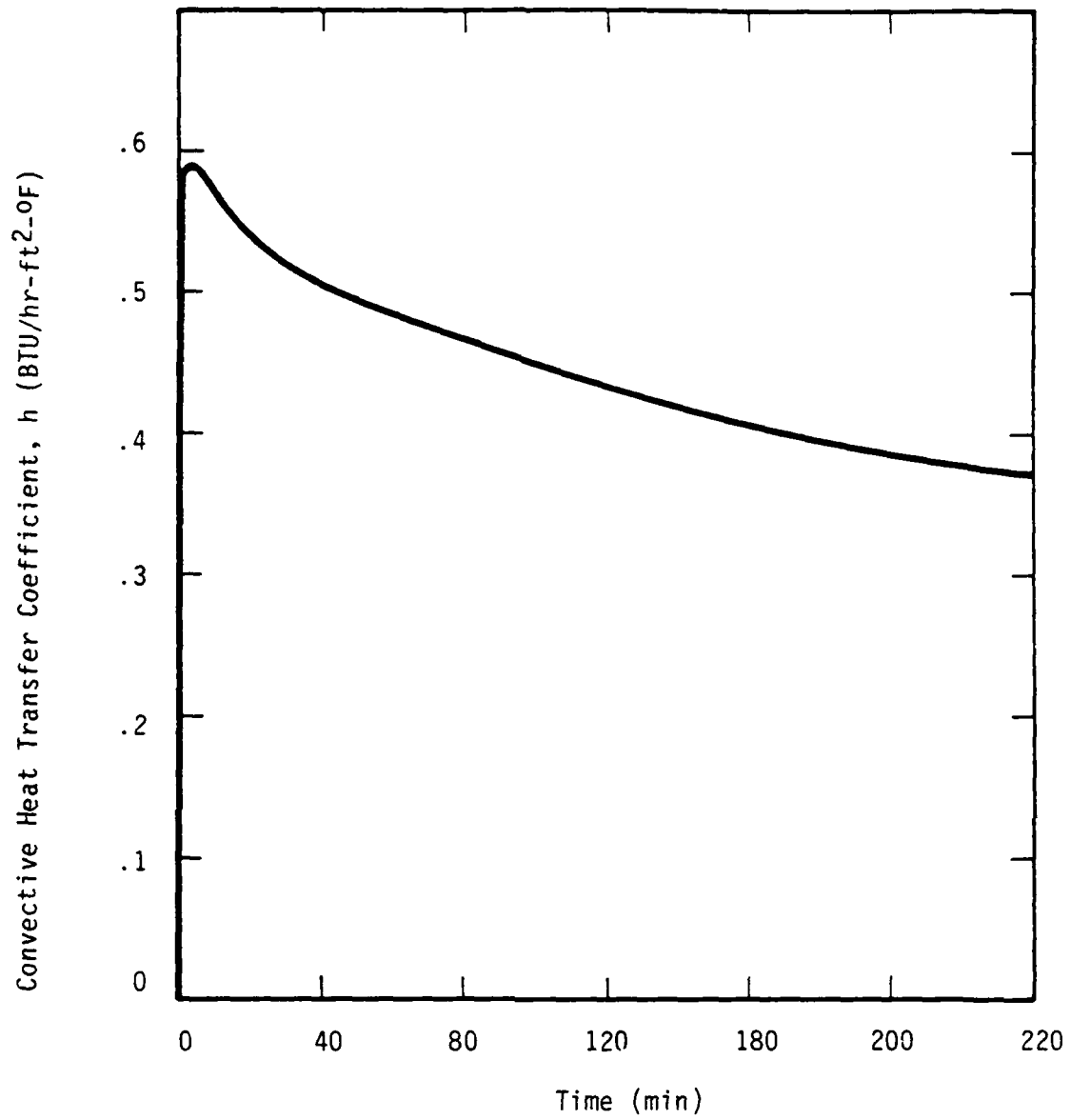


Figure 4. Transient Convective Heat Transfer Coefficient Inside the Boxcar

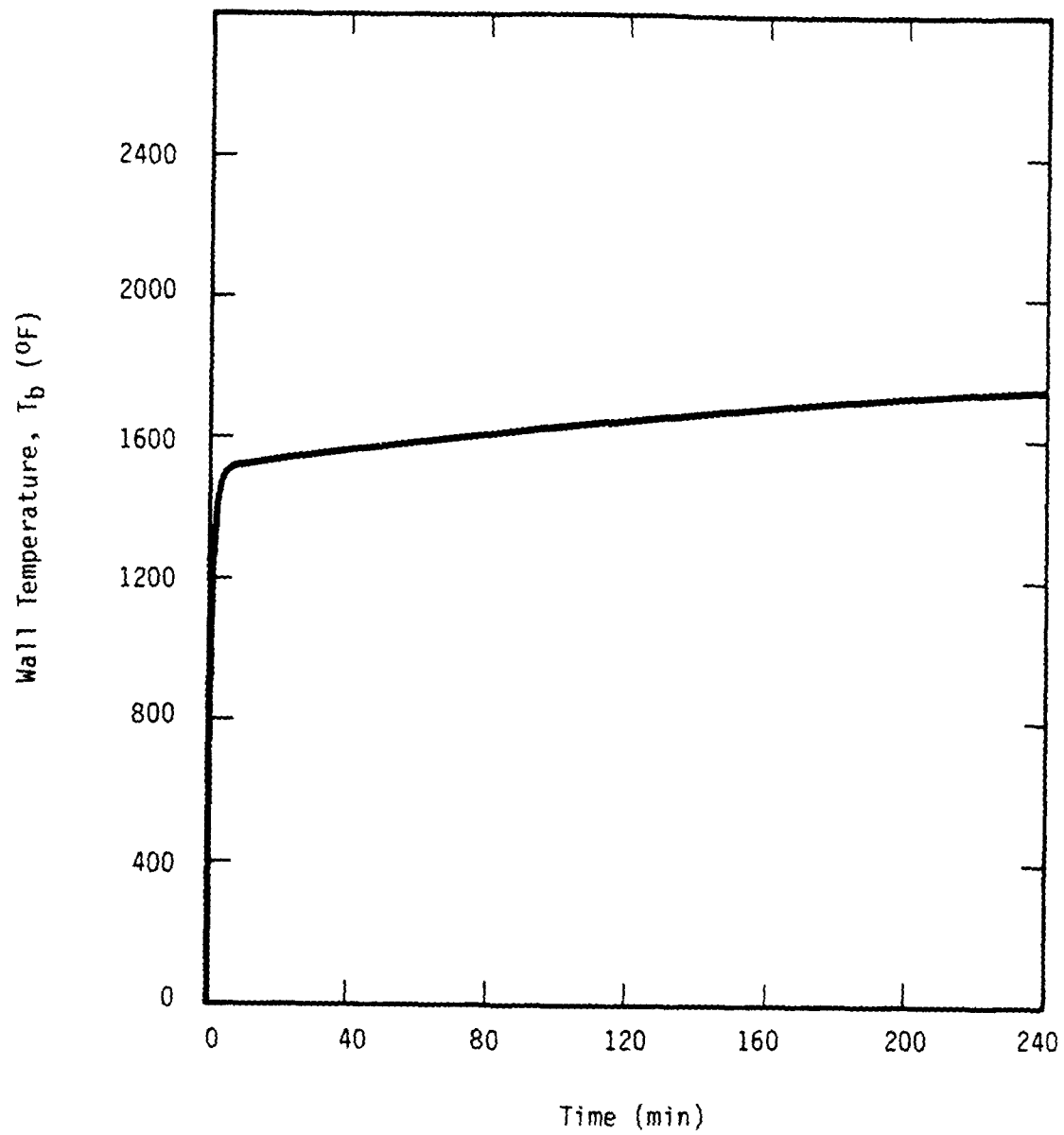


Figure 5. Transient Boxcar Wall (inner surface) Temperature

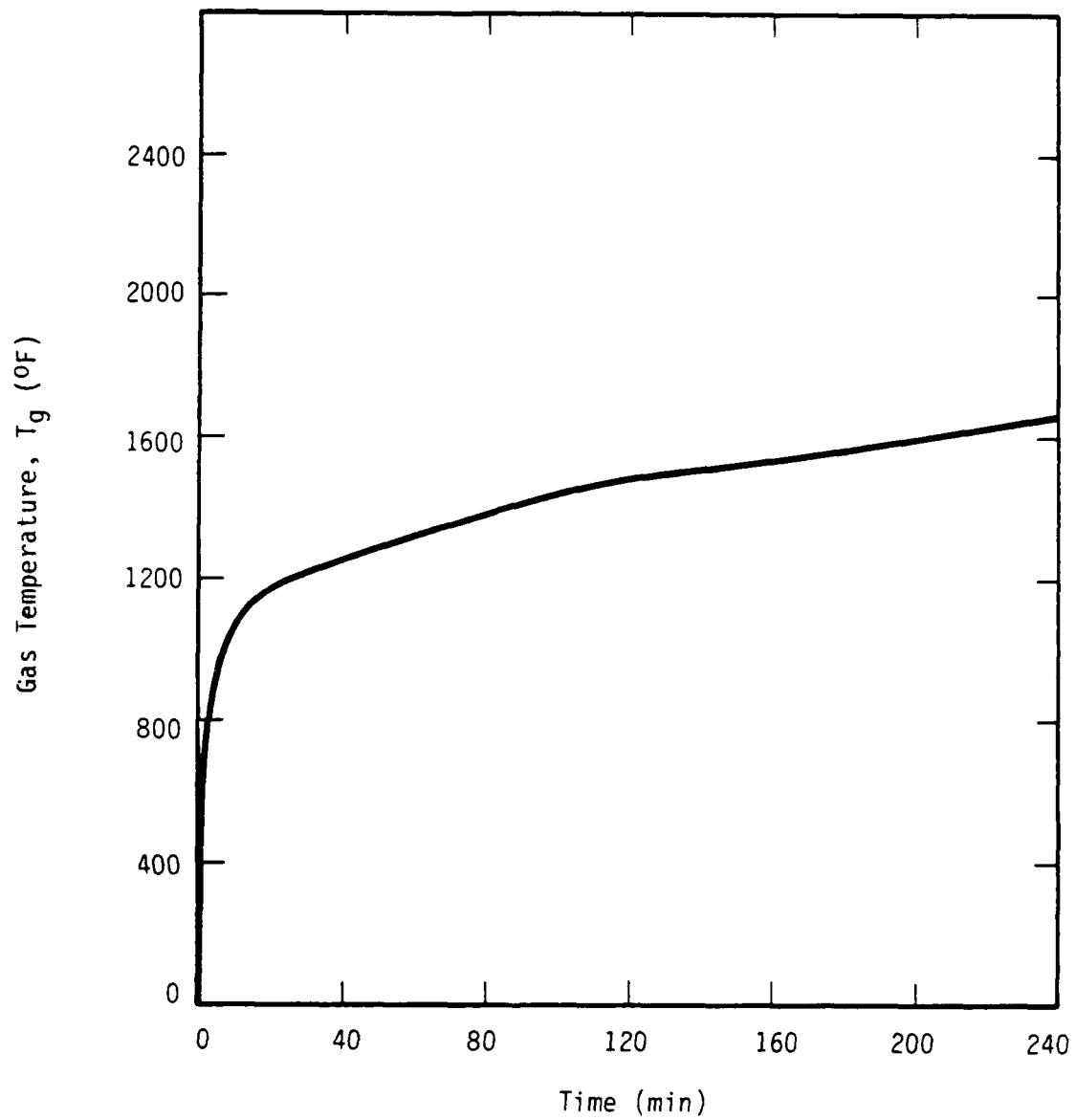


Figure 6. Transient Gas Temperature Inside the Boxcar

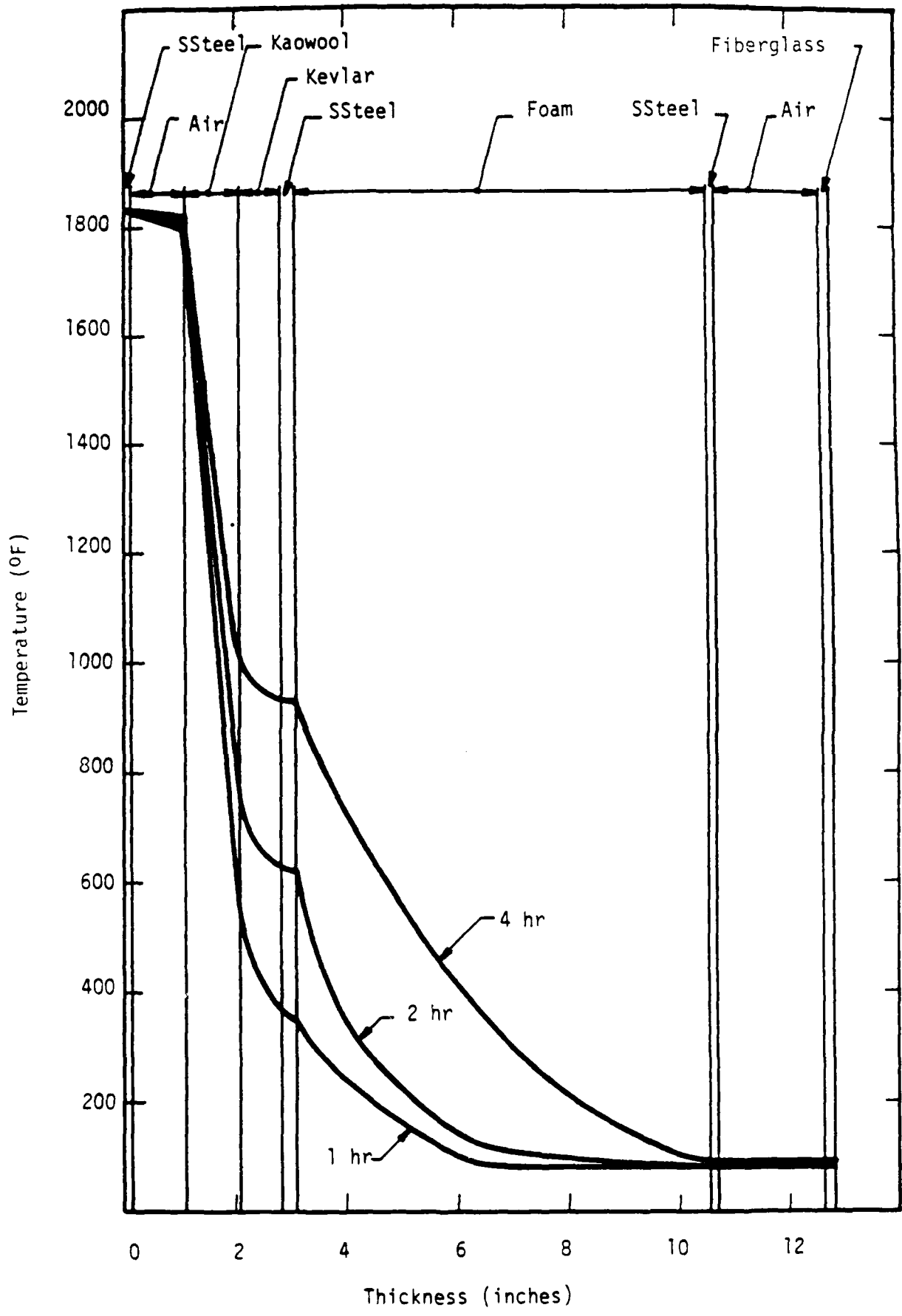


Figure 7. Temperature Contours Within the CAMPACT

exchanging surfaces and the relative angles of exposure. The general expression [12] for the configuration factor is

$$F_{d1-2} = \int_{A_2} \frac{\cos\theta_1 \cos\theta_2}{\pi r^2} dA_2 \quad (6)$$

where F_{d1-2} is the fraction of the energy leaving elemental surface 1 that strikes surface 2; r is the distance between differential areas on surfaces 1 and 2; θ_1 and θ_2 are the angles between r and the respective normals of each surface.

Figure 8 shows the geometry of the rockets, pallet framing, and carrier walls. The configuration factor is solved in Cartesian coordinates in terms of geometric variables (shown in the figure) as

$$F_{d1-2} = \int_{-\infty}^{\infty} \int_{-e}^f \frac{w^2 \cos\theta + w^2 \sin\theta}{\pi(x^2 + w^2 + y^2)^2} dx dy \quad (7)$$

Performing the integration of Equation (7) gives:

$$F_{d1-2} = \frac{e \cos\theta + w \sin\theta}{2(e^2 + w^2)} + \frac{f \cos\theta - w \sin\theta}{2(f^2 + w^2)} \quad (8)$$

where θ (without a subscript) represents the angular distance around the rocket's circumference. Note that the rocket has been assumed long in the axial (y) direction. Properties e , f , and w change with the rocket location and angular position.

The configuration factor has been determined as a function of angular position for the top center and top end locations of the rocket in the pallet. Rockets surrounding the rocket in the top center position shade it from some radiation transmitted from the carrier walls. In the top end position, the rocket is shaded by neighboring rockets and by the pallet framing. Details of the configuration factor determination are given in

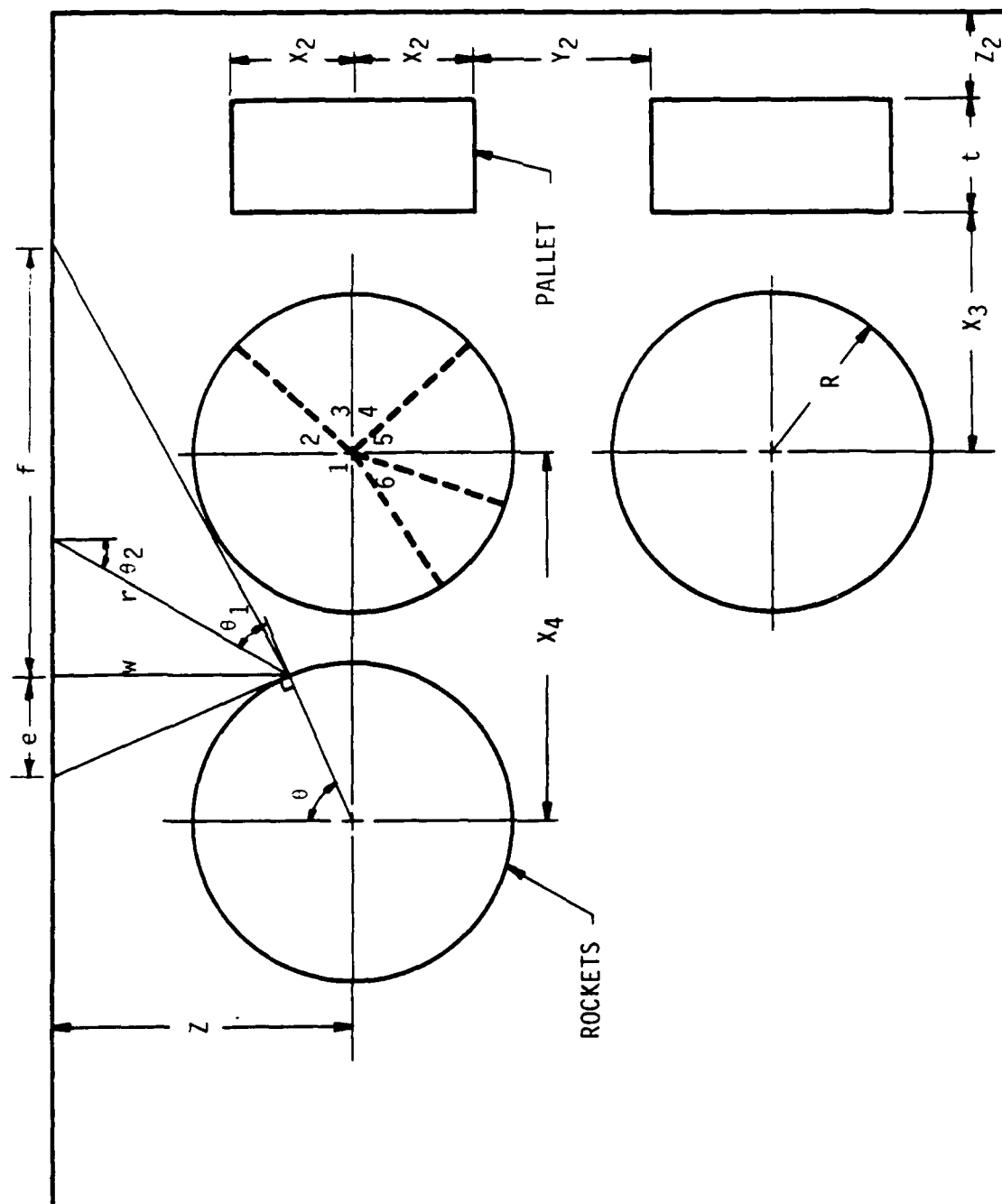


Figure 8. Configuration Factor Geometries with Rockets and Pallet

Appendix D. Dimensions extracted from copies of blueprints of the pallet are also denoted in the appendix. Figure 9 graphs the calculated configuration factors as a function of angle around the rocket's circumference.

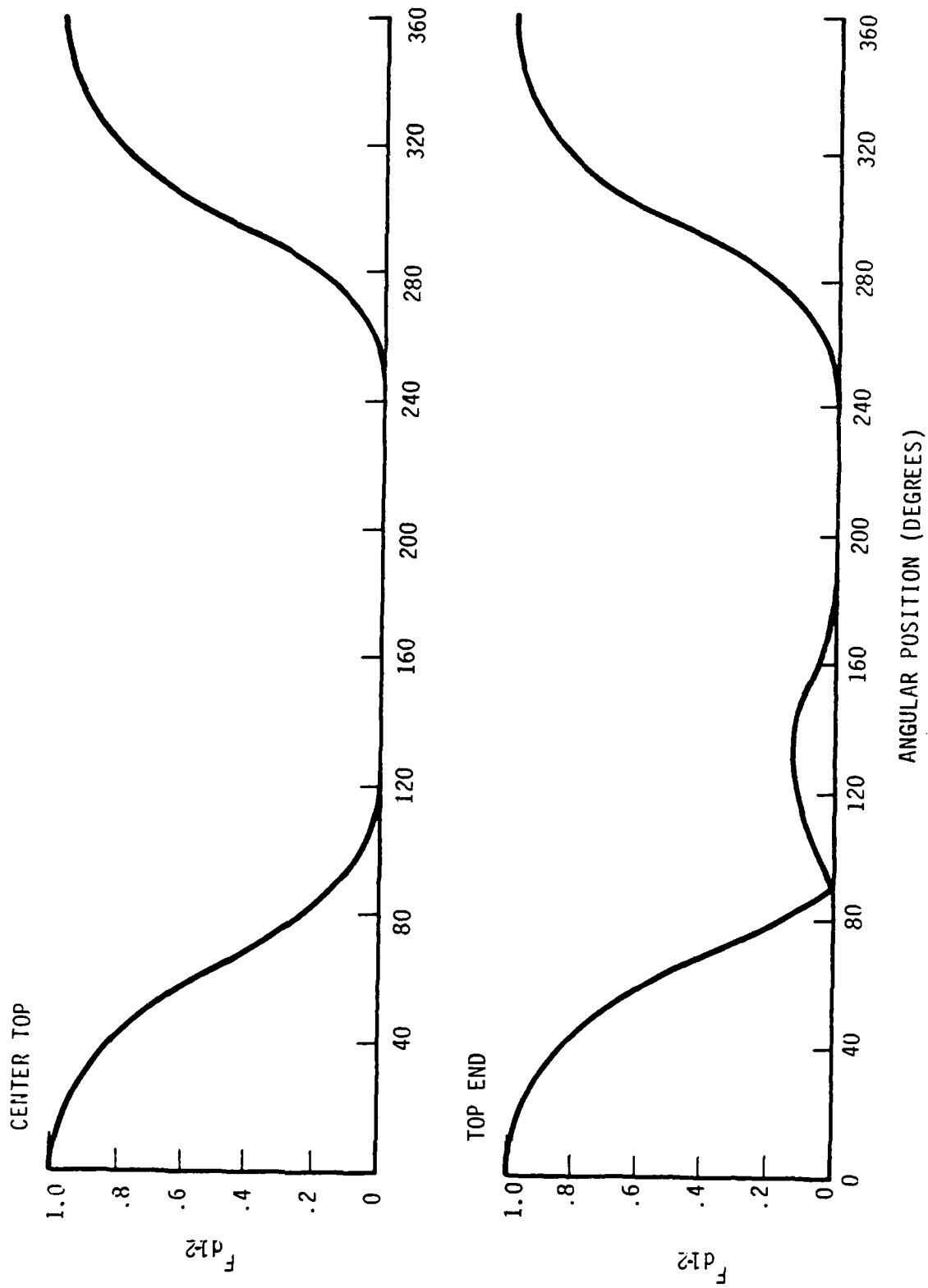


Figure 9. Configuration Factors as a Function of Angular Position

III. ROCKET RESPONSE TO THERMAL LOADS

A. Rocket Description

Four cross sections of the M55 rocket were analyzed as shown in Figure 10. The rocket is considered as stored inside its shipping case. Section A represents a typical cross section of the rocket motor; propellant is held within a steel casing. In Section B, the response of igniter contained inside of a polyethylene cap at the front of the body of propellant is examined. The cap is oriented so heat flowing radially into the rocket will pass through the casing and propellant, and into the igniter. Thus, for a heat transfer analysis, the polyethylene cap can be ignored because of the other heat path. A cross section of the agent chamber is represented in Section C. The burster, encased in an aluminum tube, is surrounded with agent, which is enclosed in a second aluminum casing. The final location analyzed, Section D, is near the burster/fuze interface. The aluminum encased burster is separated from the shipping case by an air gap created by the angled nose section.

B. Boundary Conditions

The heat flux to the rocket container defines the transient thermal load on the rockets. The configuration factor as a function of angular position is needed to establish the asymmetric loading on the rocket. This function depends on the rocket position in the pallet. Transient temperatures of the backface of the carrier walls, as determined in the transport carrier thermal analysis, is needed to define the radiative heat flux on the rocket by

$$\dot{q} = F_{d1-2} \epsilon \sigma (T_b^4 - T_r^4) \quad (9)$$

where

- \dot{q} = incident radiant heat flux (BTU/hr-ft²)
- σ = Boltzmann's constant = 0.173×10^{-8} BTU/hr-ft²-°R⁴
- F_{d1-2} = configuration factor

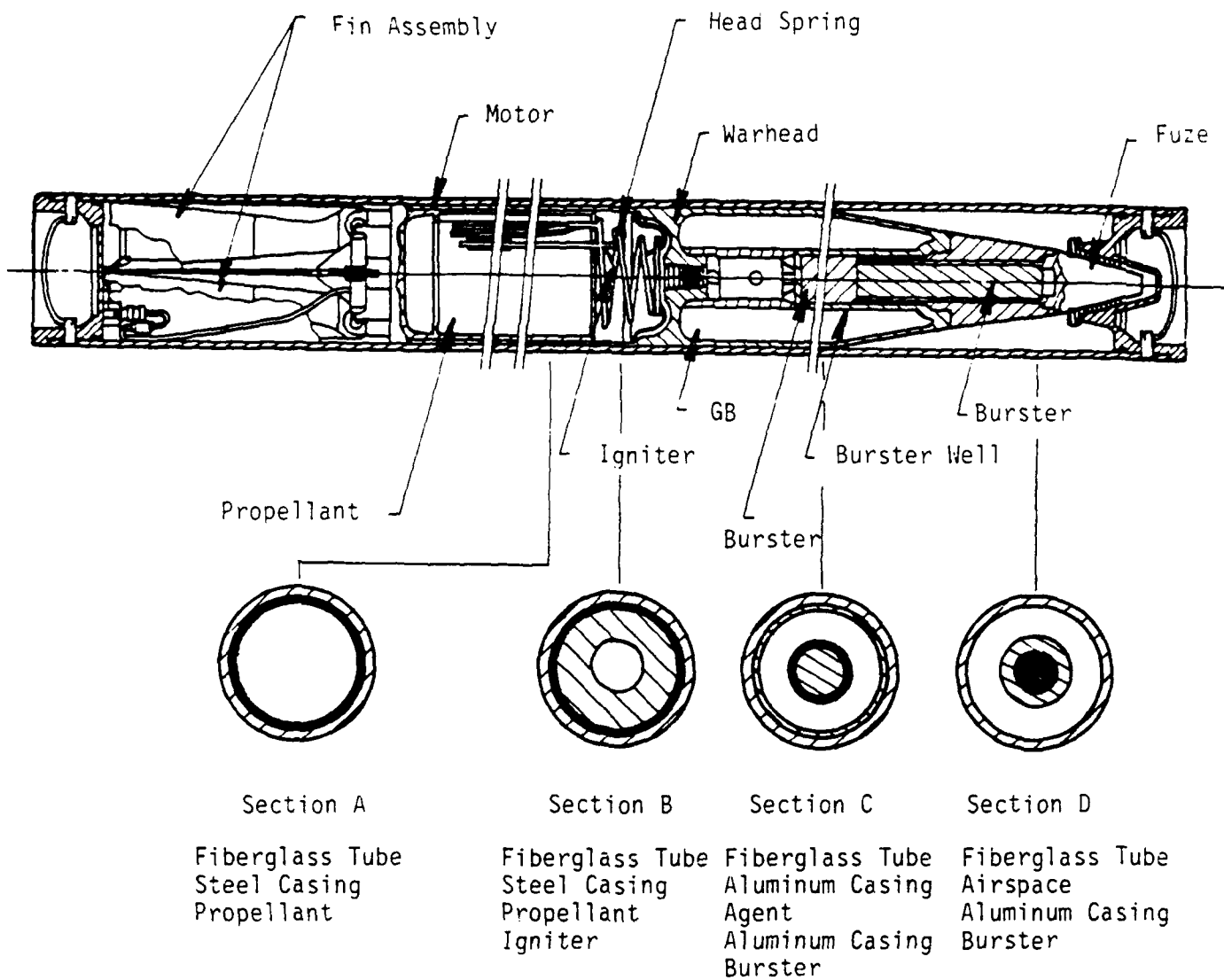


Figure 10. Rocket, 115mm, GB, M55

- ϵ = effective emissivity for radiant exchange
- T_b = absolute temperature of the backface of the carrier walls ($^{\circ}\text{R}$)
- T_r = absolute temperature of the rocket surface ($^{\circ}\text{R}$)

Convective heat transfer to the rocket is assumed to be uniform around the perimeter of the rocket. The convective flux is

$$\dot{q} = h(T_g - T_r) \quad (10)$$

where

- h = convective heat transfer coefficient ($\text{BTU/hr-ft}^2\text{-}^{\circ}\text{F}$)
- T_g = absolute gas temperature ($^{\circ}\text{R}$)
- T_r = absolute temperature of the rocket surface ($^{\circ}\text{R}$)

Both the gas temperature within the carrier and the convective heat transfer coefficient are transient properties determined in the carrier response analyses. However, after determining the thermal response of the three transport carriers, the thermal "boundary conditions" to be applied to the rockets were found to be distinctly different between the carriers. The following paragraphs summarize how the thermal loading conditions were treated for each of the transport carriers.

1. Truck

The truck walls are consumed by the fire, thus, the size and shape of the truck no longer restricts convective flows. The radiant exchange with the rockets is given by Equation (9). Natural convection to the rockets now is characterized by the diameter D , of the rockets and the temperature difference between the fire (1850°F) and the rocket surface. An average convective heat transfer coefficients to horizontal cylinders in air is defined empirically [15] by:

$$h = 0.27 (\Delta T/D)^{1/4} \quad (11)$$

where $\Delta T = T_g - T_r$. A value of $1.7 \text{ BTU/ft}^2\text{-hr-}^{\circ}\text{F}$ was used in the thermal response analyses of the rocket cross-sections. This value is an average of

the transfer coefficients over surface temperatures from 200 to 1500°F. The variation of ± 0.4 BTU/ft²-hr-°F over this temperature range was considered sufficiently small to justify approximating h as a constant.

2. Railcar

Equations (9) and (10) prescribed the thermal flux to the rockets inside a railcar. Figures 4, 5 and 6 prescribe h, T_b and T_g respectively as a function of time.

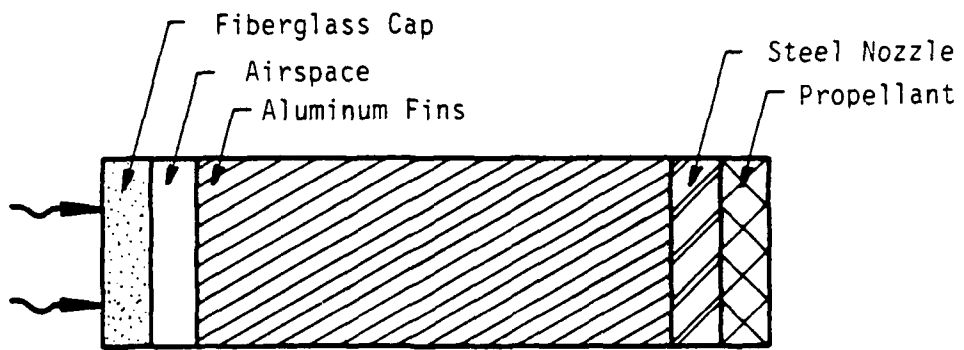
3. CAMPACT

The interior of the CAMPACT did not heat sufficiently to warrant numerical computations of the rocket sections (reference Section IIBb-(3)). From Figure 7, it is evident that the CAMPACT shipping container thermally can protect the M55 rockets from a four-hour hydrocarbon fuel fire.

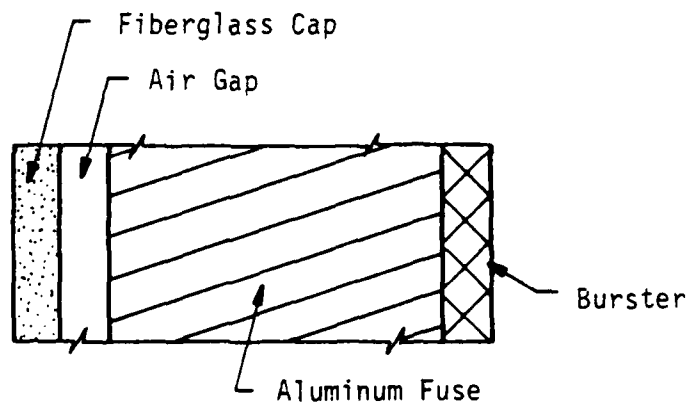
C. Axial Heating

The objective of the axial heating analysis was to determine the impact of axial heating on the thermal response of radially heated sections. Nose and tail sections were considered as one-dimensional members as shown in Figure 11. Comparison of temperatures from radial and axial heating would establish if axial heating was significant and had to be accounted for in the thermal analysis. If axial heating was found to increase temperatures by more than 10 percent of the radial temperature, then superposition of temperatures would be used to estimate the additional effects of axial heating. Table 4 lists material properties used in the axial heating analysis.

Neither the nose nor tail section showed a significant amount of axial heating when subjected to the truck's thermal environment (the most severe of the three carriers). The burster in the nose section heated to only 72°F after 10 minutes with axial heating while the same material reached 350°F with radial heating. In the tail section, propellant increased in temperature (after 15 minutes) to 84°F with axial heating and 624°F with radial heating.



A. Fin Assembly



B. Fuse Assembly

Figure 11. One Dimensional Representations of Rocket Ends

Table 4. Material Properties for Axial Heating Analysis

Section	Material	Thickness(in)	ρ (lb/ft ³)	k(BTU/ft-hr-°F)	Cp(BTU/lb°F)
Tail	Fiberglass Cap [14] (@ 100°F)	0.16	82	.02	.20
	Aluminum Fins (@ 68°F) [15] [13]	8.58	164	93	See Eq (p3)
	Steel Nozzle (@ 68°F) [15] [13]	1.62	487	25	See Eq (p4)
	Propellant [16] [17]	1.0	101	.48*	.347
Nose	Aluminum Cap [14] (@ 68°F)	0.21	164	93	See Eq (p3)
	Aluminum Fuse (@ 68°F) [15] [13]	3.31	164	93	See Eq (p3)
	Burster [16] [17]	1.0	101	.48*	.347

*Average k of mock HE explosives from Ref. 16.

Material Property Equations

(p1) For stainless steel, $k = 8.6 + .00045T$ (T in °F, k in BTU/ft hr °F).

(p2) For kaowool, $Cp = 0.2227 + 1.79 \times 10^{-5}T$ (T in °F, Cp in BTU/lb °F).

(p3) For aluminum, molar specific heat, $Cp = 4.94 + 2.96 T/1000$ (T in °K, Cp in cal/gmole °K).
Divide by 26.9 to get cal/g °K = BTU/lb °F.

(p4) For steel, molar specific heat, $Cp = 3.37 + 7.1 T/1000 + .43 \times 10^5/T^2$ (T in °K, Cp in cal/gmole °K).
Divide by 55.8 to get cal/g °K = BTU/lb °F.

As the energetic materials show a minimal temperature increase from axial heating relative to radial, the effects of axial heating were ignored.

D. Thermal Response of Rocket Sections

The four rocket cross-sections analyzed are described in terms of assumed material properties. The sections were divided into an array of nodes for a two-dimensional numerical analysis using SINDA [9]. Interior nodes transfer heat to adjacent nodes through a resistance-capacitance network. Arithmetic nodes (with no capacitance) along the outer surface of the rocket receive transient convective and radiative heat fluxes from boundary nodes. Boundary nodes input time varying gas and wall temperatures into the computer model.

It was found that the fiberglass shipping tube encasing the rockets, where exposed to high radiative flux, heated very rapidly. The auto-ignition temperature for glass-reinforced material (e.g., molded fiberglass) is 750°F as determined from test procedures in accordance with ASTM standard D1929 [21]. Once the shipping tube reached its auto-ignition temperature, the analysis procedure used was similar to the procedure used to handle the burning and consumption of wood, Section IIBb. With a burn rate of 1 in/min [22], the shipping tube was consumed within six seconds (a neglectable duration). The two-dimensional computer code was run for each scenario with the fiberglass shipping tube in place. At the point of fiberglass auto-ignition, the computer program was stopped, the burnt fiberglass nodes removed from the computational grid, and then the program was restarted.

The carrier response accounted for heat absorbed by the pallet, but was not concerned with a detailed account of this heat absorption. This was left to the more carefully treated rocket response analysis. The assumption made was that, to a good first approximation, the carrier response could be decoupled from the details of the rocket response. Once the carrier response was completed, then this information would be used as input for the transient boundary conditions to compute rocket response. However, for this analysis technique to be valid, the heat flux to the rockets should be similar in the two approaches.

The assumption of computing the thermal environment first, and then examining rocket response (without explicitly tying the two responses together), was checked by comparing the heat fluxes into the rocket. The ratio of radiative \bar{q}_r , and convective \bar{q}_c , heat fluxes are:

$$\bar{q}_r = \frac{(T_w^4 - T_s^4)_{\text{carrier}}}{(T_w^4 - T_s^4)_{\text{rocket}}}$$

and

$$\bar{q}_c = \frac{[h(T_g - T_s)]_{\text{carrier}}}{[h(T_g - T_s)]_{\text{rocket}}}$$

where the subscripts w, s, and g refer to the wall, the shipping tube or rocket surface, and gas temperatures respectively.

Table 5 lists the flux ratios as a function of time for the agent section in the boxcar. The difference in radiative heat flux was less than 2 percent between models (carrier response versus rocket response) while the convective flux varied by about 10 percent. One reason for the difference is that ignition, burning, and removal of the fiberglass was considered only in the rocket response analysis. Though the surface temperatures differ in the two analyses because of the different treatment of the shipping tube, the heat fluxes to the rocket surface differ very little. In particular, since the convective flux is approximately an order of magnitude less than the radiative flux, the very small differences in the heat fluxes (which drive the transient thermal response) validate the analysis procedure of separating the carrier and rocket response analyses.

Table 5. Transient Flux Ratios, Carrier Vs. Rocket Response

<u>Time (Sec)</u>	<u>\bar{q}_r</u>	<u>\bar{q}_c</u>
200	.989	.887
400	.988	.900
600	.987	.915
1000	.984	.949

One last numerical check was performed. ONEDIM and SINDA are based on completely different numerical algorithms. For radially symmetric heating of the rocket, a cylindrical one-dimensional analysis should agree with a two-dimensional analysis. SINDA and ONEDIM outputs were compared for each of the four cross-sections for a radiatively shielded rocket inside the truck. These computer runs, examined out to 30 minutes, confirmed the two numerical codes predicted temperatures for each cross-section reasonably consistency. There were small differences of a few percent in the numerical results attributable to the different numerical procedures, particularly at the exterior boundaries. These numerical checks also permitted confirmation of geometric and material inputs.

1. Propellant

Physical properties of the cross-section of the rocket motor containing propellant are listed in Table 6. The section is illustrated in Figure 12. A total of 211 nodes (shown in the figure) are defined for the two-dimensional SINDA analysis. Nodes are positioned every 10° around the surface of the rocket and are more widely spaced near the center. This orientation was chosen to insure spatial resolution near the propellant surface where maximum temperatures and heat fluxes occur.

Exposure of the propellant section to radiation and convection in the top center and top end pallet positions results in the ignition and burning away of the upper half of the fiberglass shipping tube within 30 seconds after wall burnthrough in the truck, and after 200 seconds in the boxcar. The network of nodes used to evaluate thermal response after fiberglass removal is shown in Figure 13.

The transient, maximum temperature of the propellant is shown in Figure 14 for a pallet of munitions in the truck and in Figure 15 for the boxcar. After the truck walls are consumed by the fire (at 6.5 minutes), the propellant shows a steeper increase in temperature with time as compared to the thermal response if in the boxcar.

Table 6. Propellant Properties

Material	Thickness (in)	Thermal Conductivity k(BTU/ft-hr-°F)	Specific Heat Cp(BTU/lb°°F)	Density ρ (lb/ft ³)	Heat of Transition h _{sf} (BTU/lb)	Transition Temperature T _m (°F)
Fiberglass Shipping Case [14] (@ 100°F)	.165	.02	.20	82		750
Steel Casing (@ 68°F) [15] [13]	.256	25.	See Eq (p4)	487		
Propellant [16] [17]	2.00	.48*	.347	101		

*Average k of mock HE explosives (Ref. 16)

Material Property Equations

(p1) For stainless steel, $k = 8.6 + .00045T$ (T in °F, k in BTU/ft hr °F).

(p2) For kaowool, $Cp = 0.2227 + 1.79 \times 10^{-5}T$ (T in °F, Cp in BTU/lb °F).

(p3) For aluminum, molar specific heat, $Cp = 4.94 + 2.96 T/1000$ (T in °K, Cp in cal/gmole °K).
Divide by 26.9 to get cal/g °K = BTU/lb °F.

(p4) For steel, molar specific heat, $Cp = 3.37 + 7.1 T/1000 + .43 \times 10^5/T^2$ (T in °K, Cp in cal/gmole °K).
Divide by 55.8 to get cal/g °K = BTU/lb °F.

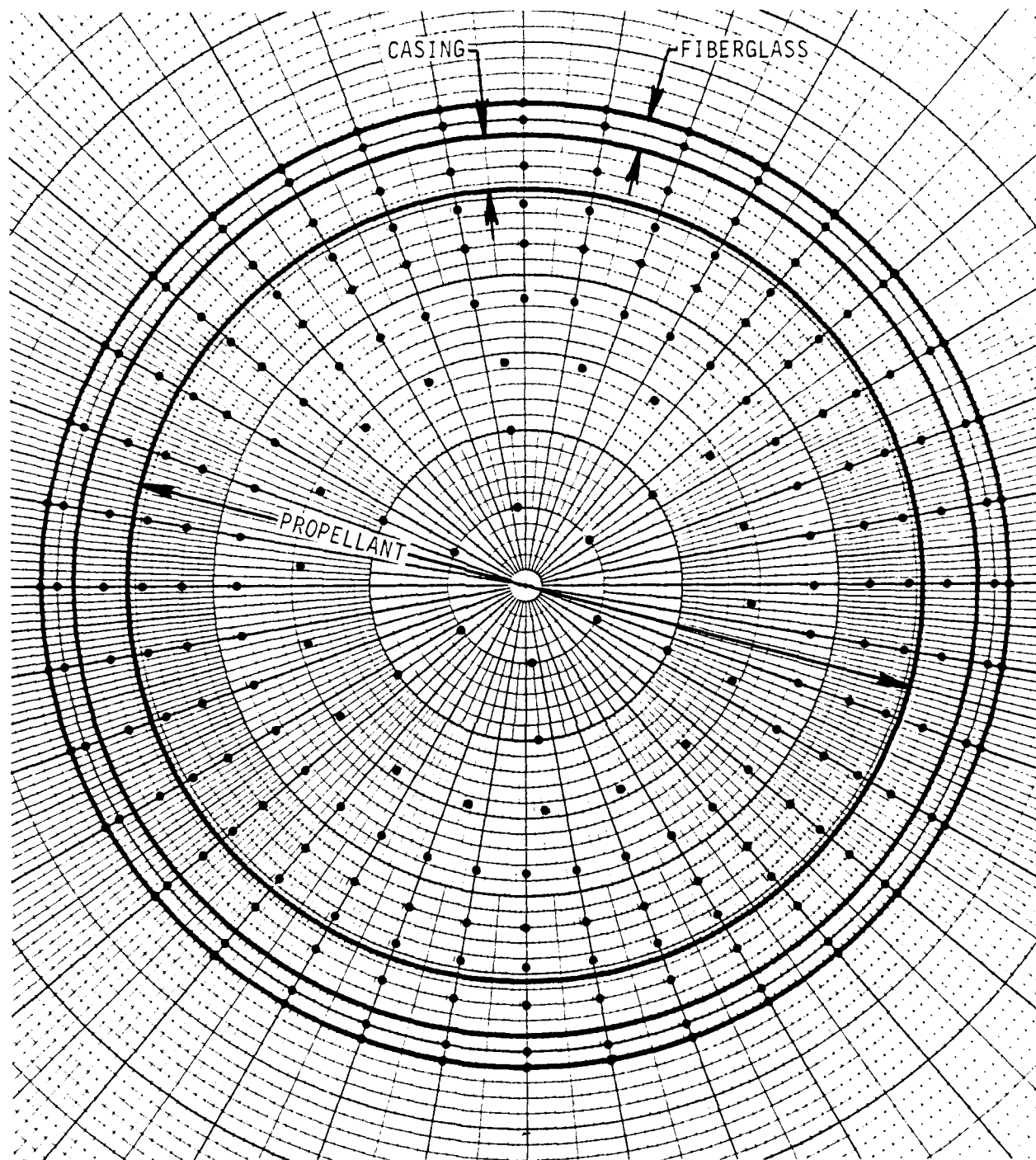


Figure 12. Node Locations for Two-Dimensional Computer Analysis of Propellant Section

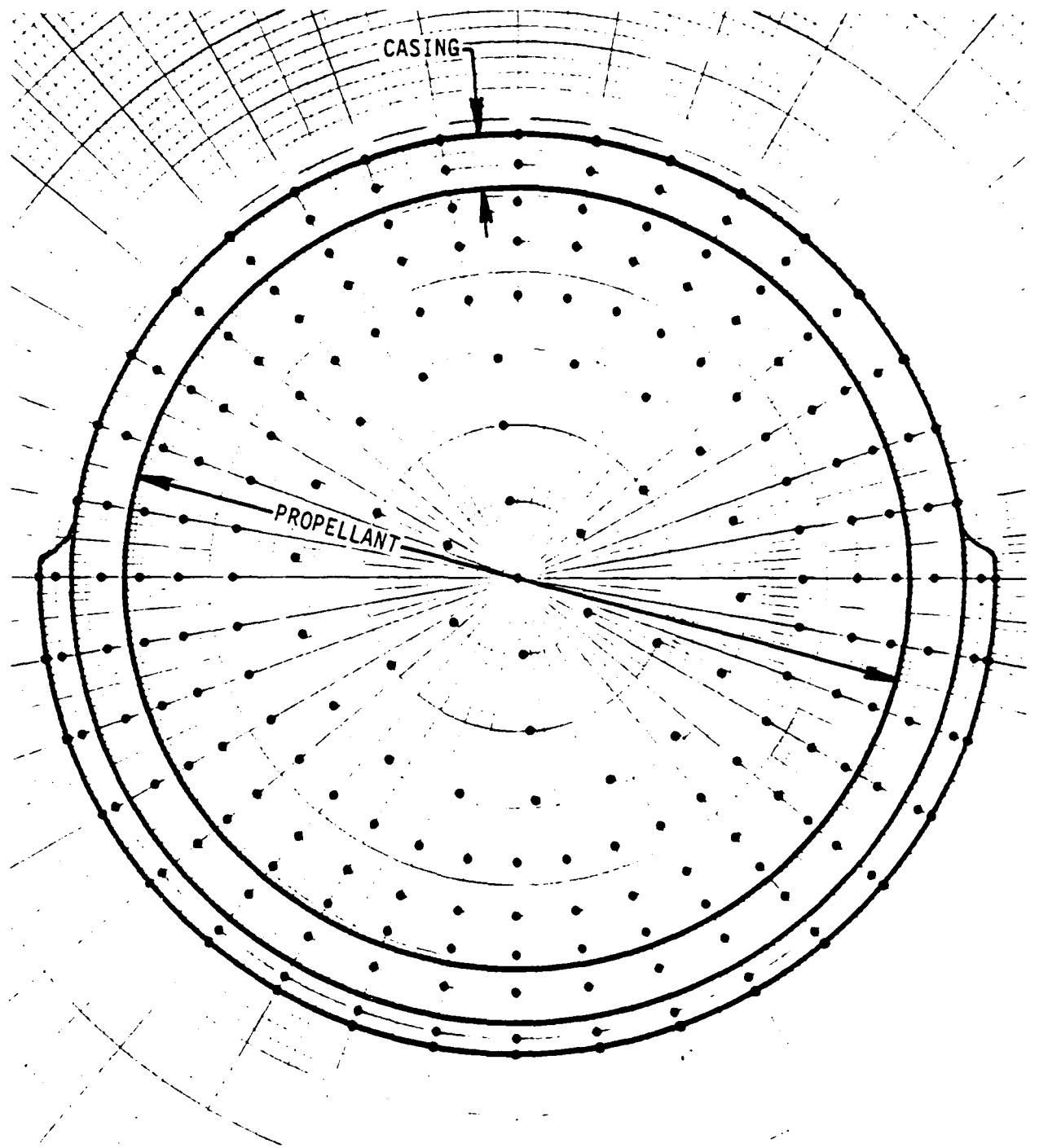


Figure 13. Node Locations for Two-Dimensional Computer Analysis of Propellant Section after Fiberglass Melt

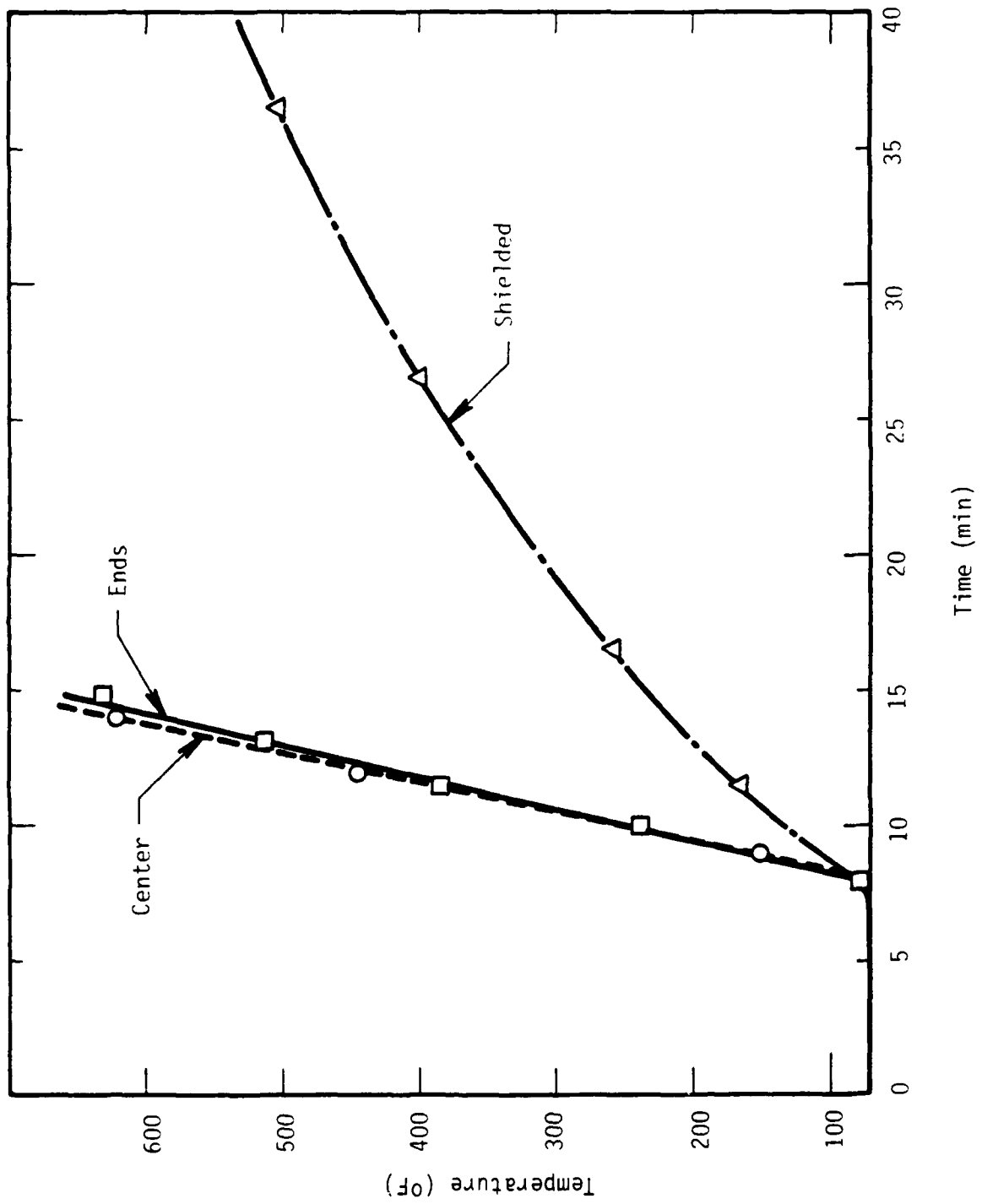


Figure 14. Temperature-Time History of Propellant for Truck

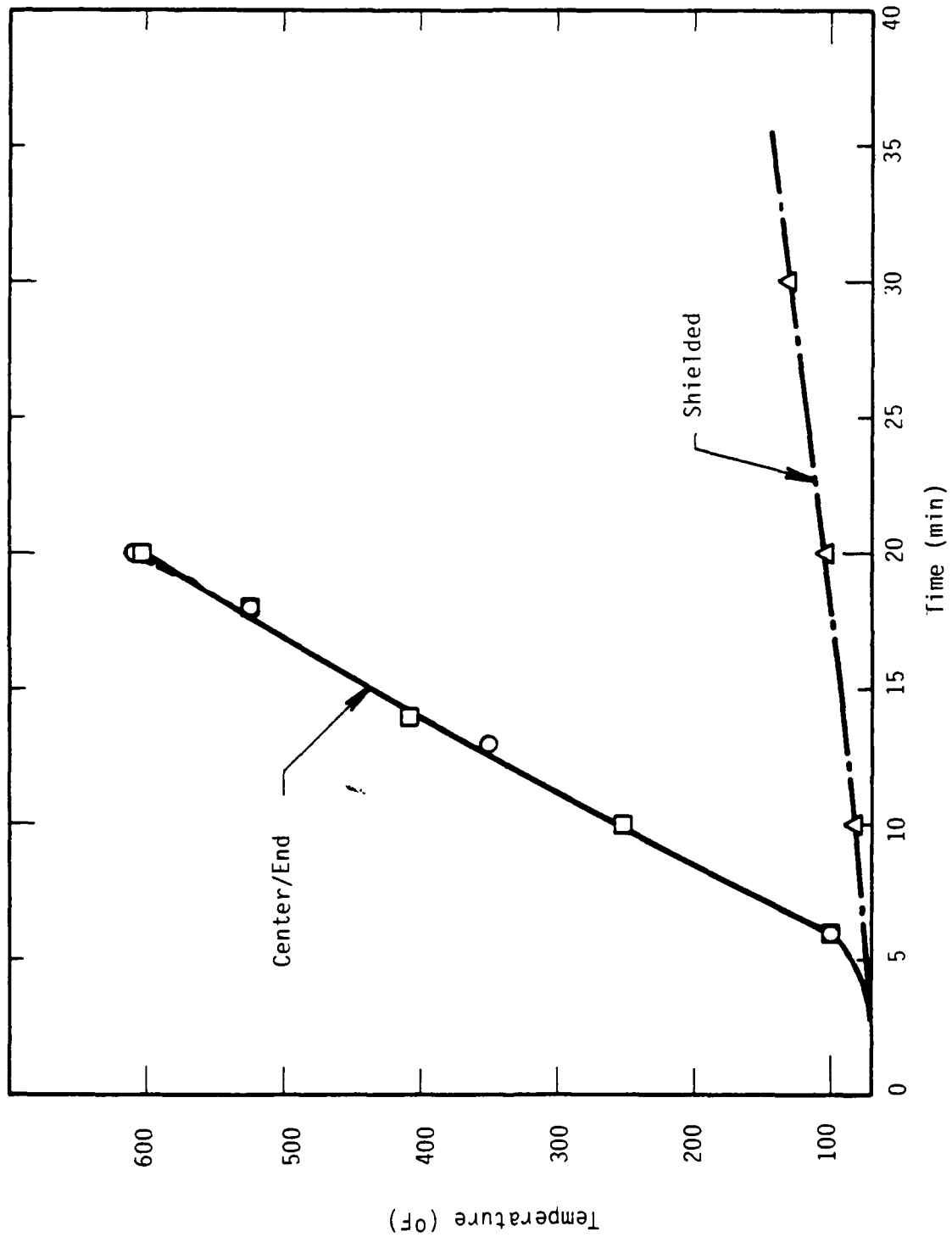


Figure 15. Temperature-Time History of Propellant for Railcar

Propellant in rockets located within the pallets, shielded from radiation by surrounding rockets, increased in temperature significantly slower than the top positions. Temperature-time profiles of the propellant for the top center and top end pallet positions are virtually identical.

2. Igniter

The geometry and physical properties of the igniter cross-section are listed in Table 7. The section is illustrated in Figure 16. Again 211 nodes are used to define the section to the SINDA program. Radially, the nodes are positioned to include the thermal response of each of the material layers to the heat diffusion. Nodes are placed at 10° increments around the rocket perimeter. The number of nodes decreases with radial distance near the rocket centerline.

The fiberglass shipping tube encasing the igniter section reaches auto-ignition temperature within three minutes for the top center or end pallet positions of the boxcar. The tube burns away in unshielded positions similar to the propellant cross-section analysis. The upper half of the fiberglass tube is consequently burned away, exposing the steel casing directly to the incident heat flux. At the point of burn through, the numerical analysis was stopped, the node network redefined (see Figure 17), and the program restarted with temperatures reflecting heating during the pre-burn phase.

The next two figures show the largest igniter temperatures as a function of time. Figure 18 presents the transient igniter temperatures for three pallet positions in the truck. Following the consumption of the truck walls by the fire, the igniter in the top center and end positions follow the same linear increase in temperature with time. The igniter in rockets in the pallet center shows a slower thermal response owing to the shielding from radiation. Figure 19 shows the same information for igniter sections inside the boxcar. Igniter in the top pallet positions again show similar thermal responses while the shielded rocket displays a much slower temperature increase because of the shielding from radiation.

Table 7. Igniter Properties

Material	Thickness (in)	Thermal		Specific Heat Cp(BTU/lb-°F)	Density ρ (lb/ft ³)	Transition Temperature T _m (°F)
		Conductivity k(BTU/ft-hr-°F)				
Fiberglass Shipping Case [14] (@ 100°F)	.165	.02		.20	82	750
Steel Casing (@ 68°F) [15] [13]	.256	25		See Eq (p4)	487	
Propellant [16] [17]	1.31	.48*		.347	101	
Igniter [16] [17]	.693	.48*		.347	101	

*Average k of mock HE explosives from Ref. 16.

Material Property Equations

(p1) For stainless steel, $k = 8.6 + .00045T$ (T in °F, k in BTU/ft hr °F).

(p2) For kaowool, $C_p = 0.2227 + 1.79 \times 10^{-5}T$ (T in °F, Cp in BTU/lb °F).

(p3) For aluminum, molar specific heat, $C_p = 4.94 + 2.96 T/1000$ (T in °K, Cp in cal/gmole °K).
Divide by 26.9 to get cal/g °K = BTU/lb °F.

(p4) For steel, molar specific heat, $C_p = 3.37 + 7.1 T/1000 + .43 \times 10^5/T^2$ (T in °K, Cp in cal/gmole °K).
Divide by 55.8 to get cal/g °K = BTU/lb °F.

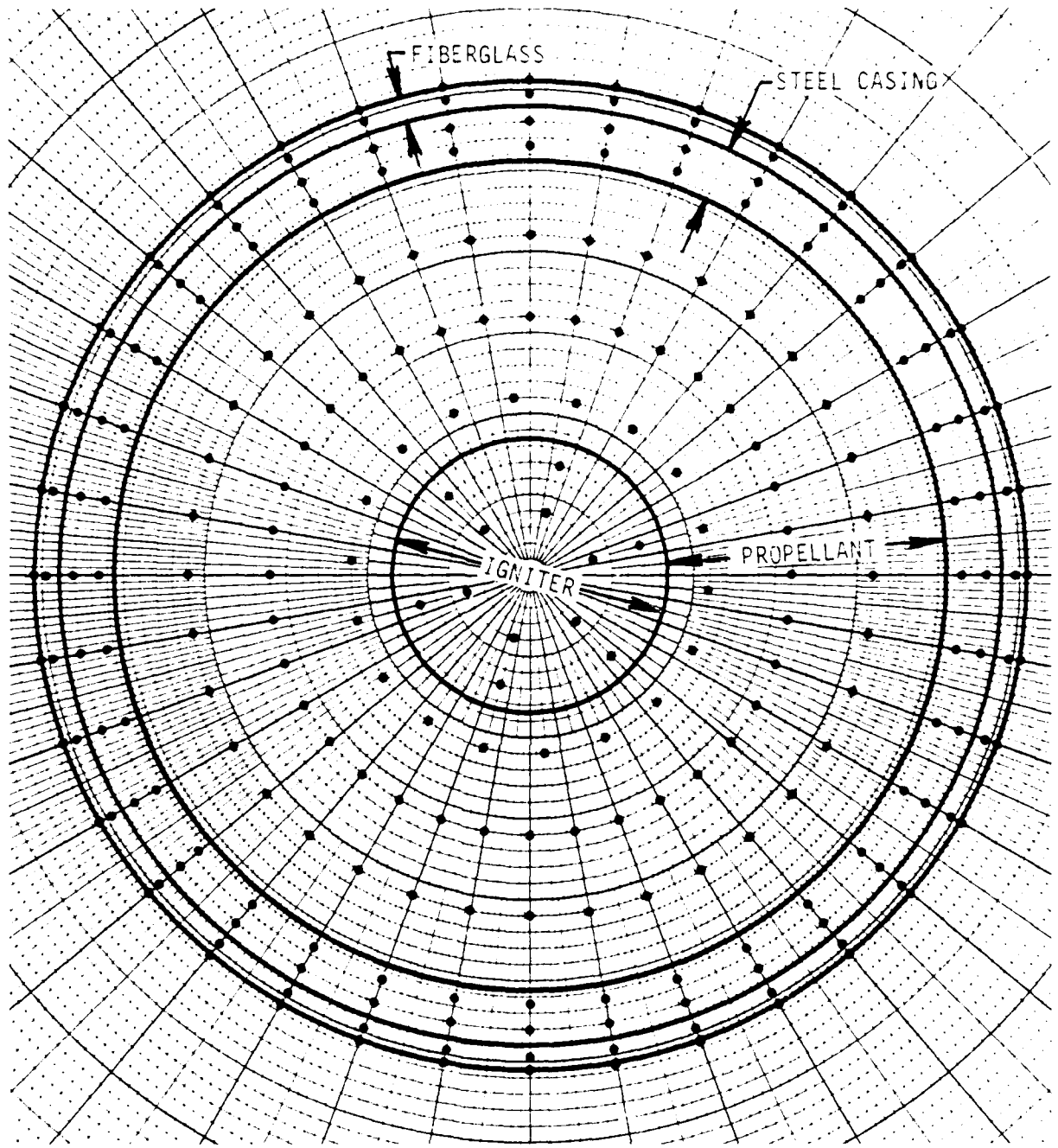


Figure 16. Node Locations for Two-Dimensional Computer Analysis of Igniter Section

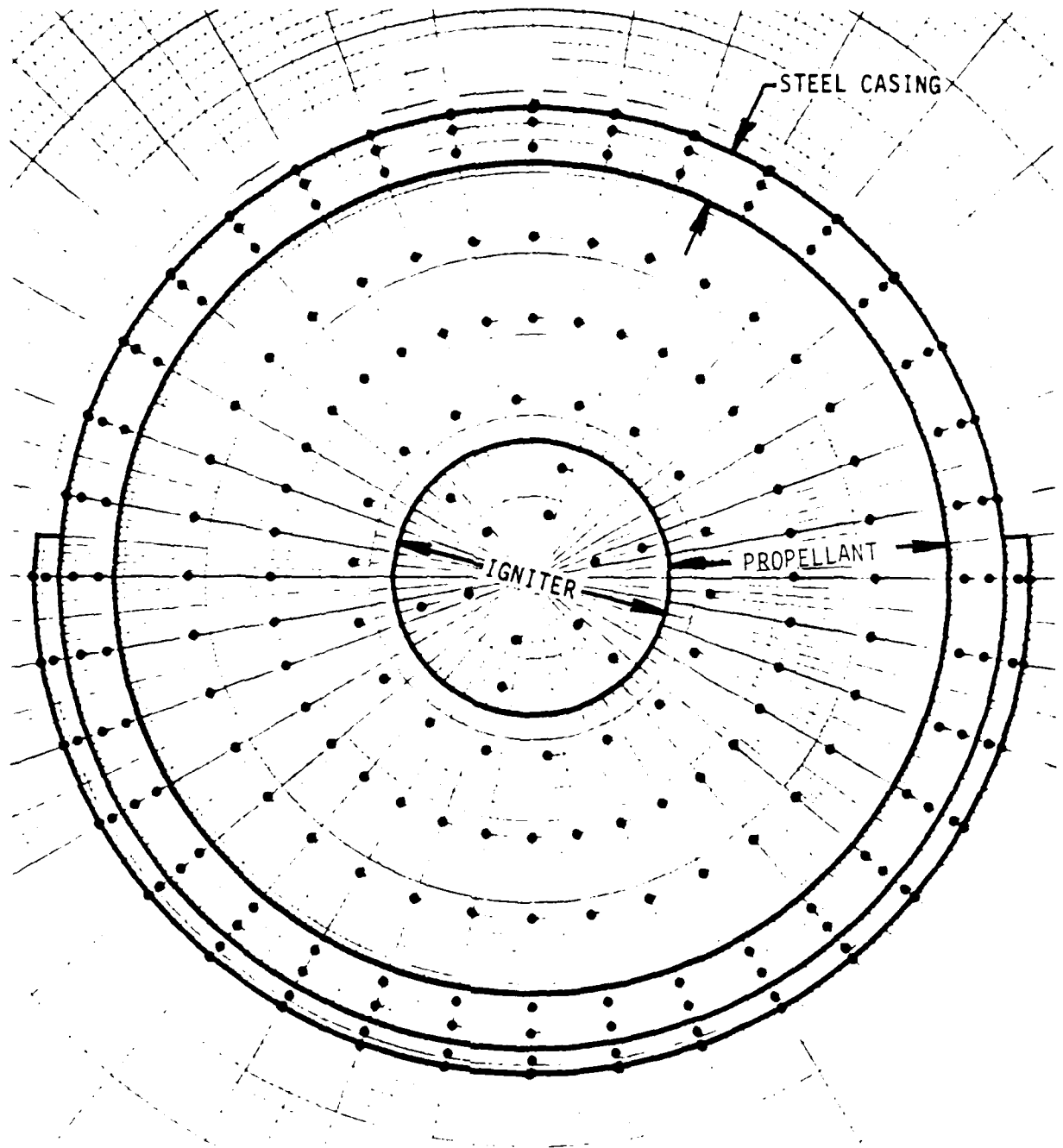


Figure 17. Node Locations for Two-Dimensional Computer Analysis of Igniter Section

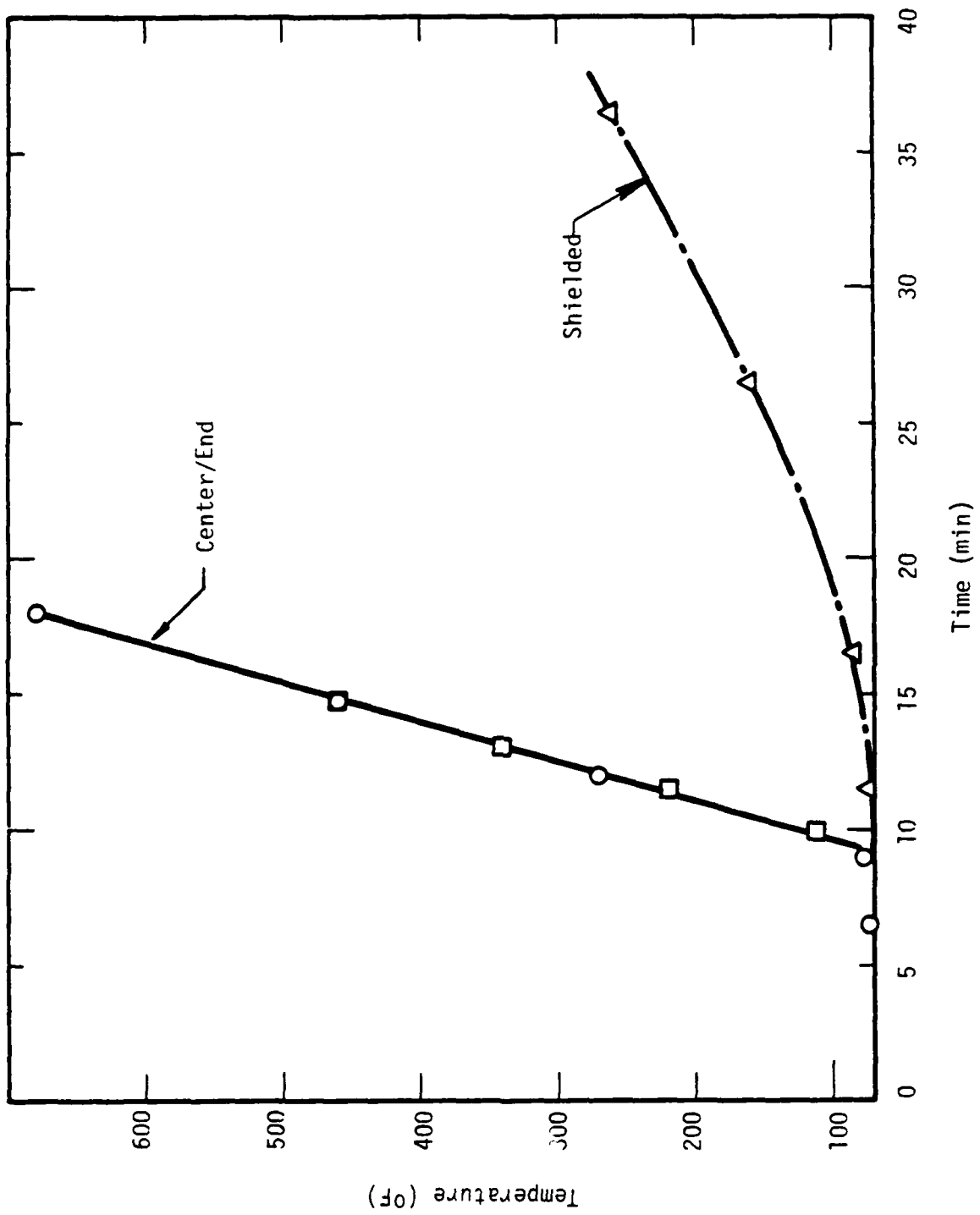


Figure 18. Temperature-Time History of Igniter for Truck

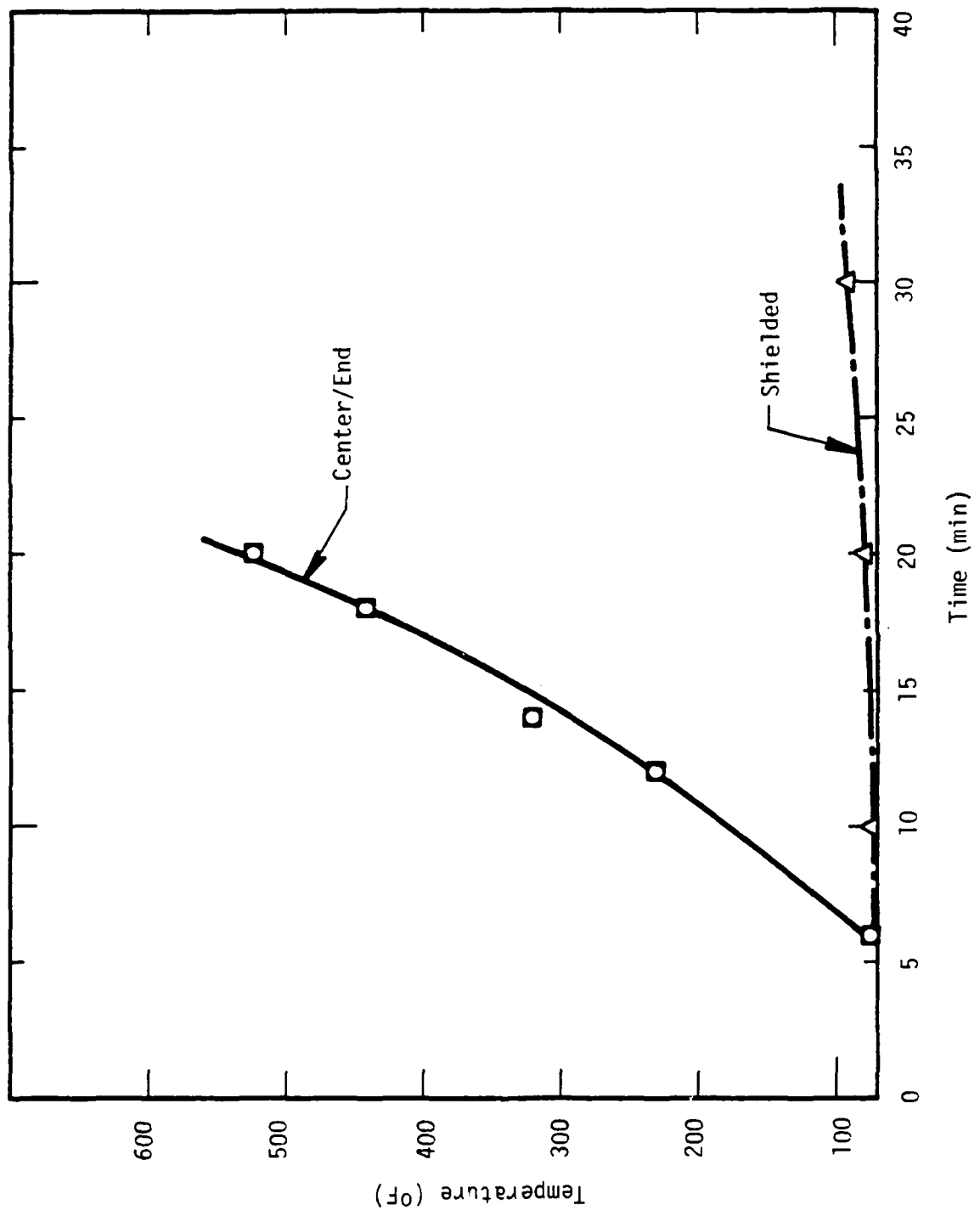


Figure 19. Temperature-Time History of Igniter for Railcar

3. Agent

The physical properties used in the numerical analysis of the agent chamber are contained in Table 8. Figure 20 shows the cross section divided into 211 nodes. Node spacing is close near the rocket surface to increase resolution in the fiberglass, aluminum casing, and outer region of the agent. A ring of nodes is located in each material layer to include the effects of circumferential heat transfer. Like the propellant and igniter sections, the fiberglass shipping tube on the agent section quickly burned away on the upper half of the rocket, necessitating a revised nodal scheme (Figure 21).

Bulk agent temperatures are reported from the thermal response of the center of three nodes layers in the agent region since some convection might be expected in the agent to redistribute temperatures (convection was not explicitly accounted for within the agent compartment). Figure 22 graphs the transient agent temperature for rockets in the truck. Agent in the top center and top end pallet locations follow the same linear rate of temperature increase. Shielded rockets have smaller rises in temperature with time. Thermal responses of the agent in rockets transported by boxcar, Figure 23, show similar trends. Because of the heating lag provided by the truck walls and the relatively high heat capacity of the agent, agent temperatures are greater in the boxcar for the first 15.5 minutes of heating.

4. Burster

Table 9 gives the physical properties used in the analysis of the burster section. Like the other cross-sections, the burster section is represented as an array of 211 nodes as shown in Figure 24. Natural convection of the air within the space between the shipping tube and the rocket was explicitly accounted for in the heat transfer to the rocket by using an effective thermal conductivity which incorporates convective heat transport [23] (See Appendix E).

Following the assumption that fiberglass ignites and burns, the shipping tube surrounding the burster section loses its upper half after 90

Table 8. Agent Properties

Material	Thickness (in)	Thermal Conductivity k (BTU/ft hr °F)	Specific Heat Cp (BTU/lb °F)	Density ρ (lb/ft ³)	Heat of Transition h_{sf} (BTU/lb)	Transition Temperature T_m (°F)
Fiberglass Shipping Case [14] (@ 100°F)	.165	.02	.20	82		750
Aluminum Casing (@ 68°F) [15] [13]	.058	93	See Eq (p4)	164	5.3×10^{-5}	1218
Agent** [20] at 0°F	1.29			58		
200		.0875	.395			
400		.0825	.505			
600		.0775	.615			
800		.0725	.730			
		.0675	.845			
Aluminum Casing (@ 68°F) [15] [13]	.034	93	See Eq (p4)	164	5.3×10^{-5}	1218
Burster [16] [17]	.836	.48*	.347	101		

*Average k of mock HE explosives from Ref. 16.

**Properties of SAE 50 wt oil used as agent simulant for thermal properties according to Ref. 18.

Material Property Equations

(p1) For stainless steel, $k = 8.6 + .00045T$ (T in °F, k in BTU/ft hr °F).

(p2) For kaowool, $Cp = 0.2227 + 1.79 \times 10^{-5}T$ (T in °F, Cp in BTU/lb °F).

(p3) For aluminum, molar specific heat, $Cp = 4.94 + 2.96 T/1000$ (T in °K, Cp in cal/gmole °K).
Divide by 26.9 to get cal/g °K = BTU/lb °F.

(p4) For steel, molar specific heat, $Cp = 3.37 + 7.1 T/1000 + .43 \times 10^{-5}/T^2$ (T in °K, Cp in cal/gmole °K).
Divide by 55.8 to get cal/g °K = BTU/lb °F.

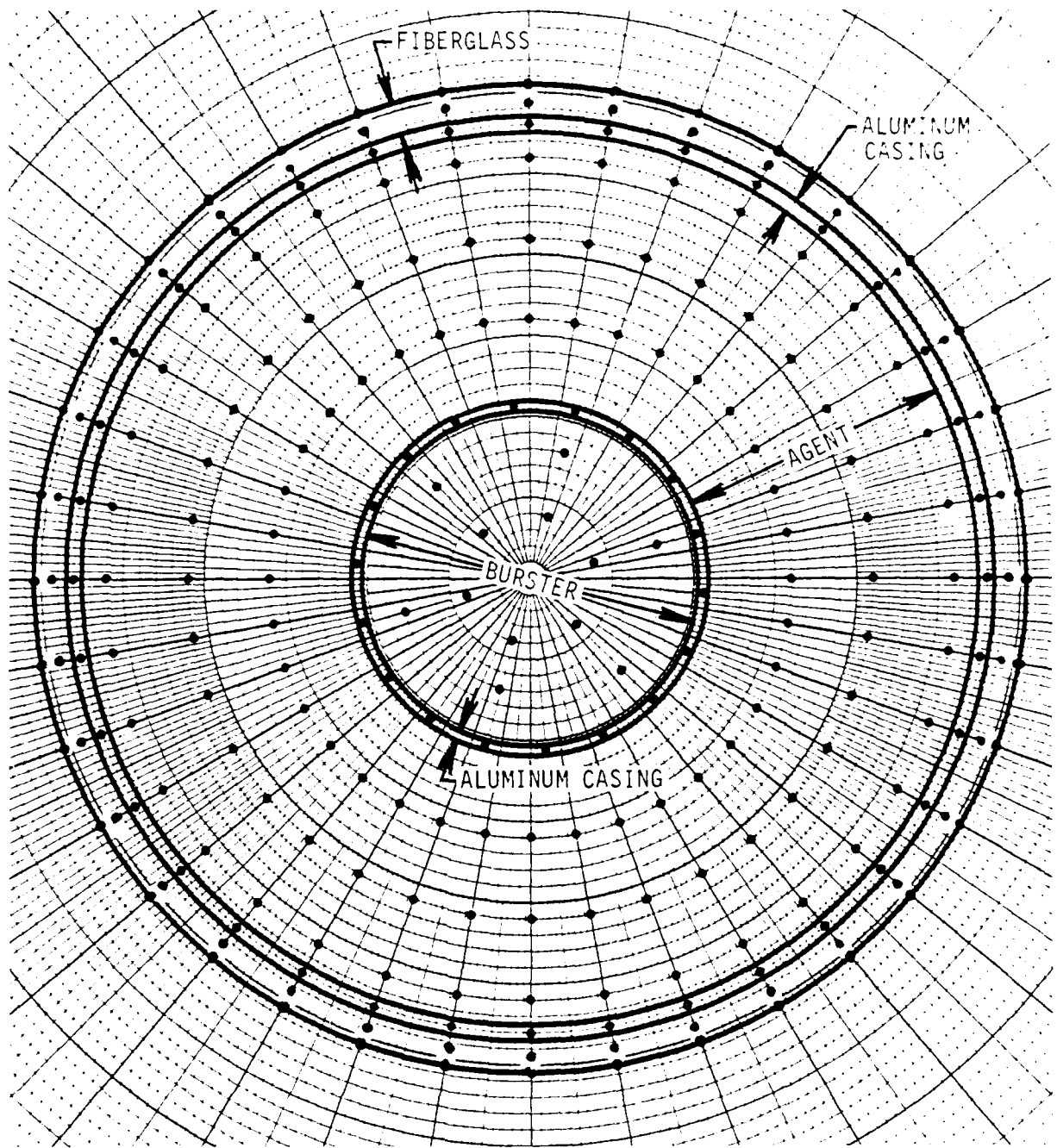


Figure 20. Node Locations for Two-Dimensional Computer Analysis of Agent Section

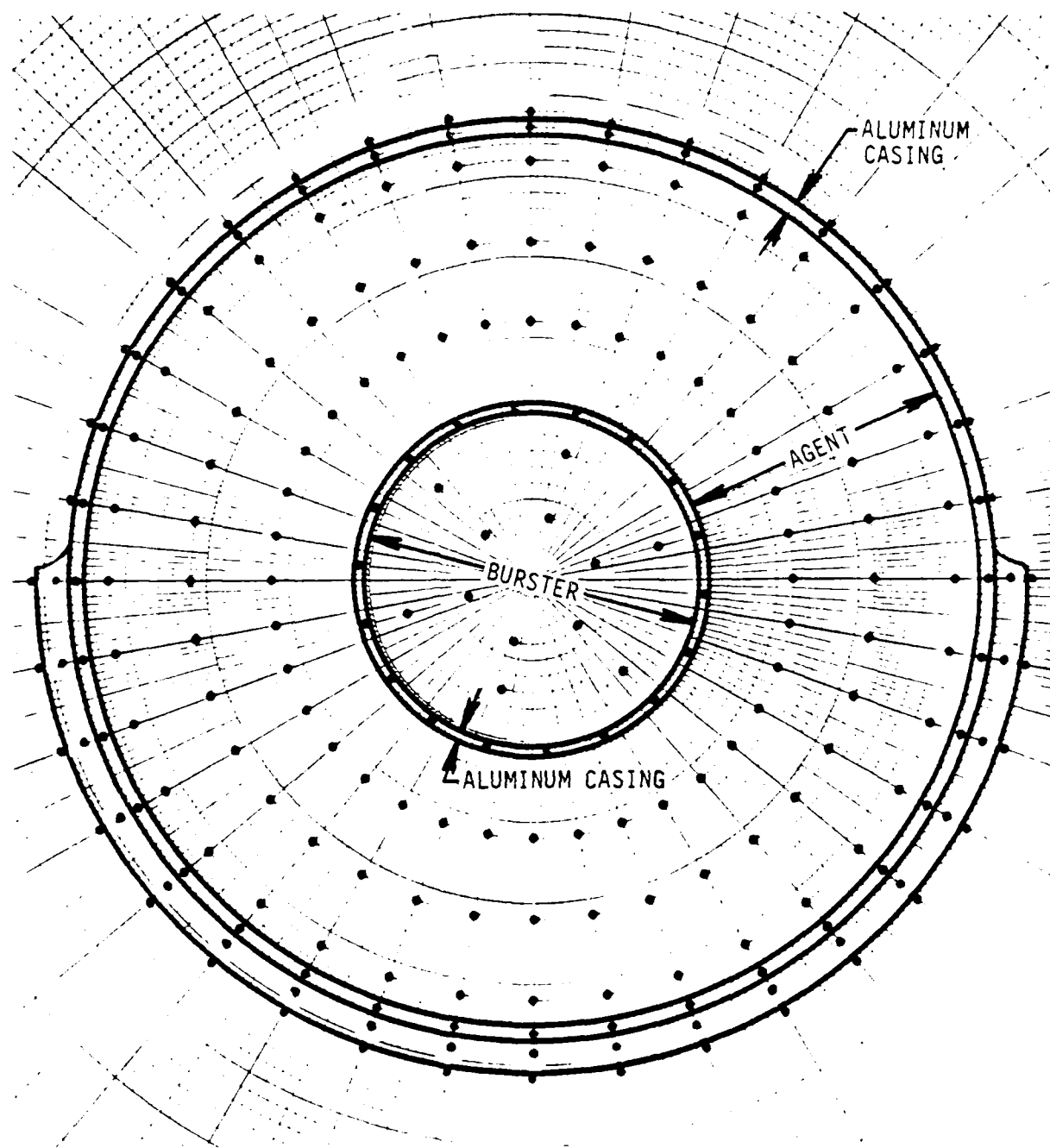


Figure 21. Node Locations for Two-Dimensional Computer Analysis of Agent Section

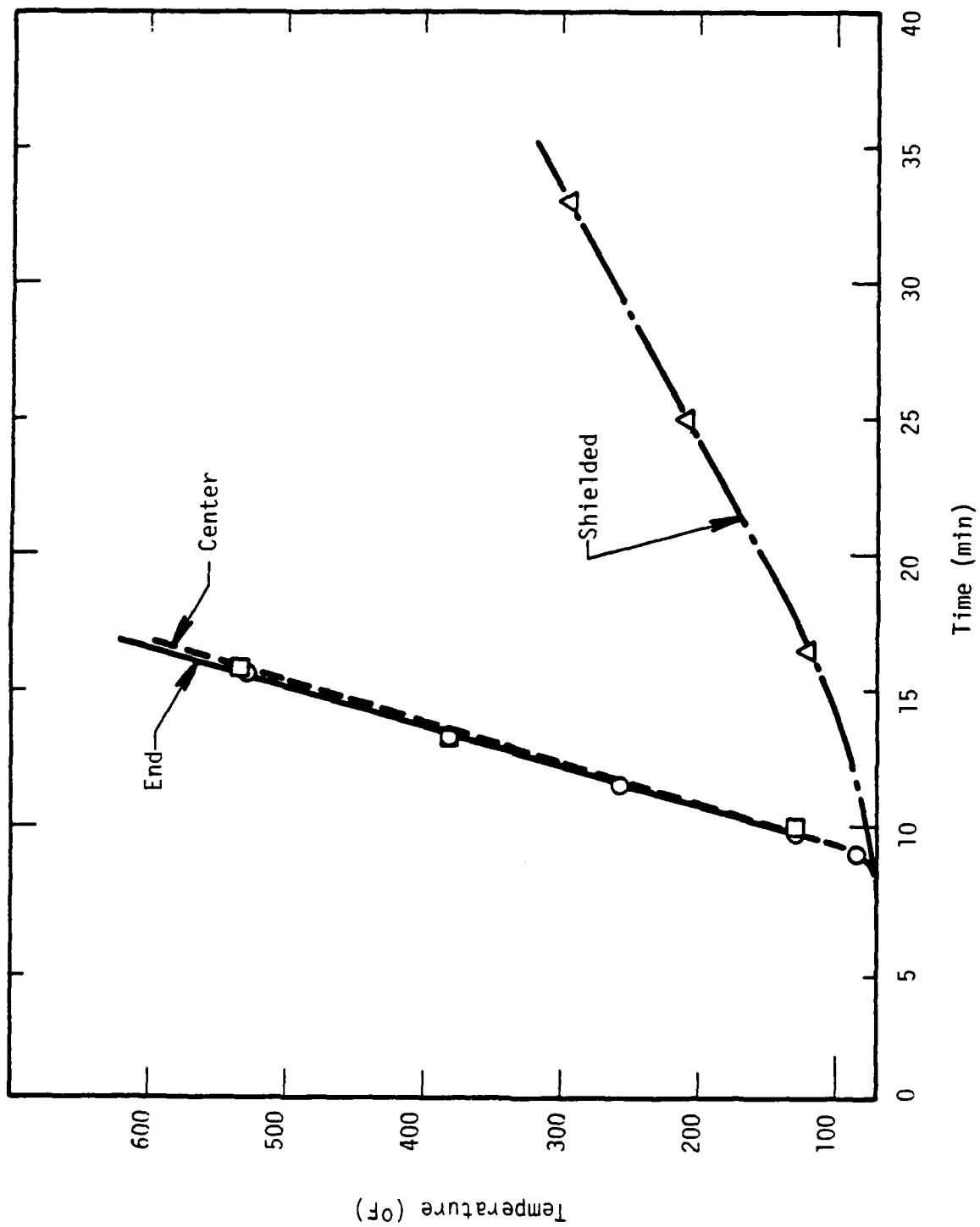


Figure 22. Temperature-Time Histories of Agent for Truck

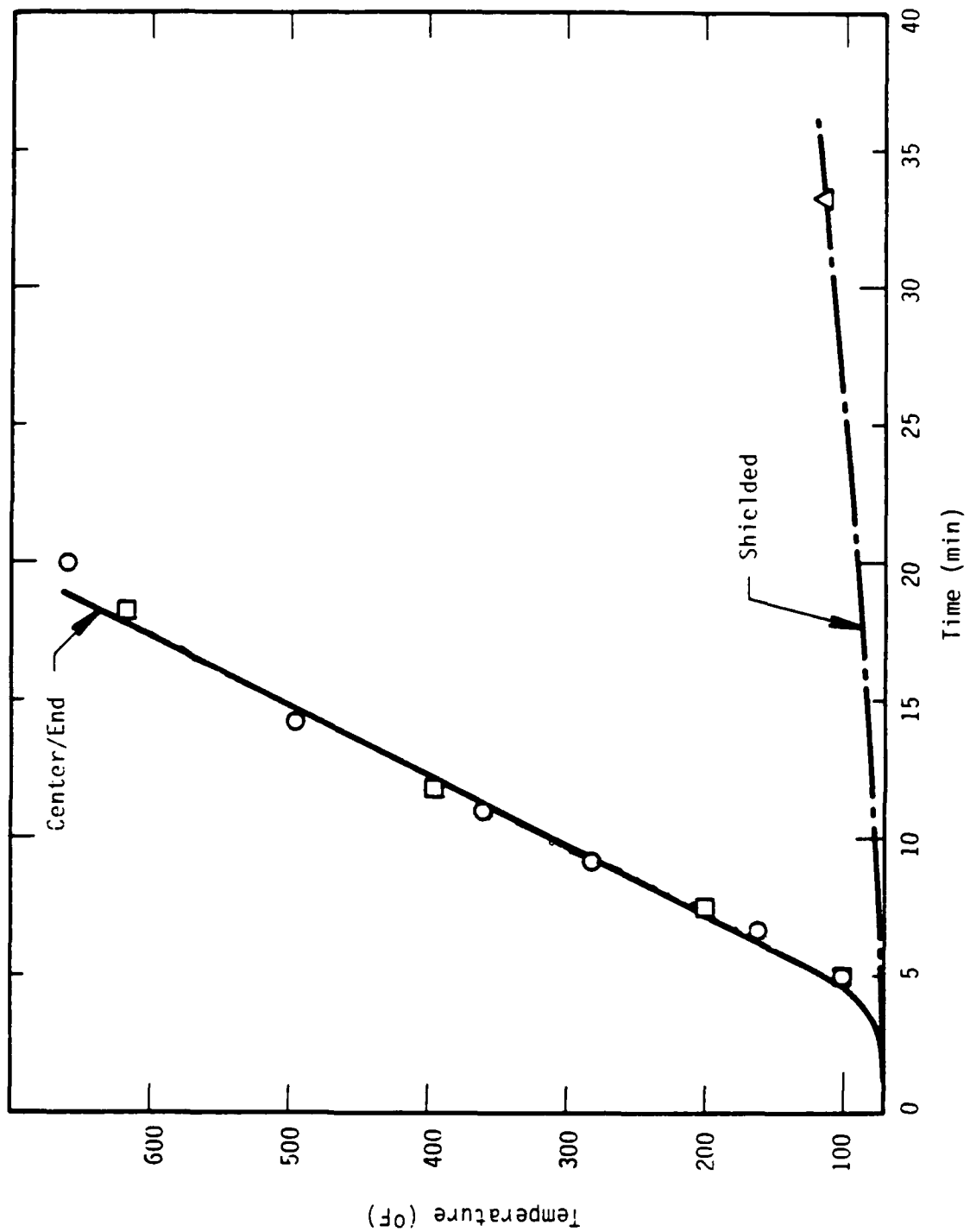


Figure 23. Temperature-Time Histories of Agent for Railcar

Table 9. Burster Properties

Material	Thickness (in)	Thermal Conductivity k (BTU/ft hr °F)	Specific Heat Cp (BTU/lb °F)	Density ρ (lb/ft ³)	Heat of Transition h _{sf} (BTU/lb)	Transition Temperature T _m (°F)
Fiberglass Shipping Case [14] (@ 1000°F)	.165	.02	.20	82		750
Airspace [15] for 800°F	1.06					
350		.01516	.2402	.0735		
620		.02142	.2438	.0489		
890		.02692	.2520	.0367		
		.03183	.2593	.0294		
Aluminum Casing (@ 680°F) [15] [13]	.465	93	See Eq (p3)	164	5.3 x 10 ⁻⁵	1218
Burster [16] [17]	.693	.48*	.347	101		

*Average k of mock HE explosives from Ref. 16.

Material Property Equations

- (p1) For stainless steel, $k = 8.6 + .00045T$ (T in °F, k in BTU/ft hr °F).
- (p2) For kaowool, $Cp = 0.2227 + 1.79 \times 10^{-5}T$ (T in °F, Cp in BTU/lb °F).
- (p3) For aluminum, molar specific heat, $Cp = 4.94 + 2.96 T/1000$ (T in °K, Cp in cal/gmole °K).
Divide by 26.9 to get cal/g °K = BTU/lb °F.
- (p4) For steel, molar specific heat, $Cp = 3.37 + 7.1 T/1000 + .43 \times 105/T^2$ (T in °K, Cp in cal/gmole °K).
Divide by 55.8 to get cal/g °K = BTU/lb °F.

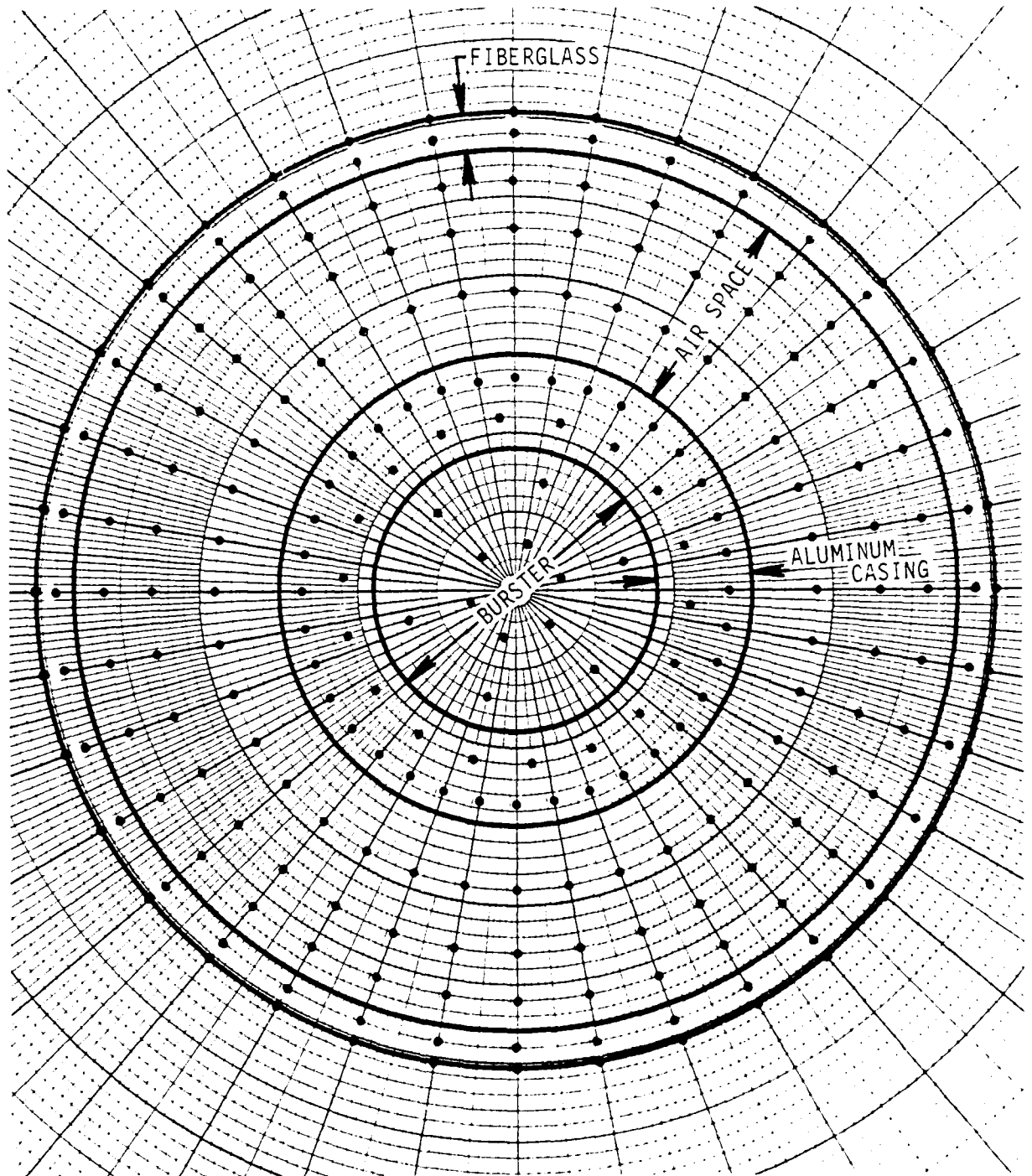


Figure 24. Node Locations for Two-Dimensional Computer Analysis of Burster Section

seconds of exposure to the radiant heat flux in the boxcar. The tube responded similarly in the truck, reaching flame temperature 30 seconds after the walls collapse. At melt-through of the fiberglass, the computer analysis was stopped and rerun from the point of melt-through with temperatures in the rocket initialized to their values at that time, but with transient thermal loads applied directly to the aluminum casing surrounding the burster (see Figure 25). Should the tube fail in some way other than complete burnoff and fully exposing the rocket to the incoming radiant heat flux, the insulative air gap between the tube and rocket will remain intact and significantly decrease the heat transfer to the burster section.

The transient, maximum temperature of the burster is shown in Figure 26 for a pallet of munitions in the truck and in Figure 27 inside the boxcar. The rate of temperature increase in the burster is greater than for any other energetic material. The burster in top center and top end pallet locations have near identical thermal responses, while the burster in shielded rockets heats more slowly because of the lower heat fluxes.

E. Comparison of Cross-Sectional Thermal Responses

Figures 28 and 29 compare the thermal response of the four cross-sections for both the truck and the railcar. There are small differences in the thermal response of the four energetic materials as a result of their different thermal properties and whether they are bounded by aluminum or steel.

Note in Figure 28 that for times less than 7 to 10 minutes (depending upon the cross-section of the rocket), the temperatures are higher for the railcar than the truck. This is because the truck is a better "insulator" until the plywood behind the aluminum walls burns away; then the rocket is exposed to the direct heat of the fire after which the temperature increases very rapidly. This effect is somewhat enhanced for the agent, Figure 29, because a bulk temperature is used for the agent.

For each scenario, shielded rockets show a drastically slower heating than rockets exposed to direct thermal radiation. Figures 30 and 31

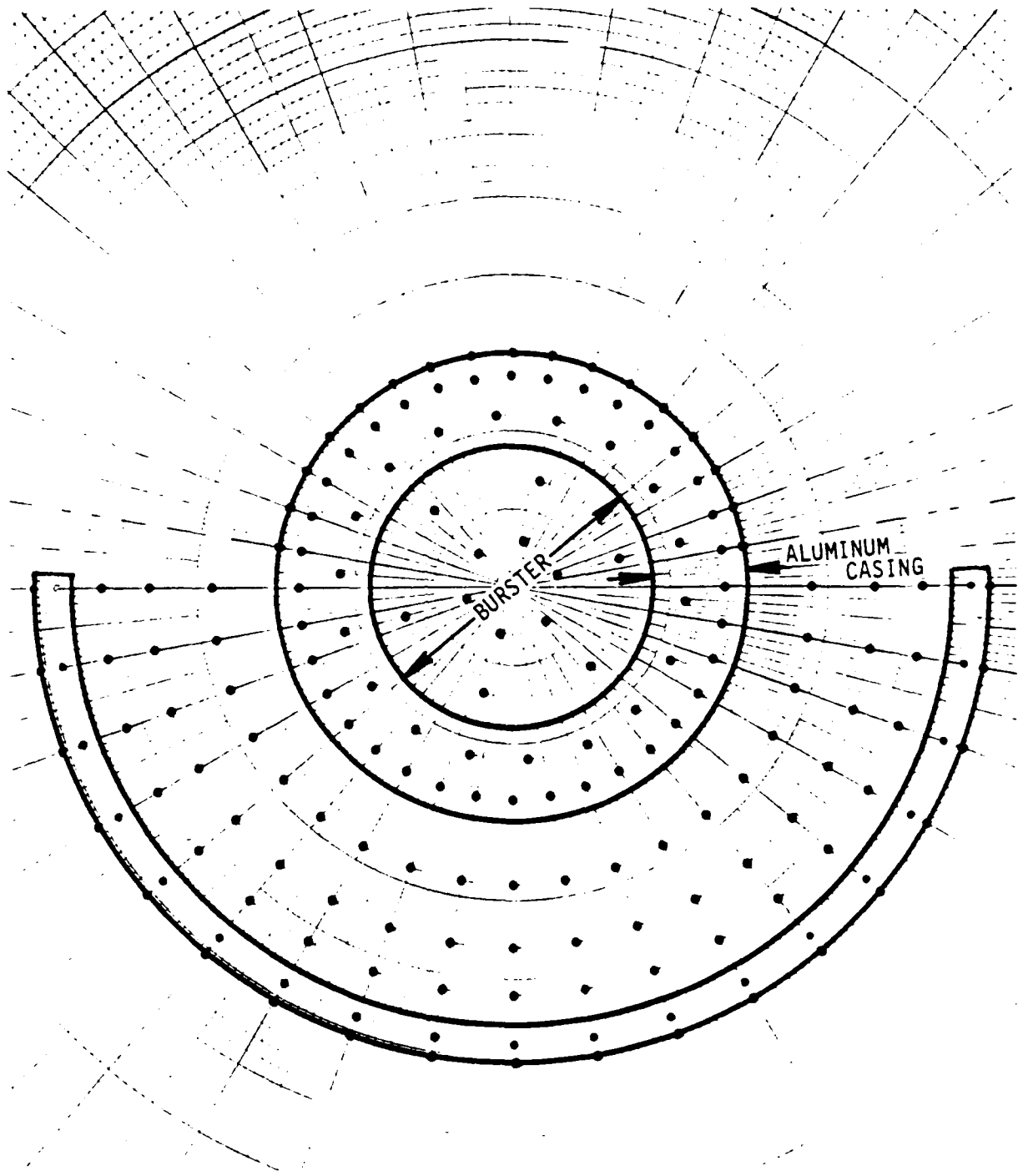


Figure 25. Node Locations for Two-Dimensional Computer Analysis of Burster Section

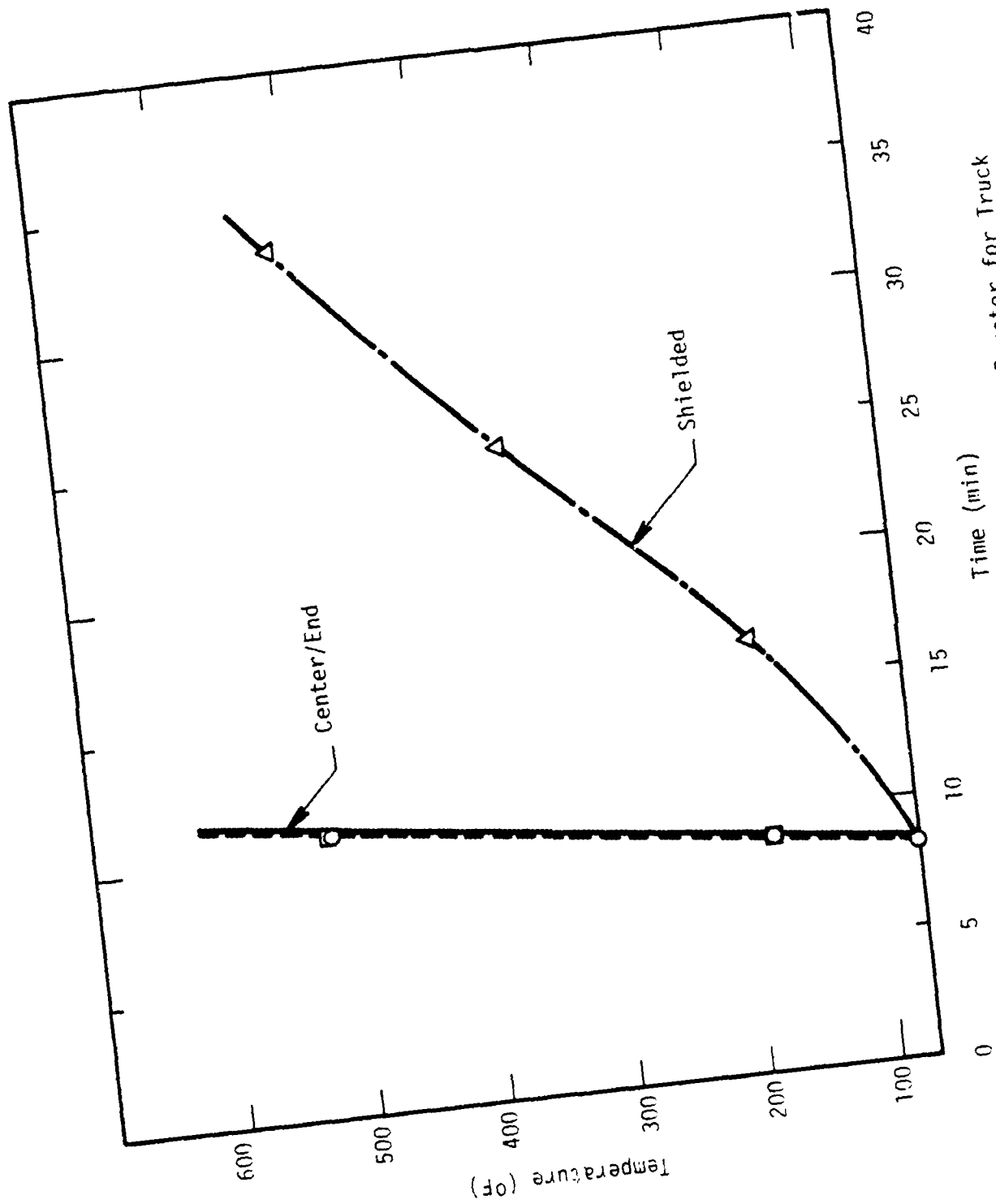


Figure 26. Temperature-Time History of Burster for Truck

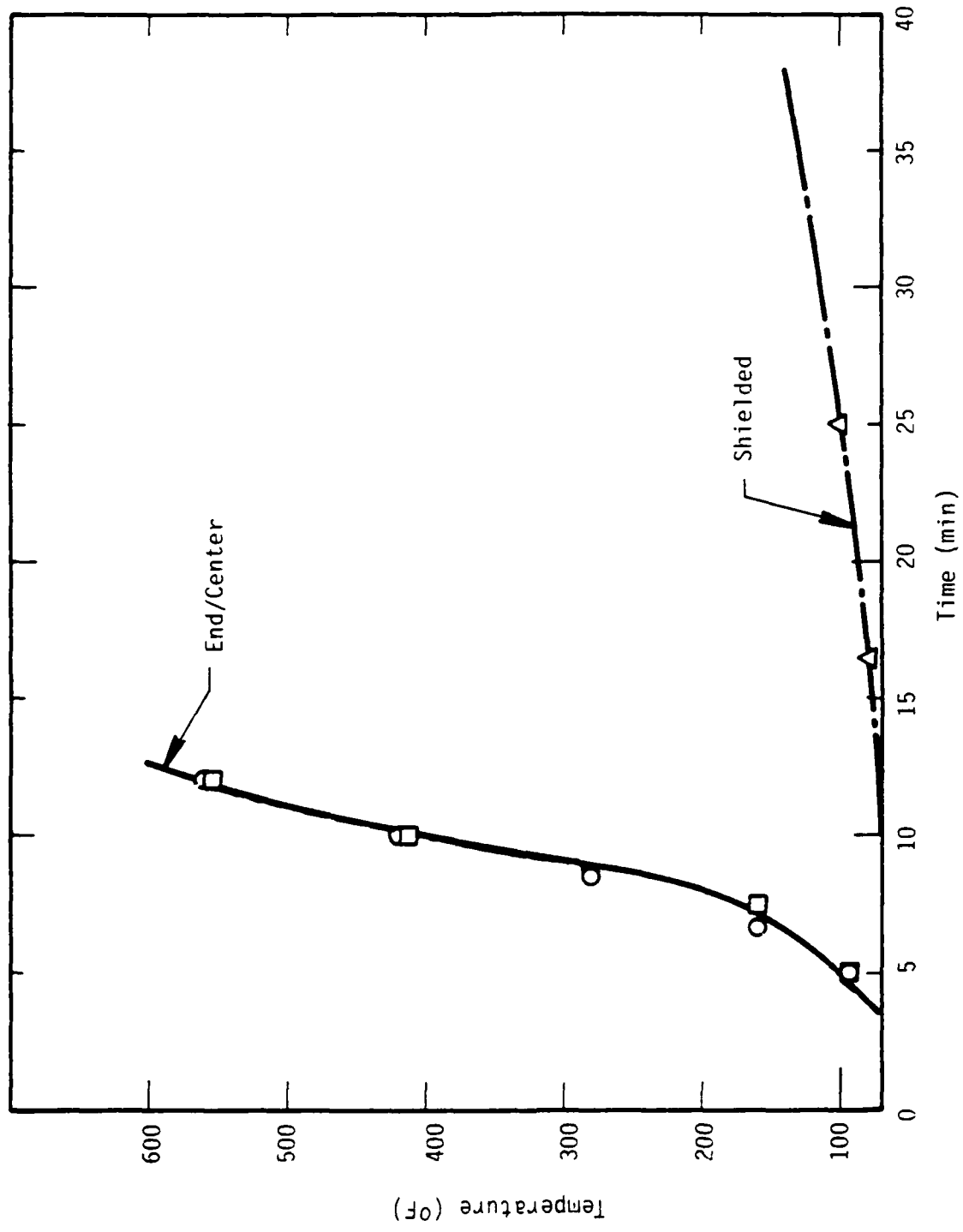


Figure 27. Temperature-Time Histories of Burster for Railcar

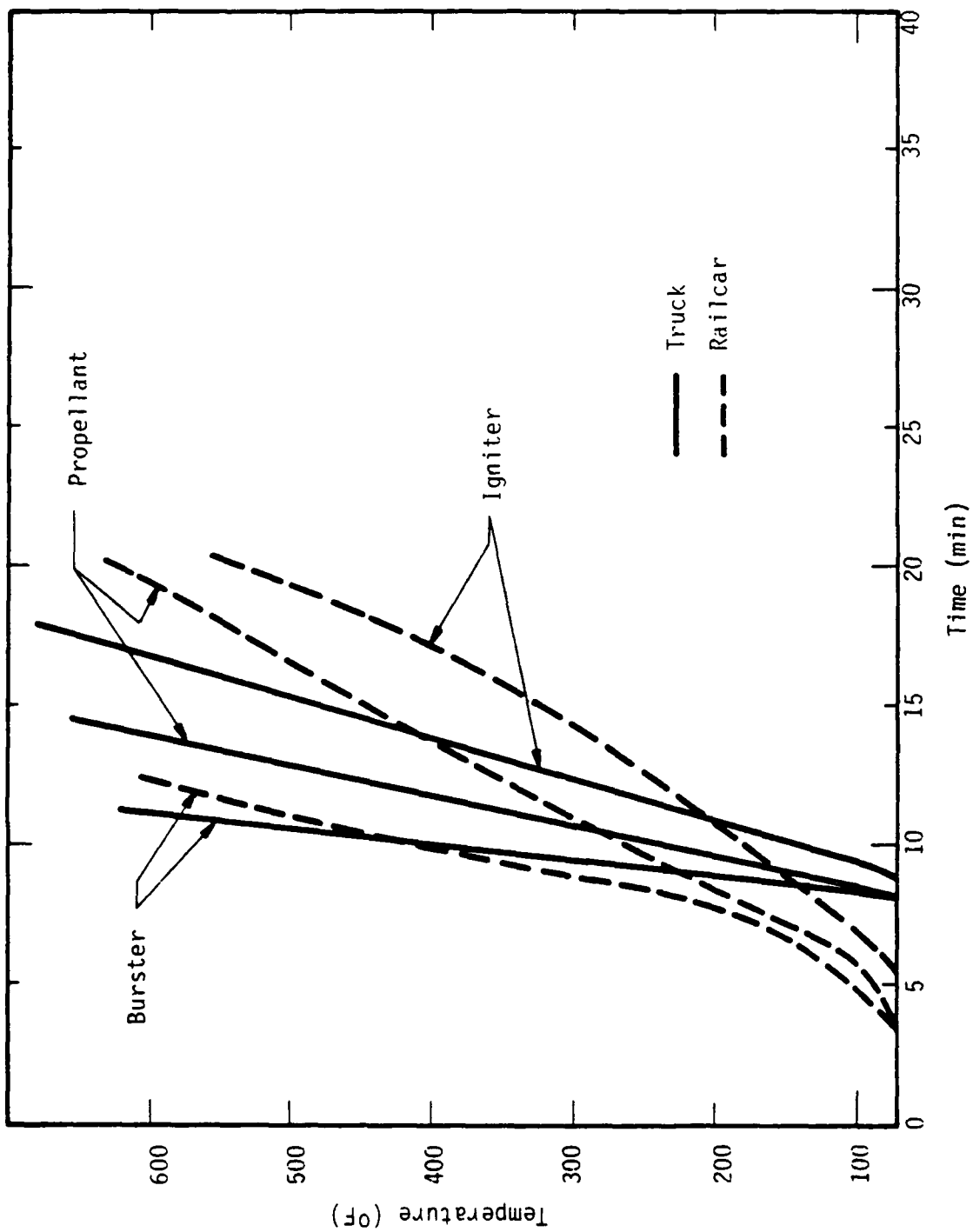


Figure 28. Comparison of Truck versus Railcar Thermal Response for Burster, Propellant and Igniter

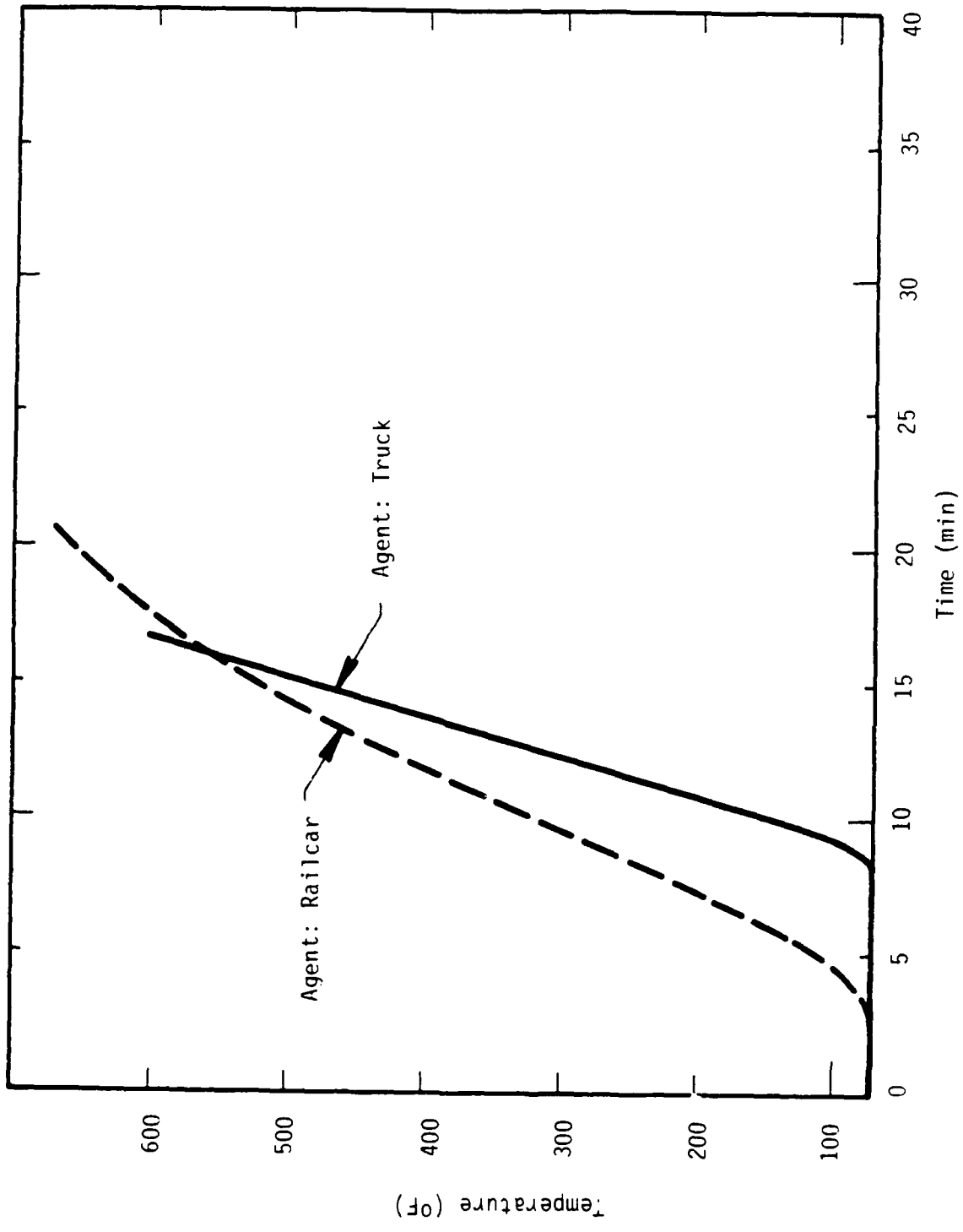


Figure 29. Comparison of Truck versus Railcar Thermal Response for Agent Section

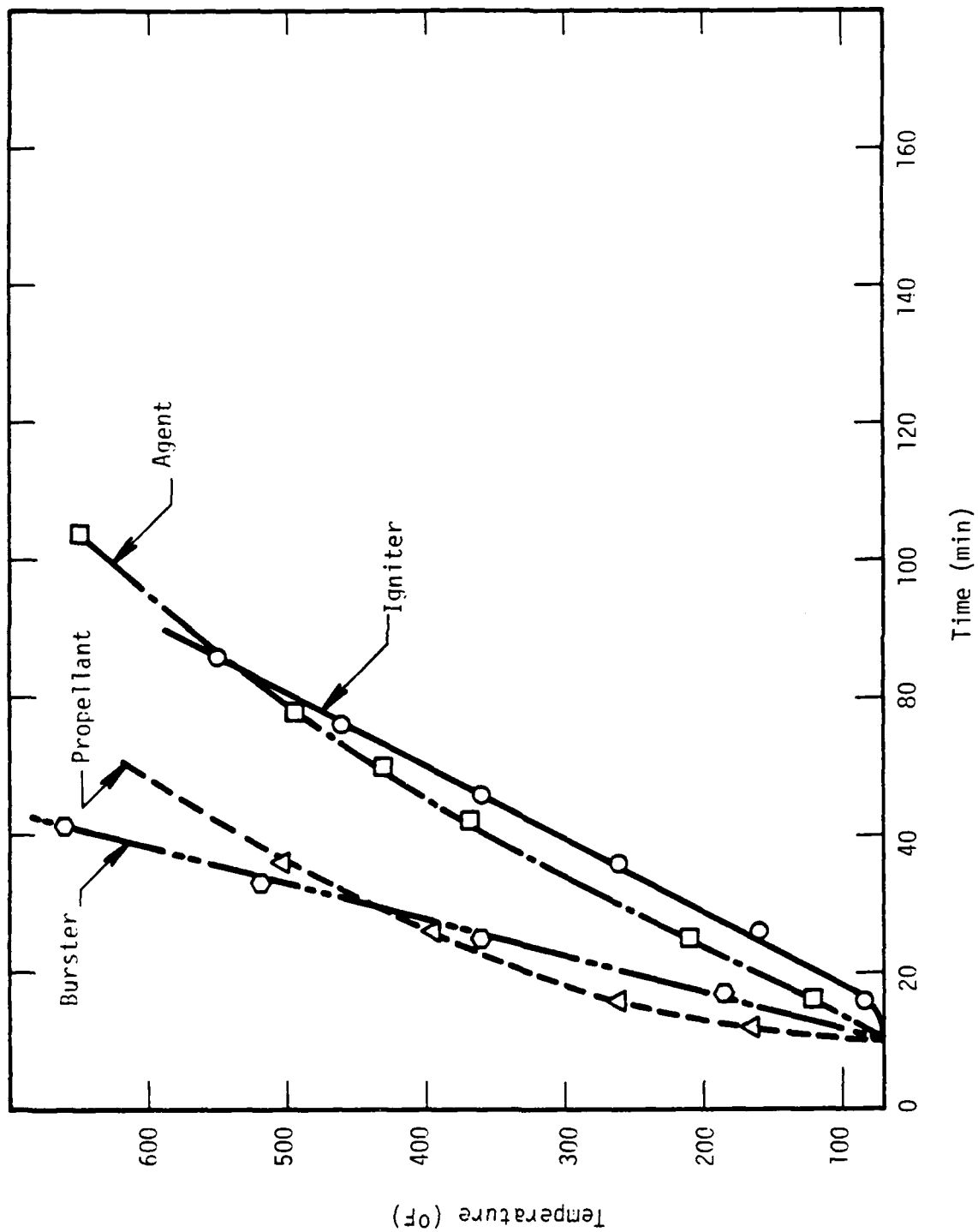


Figure 30. Comparison of Thermal Histories for the Energetic Materials - Shielded Rockets in Truck

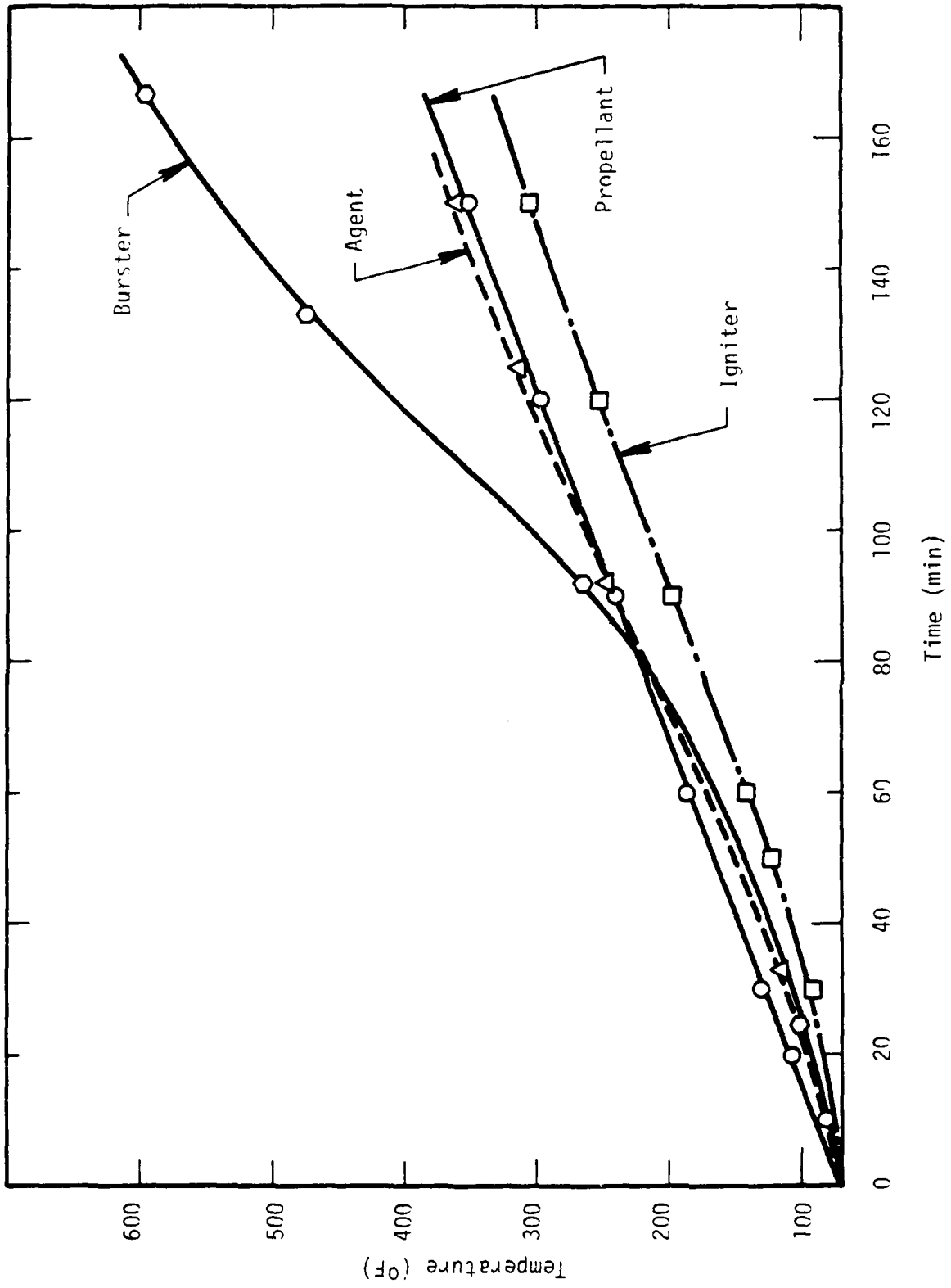
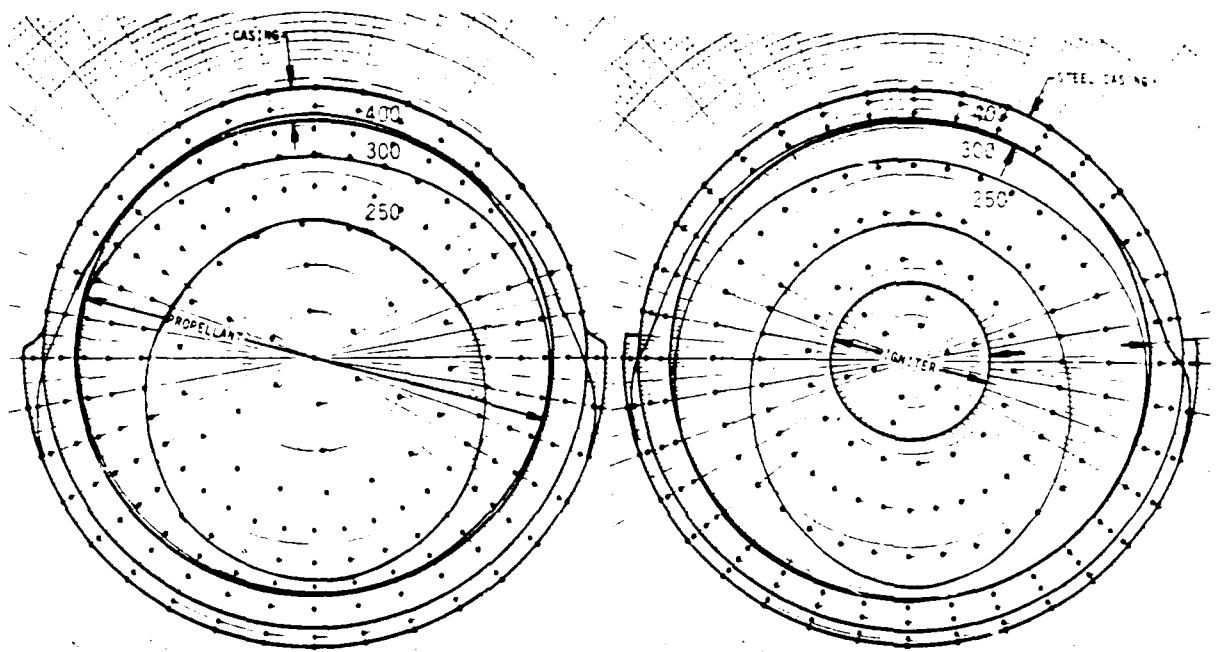


Figure 31. Comparison of Thermal Histories for the Energetic Materials - Shielded Rockets in Railcar

illustrate the response of materials in radiatively shielded rockets. Comparing these two graphs it is evident that the boxcar provides superior protection for the shielded rockets. In remaining intact during the fire, the boxcar's enclosure restricts convective flows and prevents direct exposure to the strong turbulent flows within the fire, and thus, less convective flux to the rockets.

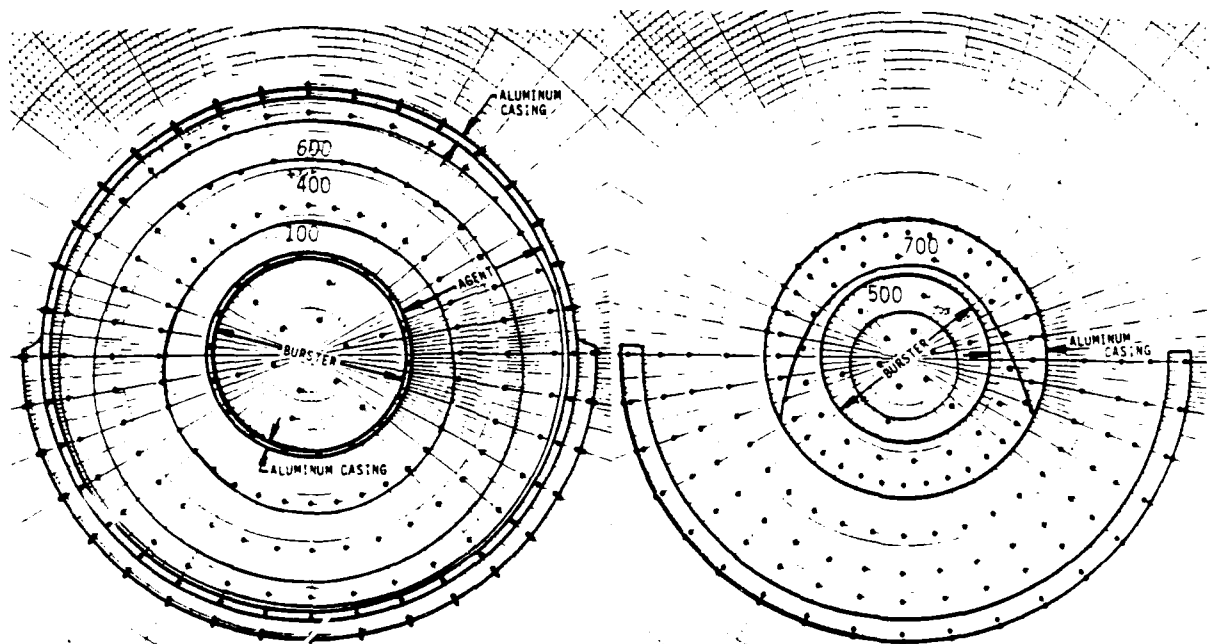
The burster section of the shielded rockets inside the boxcar shows an increase in the rate of heating after 50 minutes owing to the fact that the fiberglass shipping tube burns off at that time. The airgap in that section inhibits heat from leaving the fiberglass, so the tube eventually rises to its auto-ignition temperature. Other sections of the rocket retain the shipping tube since heat can be conducted into the underlying metal skin of the rocket.

The vastly different thermal response of the rocket between Figures 28-29 and Figures 30-31 result from the combination of two important factors. Firstly, the radiative flux is approximately an order of magnitude greater than the convective flux. Secondly, because the radiative flux intensity is sufficiently large to melt/burn the fiberglass shipping container, this flux after melt/burn of the fiberglass, is applied directly to the metal case of the rocket, increasing the rate of heat transfer to the interior of the rocket. This last effect is demonstrated in Figure 32 which shows temperature contours of the four cross-sections at the same instant in time. This graph depicts the spatial temperature distribution of the four rocket cross-sections inside the boxcar after 12 minutes of heating. The top portion of the fiberglass shipping tube has burned away for all four cross-sections. Contours are symmetrical with respect to the vertical axis within sections, but show stronger heat diffusion into the top half of the rocket resulting from the asymmetric heating. Note that the fiberglass does provide thermal protection--the lower portions of each cross section--due to its low thermal conductivity relative to metal. The large differences between Figures 30 and 31 result because of the higher convective flux from direct exposure to the fire (Figure 30) since the walls of the truck are consumed by the fire.



A. Propellant Section

B. Igniter Section



C. Agent Section

D. Burster Section

Figure 32. Temperature Contours After 12 Minutes Heating (Railcar)
(Top Center Pallet Position)

F. Failure Temperatures and Expected Times to Failure

M28 propellant found in the M55 rocket is composed of 59% nitrocellulose, 26% nitroglycerin, 9% triacetin, and 6% other compounds [24]. Auto-ignition temperatures of the major components, nitrocellulose and nitroglycerin, are reported in Reference 25 to be 472°F and 450°F respectively. As the auto-ignition temperature of the M55 propellant, burster, or igniter was not specified in any available references, all three materials were assumed to ignite at 450°F, i.e., the lowest auto-ignition temperature of one of the major active components of the M28 propellant. The effects of aging on this property are uncertain and were not considered further in this analysis.

A brief analysis of the temperatures required to burst the agent section is found in Appendix F. Under the applied heat load, the agent vaporizes and exerts a pressure on the thermally weakened aluminum casing, which eventually fails. The analysis follows a three step procedure: 1) the ultimate tensile strength of the aluminum is estimated for the casing temperature at the time of failure; 2) the maximum internal pressure required to rupture a thin walled cylinder of that strength is found; and 3) the temperature of saturated steam (assumed representative of the agent) that produces that pressure is determined. An iterative procedure was used to determine the temperature of the agent such that its vapor pressure was sufficiently high to rupture the thermally weakened aluminum shell.

Results show the ultimate strength of the aluminum casing is reduced to about 22 percent of its original strength by the heating, when the agent temperature reaches 439°F producing an internal pressure of 378 psi which will fail the casing. [It is recognized that saturated steam may not be representative of the vapor pressure of the agent. No information could be found on specific properties of the agent. Oil is used to simulate agent for thermal (heat capacity) effects. Recognizing that the agent properties are not really known, and that any assumption could be suspect, the authors chose saturated steam for vapor pressure calculations because of the availability of these numbers and to assert that the true properties are unknown.]

The critical temperatures of the M55 rocket energetic materials are: propellant - 450°F, igniter - 450°F, agent - 439°F, burster - 450°F. These numbers are engineering estimates based on assumptions discussed in the preceding paragraphs. However, if temperatures other than the ones used are determined to be more appropriate as "failure criteria," then the figures in this report can be used to estimate a "revised" time to failure.

Combining the transient temperature results of the energetic materials with the critical temperatures just discussed permits an estimation of the time to failure. Table 10A summarizes the findings for the rocket sections exposed to direct thermal radiation. The burster section is expected to ignite first, at 10.5 minutes into the heating in both the truck and railcar.

Table 10. Time To Failure

A. Rocket Sections Receiving Thermal Radiation

<u>Material</u>	<u>Pallet Location</u>	<u>Time To Failure (Min)</u>	
		<u>Truck</u>	<u>Boxcar</u>
Propellant	Top Center	12.2	16.0
	Top End	12.2	16.0
Igniter	Top Center	14.5	18.3
	Top End	14.5	18.3
Agent	Top Center	13.3	12.0
	Top End	13.3	12.0
Burster	Top Center	10.5	10.5
		10.5	10.5

B. Rocket Sections with Convective Heating Only

<u>Material</u>	<u>Pallet Location</u>	<u>Time To Failure (Min)</u>	
		<u>Truck</u>	<u>Boxcar</u>
Propellant	Shielded	30.	200.
Igniter	Shielded	55.	230.
Agent	Shielded	43.	164.
Burster	Shielded	30.	129.

For the first few minutes of the fuel fire, the truck is a better insulator than the railcar by virtue of the thermal protection of the plywood. However, the higher heat fluxes after melt and burn-through of the truck wall result in high heating rates of the rocket sections for the truck scenario, as compared to the railcar, after the first several minutes of fire exposure. This is evident in Figures 28 through 31. Only for the agent section does the "time to failure" occur slightly sooner in the railcar than the truck.

The rockets shielded from direct radiative fluxes take considerably longer to fail, Table 10B. The railcar provides considerably more protection than the truck since the confinement of an enclosure has the effect of stagnating the convective flux, resulting in a lower convective heat transfer coefficient.

IV. CONCLUSIONS

This report determined the thermal response of M55 rockets stacked in pallets and loaded inside one of three transport carriers engulfed in a fuel fire. The carriers considered were a standard trailer truck, a standard boxcar, and a CAMPACT on a flatcar. Two transient heat transfer computer programs were used in evaluating the accident scenario. A one-dimensional analysis was used to calculate the transient heating of the carrier walls and the thermal environment created inside the carriers. A two-dimensional analysis then was used to determine the transient temperatures of the M55 rockets exposed to these environments.

The rockets were analyzed at four cross-sectional locations to examine the thermal response of the differing energetic materials in the rocket: propellant, igniter, agent, and burster. Failure of the rockets was determined from an "auto-ignition" temperatures of the propellant, igniter and burster; or the failure of the thermally weakened aluminum case from thermally induced vapor pressures of the agent. For the truck or the railcar, failure times showed a strong dependence on rocket location in the pallet. Those rockets completely shielded from thermal radiation (i.e., those rockets receiving only convective heat flux), could survive the fire environments for 30 to 230 minutes, depending upon the carrier and rocket cross-section. More significant, rockets in either the truck or the boxcar failed in approximately 11 to 16 minutes if exposed to thermal radiation. In the case of the truck, the fire rather rapidly melts the aluminum skin and then burns the plywood (6.5 minutes); thus the thermal radiation to the rockets is directly from the fire. The boxcar walls, constructed of steel, do not melt, but heat rapidly to temperatures of the order of the fire temperature. The analysis of all four cross sections of the rocket shows that failure would occur at approximately the same time. Since the failure times are about the same, this would imply that the failure of an M55 rocket in a fire could occur at any of the cross-sectional areas depending on the relative intensities of the heating along the axial length of the rocket. This conclusion has been observed experimentally [7].

The vastly different "times to failure" between the shielded and unshielded rockets show that the driving heat transfer mechanism to the rockets is radiation from the carrier wall (boxcar) or directly from the fire (the truck). Thermal shielding of the rockets, as for those near the pallet center, shows a dramatic increase in the time required to fail. Fireproofing and insulating the walls of the truck or railcar, which may be done in a variety of ways, would significantly improve the transported rocket's thermal resistance to an accidental fuel fire. This is reinforced by the analysis of the CAMPACT shipping container, which showed that the temperatures in the interior of the CAMPACT had not increased substantially after four hours of fire exposure.

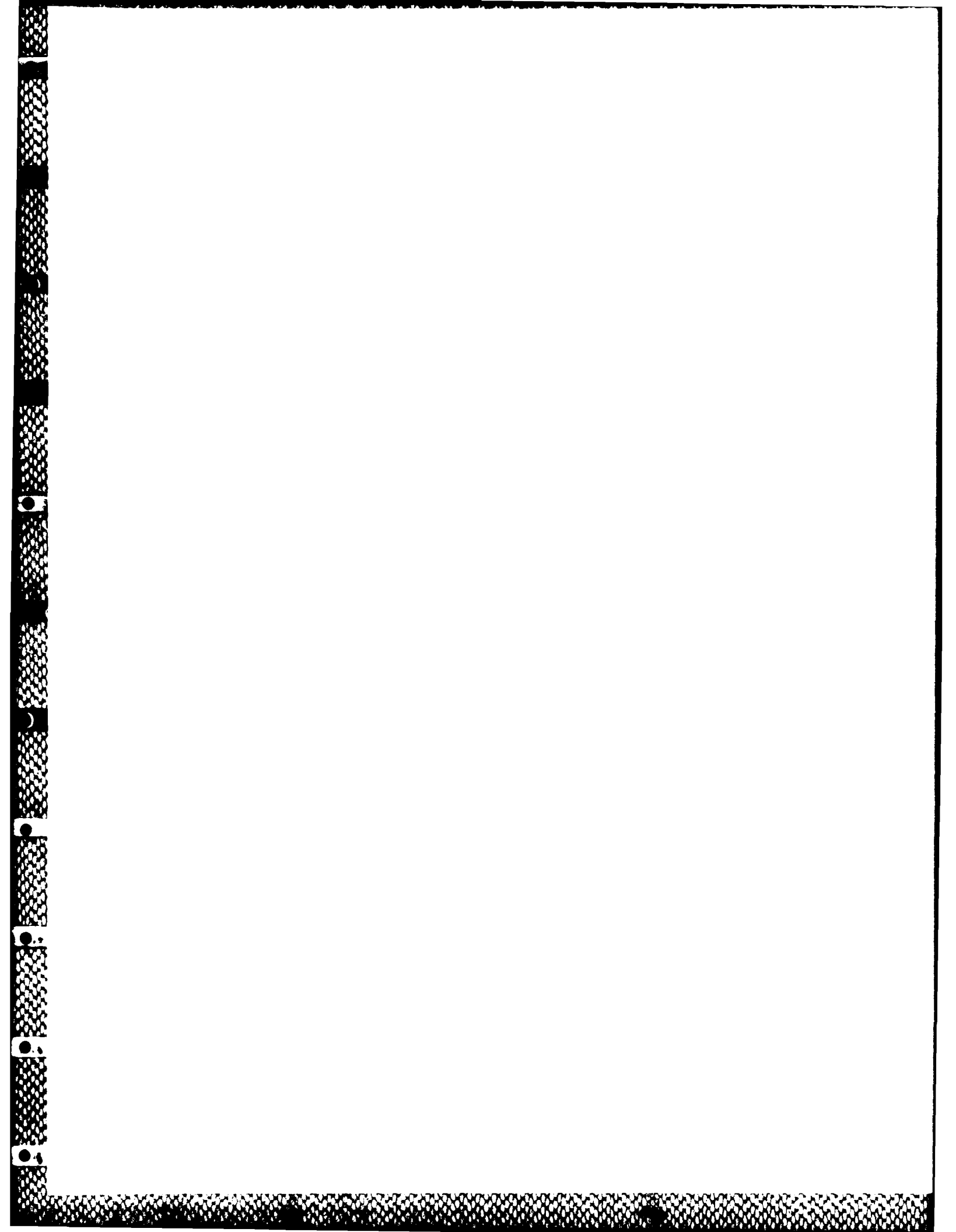
V. REFERENCES

1. Whitney, M. G., Friesenhahn, G. J., Baker, W. E., and Vargas, L.M., "A Manual to Predict Blast and Fragment Loadings From Accidental Explosions of Chemical Munitions Inside an Explosion Containment Structure," Final Report for Contract No. DACA87-81-C-0099, SwRI prepared for U. S. Army Toxic and Hazardous Materials Agency and U. S. Army Corps of Engineers, Huntsville Division, April 1983.
2. Whitney, M. G., Ketchum, D. E., and Moseley Bowles, P. L., "ECR Pressure-Temperature Analysis," SwRI Final Report No. 7918, Prepared for The Ralph M. Parsons Co., March 1984.
3. Ketchum, D. E., and Anderson, C. E., "Thermal Response of an M55 Rocket to the Detonation and Burning of a Second Rocket," SwRI Final Report No. 8069/202, Prepared for U. S. Army Corps of Engineers, Huntsville Division, August 1984.
4. Whitney, M., Ketchum, D. and Bowles, T., "Blast Closure System Evaluation," SwRI Final Report No. 8069/203, Prepared for U. S. Army Corps of Engineers, Huntsville Division, September 1984.
5. Clarke, R. K., Foley, J. T., Hartman, W. F., and Larson, D. W., "Severities of Transportation Accidents Volume III - Motor Carriers," Sandia Laboratories Report No. SLA-74-001, July 1976.
6. Clarke, R. K., Foley, J. T., Hartman, W. F., Larson, D. W., "Severities of Transportation Accidents Volume IV - Train, Sandia Laboratories Report No. SLA-74-0001, September 1976.
7. Personal communication with Dr. W. R. Rhyne, H&R Technical Associates, Inc., Oakridge, TN.
8. Gabrielson, V. K., Grange, B. W., Christian, K. D., "ONEDIM - A Computer Code For Solving One-Dimensional Nonlinear Heat Transfer Problems," Sandia Laboratories Report No. SCL-DR-69-99, February 1970.
9. Smith, J. P., "SINDA User's Manual," Lockheed Engineering and Management Services Co., Inc., Contract NAS9-15800, March 1983.
10. Thomas, P. H., "The Size of Flames from Natural Fires," Ninth Symposium on Combustion, Academic Press, NY 1963.
11. Welty, J. R., Engineering Heat Transfer, John Wiley & Sons, New York, 1974.
12. Hamilton, D. C., Morgan, W. R., "Radiant-Interchange Configuration Factors," National Advisory Committee for Aeronautics, Technical Note 2836, 1952.

13. Anderson, C. E. and Ketchum, D. E., "Heat Transfer Considerations For Selective Failure of a Solid Rocket Motor Case using Thermite," SwRI Report No. 7958/802, prepared for Naval Surface Weapons Center.
14. Malloy, J. F., Thermal Insulation, Insulation Distributor - Contractors National Association, Van Nostrand-Reinhold.
15. Karlekar, B. V., Desmond, R. M., Engineering Heat Transfer, West Publishing Co., St. Paul, 1977.
16. Dobratz, B. M., LLNL Explosives Handbook. Properties of Chemical Explosives and Explosive Stimulants, Lawrence Livermore National Laboratory, Livermore, CA, March 1981.
17. CPIA/M2 Solid Propellant Manual, Johns Hopkins University, Applied Physics Laboratory, Johns Hopkins Road, Laurel, MD 20810, March 1979.
18. Darling, B. W., 115mm Sensitivity Tests, AEO Project T-222. Chemical Demil Project No. 200, Tooele Army Depot, April 1974.
19. N.F.P.A. Inspection Manual, 60 Battery March St., Boston 10, Mass., 1959.
20. Nelson, W. L., Petroleum Refinery Engineering, 4th Ed., McGraw-Hill Book Co., NY.
21. Personal Communication with Dr. A. Grand, Dept. of Fire Technology, SwRI.
22. Rosato, D., Grove, C., Filament Winding, John Wiley & Sons, Inc., New York, 1964.
23. Eckert and Drake, Analysis of Heat and Mass Transfer, McGraw-Hill Book Co., New York, 1972.
24. CPIA/MI Rocket Motor Manual, MIL-P-60071A(1), Chemical Propulsion Information Agency, Laurel, Maryland, 1979.
25. Engineering Design Handbook, Properties of Explosives of Military Interest, AMCP-706-177, U.S. Army Materiel Command, January 1971.

APPENDIX A - LIST OF COMPUTER RUNS

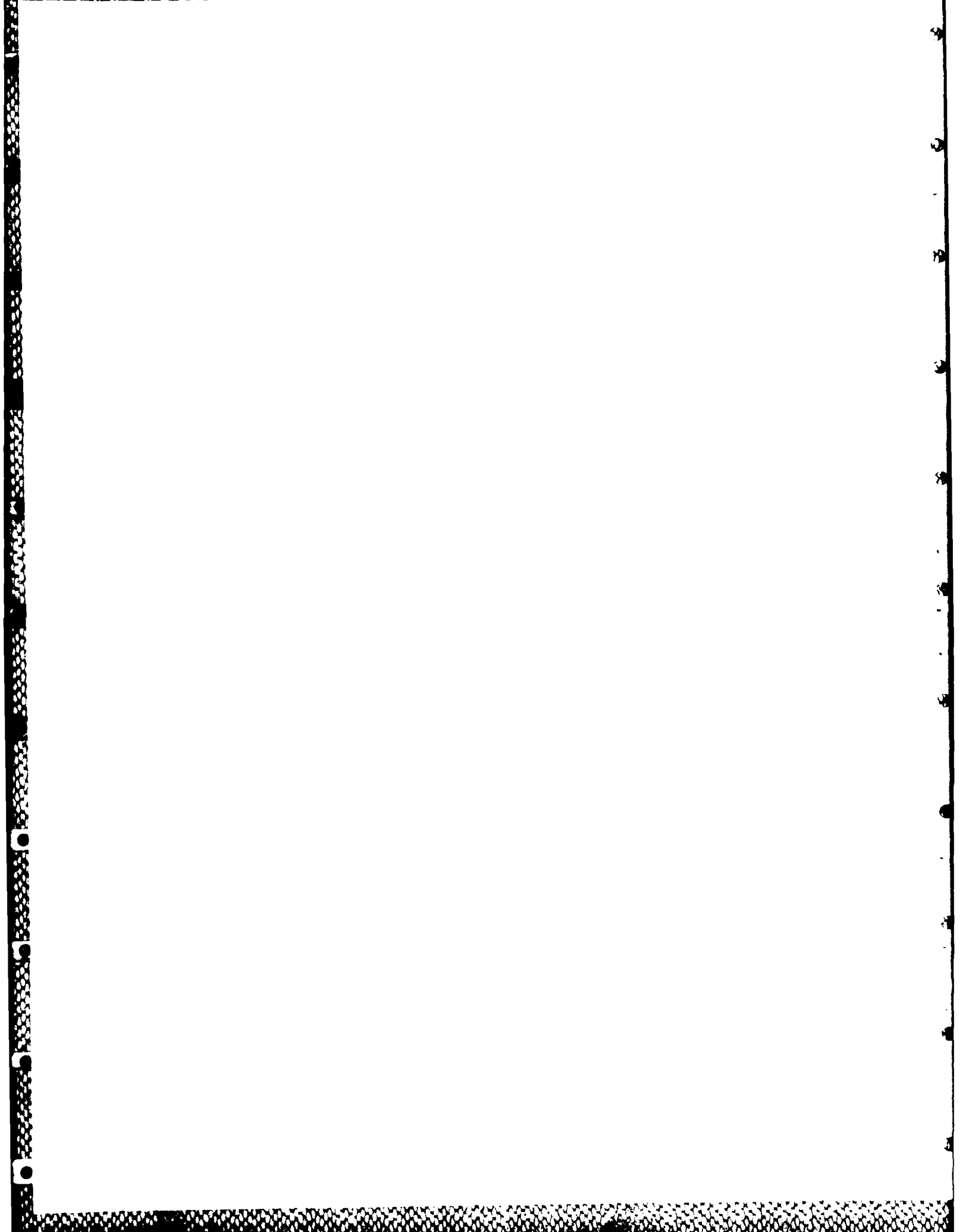
RUN NO. -----	CODE -----	DESCRIPTION -----
1 - 3	ONEDIM	TRANSIENT, 1D ANALYSES OF CARRIER (TRUCK, RAILCAR, AND CAMPACT) THERMAL RESPONSE TO FIRE. CONSTANT TEMPERATURE BLACKBODY RADIATION ON THE FRONT SURFACE IS ASSUMED AS THE LOADING CONDITION. CONVECTION AND RADIATION ARE DETERMINED OFF THE BACKFACE THROUGH AN AIR GAP TO A FIBERGLASS LAYER. MELTING AND VARIABLE MATERIAL PROPERTIES ARE USED WHENEVER DATA IS AVAILABLE. THE TRANSIENT BACKFACE AND GAP TEMPERATURES, TRANSIENT CONVECTIVE HEAT TRANSFER COEFFICIENT, AND TEMPERATURES THROUGHOUT THE CARRIER ARE DETERMINED.
4 - 7	ONEDIM	TRANSIENT, 1D THERMAL RESPONSE OF THE ROCKET SECTIONS TO CONVECTION WITHIN THE TRUCK.
8 - 11	SINDA	TRANSIENT, 2D THERMAL RESPONSE OF THE FOUR ROCKET SECTIONS TO CONVECTION IN THE TRUCK. THE OBJECTIVE OF THESE COMPUTER RUNS (4-11) IS TO ASSURE THE VALIDITY OF SINDA BY COMPARISON OF THERMAL RESPONSES WITH ONEDIM. TESTS 4 - 33 USE TRANSIENT LOAD CONDITIONS DETERMINED IN RUNS 1-3 AS INPUT.
12, 13	ONEDIM	ONE DIMENSIONAL STUDY OF END EFFECTS (AXIAL HEATING). NOSE AND TAIL SECTIONS ARE MODELED, WITH THEIR THERMAL RESPONSE TO AN APPLIED LOAD COMPARED TO CROSS-SECTIONAL RESPONSES TO THE SAME LOADS.
14-17	SINDA	PROPELLANT SECTION RESPONSE TO THE THERMAL ENVIRONMENT INSIDE THE TRUCK AND RAILCAR ARE DETERMINED. TOP CENTER AND TOP END ROCKET/PALLET POSITIONS ARE CONSIDERED. TRANSIENT, 2D TEMPERATURE RESPONSE TO THE ASSYMETRIC HEATING IS REPORTED.
18-21	SINDA	IGNITER SECTION RESPONSE TO THE THERMAL ENVIRONMENT INSIDE THE TRUCK AND RAILCAR ARE DETERMINED. TOP CENTER AND TOP END ROCKET/PALLET POSITIONS ARE CONSIDERED. TRANSIENT, 2D TEMPERATURE RESPONSE TO THE ASSYMETRIC HEATING IS REPORTED.
22-25	SINDA	AGENT SECTION RESPONSE TO THE THERMAL ENVIRONMENT INSIDE THE TRUCK AND RAILCAR ARE DETERMINED. TOP CENTER AND TOP END ROCKET/PALLET POSITIONS ARE CONSIDERED. TRANSIENT, 2D TEMPERATURE RESPONSE TO THE ASSYMETRIC HEATING IS REPORTED.
26-29	SINDA	BURSTER SECTION RESPONSE TO THE THERMAL ENVIRONMENT INSIDE THE TRUCK AND RAILCAR ARE DETERMINED. TOP CENTER AND TOP END ROCKET/PALLET POSITIONS ARE CONSIDERED. TRANSIENT, 2D TEMPERATURE RESPONSE TO THE ASSYMETRIC HEATING IS REPORTED.
30-33	ONEDIM	TRANSIENT, 1D ANALYSIS OF THE THERMAL RESPONSE OF THE FOUR ROCKET SECTIONS TO CONVECTIVE HEAT TRANSFER INSIDE THE RAILCAR.



APPENDIX B - ANALYTICAL TOOLS

Two computer programs were used in the analysis, ONEDIM and SINDA. ONEDIM is a general one-dimensional heat transfer code developed at Sandia Laboratories, Livermore. Reference 8 verifies the accuracy of the code with several detailed comparisons of computer results to closed-form, analytical solutions and experimental data. ONEDIM can solve transient and steady-state heat transfer problems for composite structures that can be modeled as slabs, cylinders, or spheres. Special features include variable material properties with phase changes, plus radiation and convection options at the surface. One-dimensional computations were used to assist in the definition of the thermal environment in the interior of the differing transport carriers, i.e., the interaction of the fire with the walls of the transport carrier and the heating of the inside of the container. Also, if the walls of the carrier melt, then the time to melt-through is established, after which the pallet is exposed directly to the radiation from the fire.

The rocket has been analyzed as a series of concentric rings of different material. As the rocket has an asymmetric thermal load applied to its surface because of radiation shadowing by the pallet and other rockets, a two-dimensional heat transfer code is required for the analysis. SINDA (the Systems Improved Numerical Differencing Analyzer [9]), was used for the analysis of thermal response of the M55 rockets. SINDA is a software system developed by NASA for solving problems governed by diffusion-type equations such as the heat equation. SINDA is most widely used as a general thermal analyzer with thermal resistance-heat capacitance network representations, but may be adapted to a wide range of problems represented by parabolic differential equations. In solving thermal analysis problems, SINDA can handle such interrelated complex phenomena as phase changes, including sublimation, diffuse radiation within enclosures, transport delay effects, sensitivity analysis, and thermal network error correction.



APPENDIX C - CALCULATION OF CONVECTIVE HEAT TRANSFER COEFFICIENTS

Natural convection inside of the carriers increases as the walls heat. For a specific fluid, in this case air, it is possible to define the convective heat transfer coefficient h , as a function of the temperature difference between the walls of the carrier and the rocket filled pallet inside the carrier.

Reference 11 defines the convective heat transfer coefficient as

$$h = a \left(\frac{T_b - T_r}{L} \right)^b$$

where T_b is the wall temperature, T_r is the rocket surface temperature, L is a characteristic dimension, and a and b are empirically derived constants listed in Table 1 of the text.

For the analysis, h values from vertical walls were weighted with the horizontal ceiling by area to find an average convective heat transfer coefficient. The characteristic lengths used were the height for the vertical walls and an average of the width and length for the horizontal surface. A computer program MCALC was written to obtain h as a function of $T_b - T_r$ (i.e., ΔT). A listing of this program follows; a tabulation of the heat transfer coefficients as a function of ΔT is given in Table 2 of the text.

PROGRAM HCALC

PROGRAM HCALC DETERMINES THE CONVECTIVE HEAT TRANSFER COEFFICIENT AS A FUNCTION OF TEMPERATURE DIFFERENCE BETWEEN THE CARRIER WALLS AND CONTENTS. VALUES FOR VERTICAL AND HORIZONTAL WALLS ARE DETERMINED FROM EQUATIONS CITED IN REFERENCE B. AN AVERAGE CONVECTIVE HEAT TRANSFER COEFFICIENT IS FOUND BY WEIGHTING VERTICAL AND HORIZONTAL VALUES WITH THEIR SURFACE AREAS.

Transport carrier dimensions are in feet
H is in btu/hr sq ft deg f

```

DIMENSION TEMP(100),HBAR1(100),HBAR2(100),W(3),H(3),
1          HT(3),HS(3),AT(3),AE(3),AS(3),HBAR3(100)
REAL L(3),LEN(3)
OPEN(UNIT=2,NAME='HCALC.DAT',TYPE='NEW')
    
```

```

C      For truck.....
C      TYPE*, 'ENTER TRUCK LENGTH,WIDTH,HEIGHT (FEET)'
C      ACCEPT*,L(1),W(1),H(1)
C      LEN(1)=L(1)+W(1)/2.
C      AT(1)=L(1)*W(1)
C      AS(1)=2.*(L(1)*W(1))
C      AE(1)=2.*(W(1)*H(1))
    
```

```

C      For railcar.....
C      TYPE*, 'ENTER RAILCAR LENGTH,WIDTH,HEIGHT (FEET)'
C      ACCEPT*,L(2),W(2),H(2)
C      LEN(2)=L(2)+W(2)/2.
C      AT(2)=L(2)*W(2)
C      AS(2)=2.*(L(2)*W(2))
C      AE(2)=2.*(W(2)*H(2))
    
```

```

C      For compact.....
C      TYPE*, 'ENTER COMPACT LENGTH,WIDTH,HEIGHT (FEET)'
C      ACCEPT*,L(3),W(3),H(3)
C      LEN(3)=L(3)+W(3)/2.
C      AT(3)=L(3)*W(3)
C      AS(3)=2.*(L(3)*W(3))
C      AE(3)=2.*(W(3)*H(3))
    
```

```

C      WRITE(2,900)L(1),W(1),H(1),L(2),W(2),H(2),L(3),W(3),H(3)
900  FORMAT(1H1,///,5X,'CONVECTIVE HEAT TRANSFER',
1      ' COEFFICIENT (BTU/HR SQ FT F)',///,
1      5X,'DIMENSIONS: Length   Width   Height (FT)',
1      //,5X,'Truck           ',F5.1,5X,F5.1,5X,F5.1,
1      /,5X,'Railcar          ',F5.1,5X,F5.1,5X,F5.1,/,
1      5X,'Compact           ',F5.1,5X,F5.1,5X,F5.1,/,/,
2      4X,'Delta Temp (deg F)',3X,'Truck',5X,'Railcar',5X,
3      'Compact',/)
    
```

```

C      DELT=100.      ! DEGREES F
C      NINC=21
C      TEMP(1)=0.
C      HBAR1(1)=0.
C      HBAR2(1)=0.
C      HBAR3(1)=0.
    
```

```

C      DO 100 I=1,NINC
C      For truck*****
C      HT(1)=0.12*(TEMP(I)/LEN(1))**.25
C      HSTK1=0.29*(TEMP(I)/H(1))**.25
C      HSTK2=0.19*(TEMP(I)/H(1))**.3333
    
```

```
HS(1)=AMAX1(HSTK1,HSTK2)
HBAR1(I)=(HT(1)*AT(1)+HS(1)*(AS(1)+AE(1)))/
1      (2.*(L(1)*W(1)+L(1)*H(1)+W(1)*H(1))-L(1)+W(1))
```

```
For railcar*****
```

```
HT(2)=0.12*(TEMP(I)/LEN(2))*0.25
HSRC1=0.29*(TEMP(I)/H(2))*0.25
HSRC2=0.19*(TEMP(I)/H(2))*0.3333
HS(2)=AMAX1(HSRC1,HSRC2)
HBAR2(I)=(HT(2)*AT(2)+HS(2)*(AS(2)+AE(2)))/
1      (2.*(L(2)*W(2)+L(2)*H(2)+W(2)*H(2))-L(2)+W(2))
```

```
For compact*****
```

```
HT(3)=0.12*(TEMP(I)/LEN(3))*0.25
HSCP1=0.29*(TEMP(I)/H(3))*0.25
HSCP2=0.19*(TEMP(I)/H(3))*0.3333
HS(3)=AMAX1(HSCP1,HSCP2)
HBAR3(I)=(HT(3)*AT(3)+HS(3)*(AS(3)+AE(3)))/
1      (2.*(L(3)*W(3)+L(3)*H(3)+W(3)*H(3))-L(3)+W(3))
```

```
WRITE(2,1000)TEMP(I),HBAR1(I),HBAR2(I),HBAR3(I)
1000  FORMAT(5X,E12.4,3X,3E12.4)
TEMP(I+1)=TEMP(I)+DELT
```

```
100 CONTINUE
CALL EXIT
END
```

APPENDIX D - THERMAL RADIATION INSIDE THE CARRIERS
CONFIGURATION FACTOR CALCULATION

This Appendix summarizes the calculation of the configuration factor as a function of angular position on the rockets. Two rocket locations were examined; top center and top end. The configuration factor is first translated from its general form through integration to an expression in terms of geometric variables e , f , w and θ . These variables are then determined in terms of physical dimensions Z , R , X_2 , X_3 , X_4 , t , Y_2 and Z_2 . The values of the dimensions are shown in a sketch of the rocket, pallet, and carrier walls. Note that the pallet is assumed to be about two inches away from the walls of the carrier.

The center rocket receives radiation only from the roof, while the end sees heat from both roof and walls. Because of this and the shielding effect of pallet boards, calculated variables w , e , and f are determined differently in each of 6 sections around the circumference of the rocket, Figure D1 or D2. Algebraic terms used to define the variables are shown in the accompanying table. A computer program SHAPE was written to evaluate the configuration factor over the rocket surfaces. A listing of the program is given, and tabulated results of the configuration factor are given. The angular distribution of the configuration factor is shown in Figure 9.

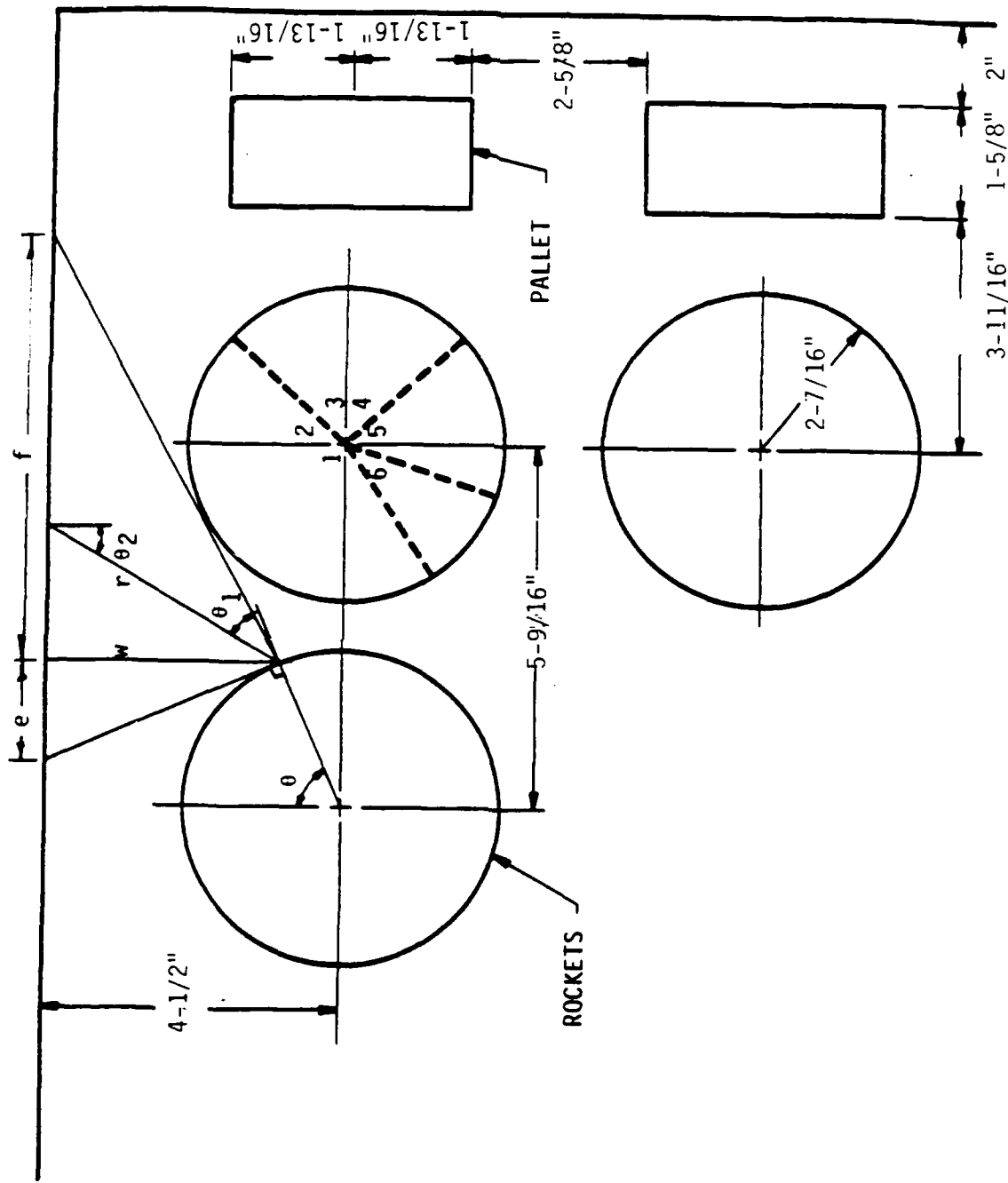
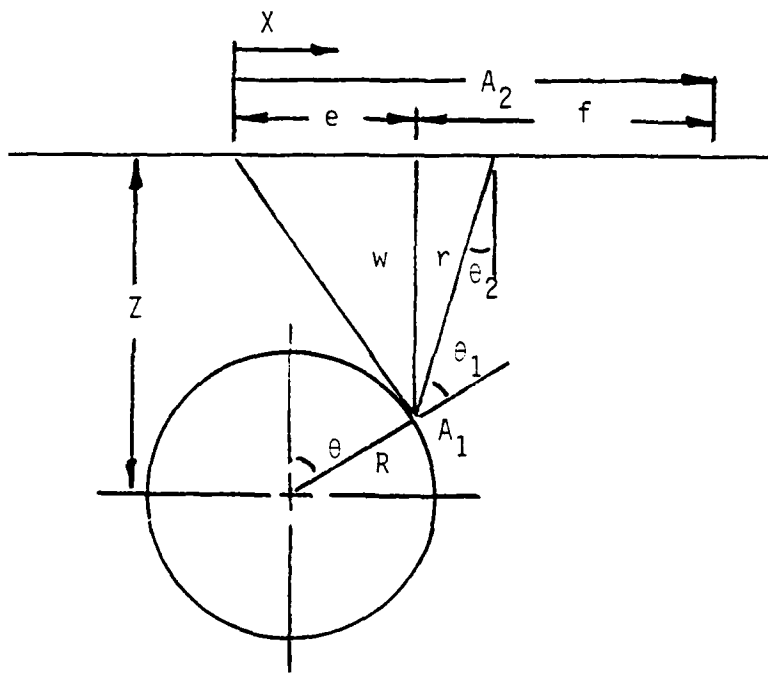


Figure D2. Rocket/Pallet Geometry with Dimensions



$$w = z - R \cos \theta$$

$$\frac{w}{r} = \cos \theta_2$$

$$\theta_1 = \theta - \theta_2$$

$$\cos \theta_1 = \cos(\theta - \theta_2)$$

$$= \frac{w}{r} \cos \theta + \frac{x}{r} \sin \theta$$

$$r = \sqrt{x^2 + w^2 + y^2}$$

General Configuration Factor

$$F_{d1-2} = \int_{A_2} \frac{\cos \theta_1 \cos \theta_2}{\pi r^2} dA_2$$

$$= \int_{A_2} \frac{\frac{w}{r} \cos \theta + \frac{x}{r} \sin \theta}{\pi r^2} \frac{w}{r} dA_2$$

$$= \iint \frac{w^2 \cos \theta + wx \sin \theta}{\pi r^4} dx dy$$

$$= \int_{-\infty}^{\infty} \int_{-e}^f \frac{w^2 \cos \theta + wx \sin \theta}{\pi (x^2 + w^2 + y^2)^2} dx dy = \frac{w^2 \cos \theta + wx \sin \theta}{\pi}$$

$$\frac{1}{2(x^2 + w^2)} \left[\frac{y}{x^2 + w^2 + y^2} - \frac{1}{\sqrt{x^2 + w^2}} \tan^{-1} \frac{y}{\sqrt{x^2 + w^2}} \right] \Big|_{-\infty}^{\infty}$$

$$= \int_{-e}^f \frac{w^2 \cos\theta + wx \sin\theta}{2\pi(x^2+w^2)^{3/2}} (\pi) dx$$

$$= \int_{-e}^f \frac{w^2 \cos\theta}{2(x^2+w^2)^{3/2}} dx + \int_{-e}^f \frac{w \sin\theta x dx}{2(x^2+w^2)^{3/2}}$$

$$= \left(\frac{w^2 \cos\theta}{2} \right) \left(\frac{x}{w^2 \sqrt{x^2+w^2}} \right) \Big|_{-e}^f + \frac{w \sin\theta}{2} \frac{-1}{\sqrt{x^2+w^2}} \Big|_{-e}^f$$

$$F_{d1-2} = \frac{e \cos\theta + w \sin\theta}{2 \sqrt{e^2 + w^2}} + \frac{f \cos\theta - w \sin\theta}{2 \sqrt{f^2 + w^2}}$$

Rocket	$\theta_{\text{min}}/\theta_{\text{max}}$	Section	w	e	f
center	$\cos^{-1} \frac{2R}{X_4} + \frac{\pi}{2}$		Z - Rcos θ	w/Lano	$\frac{M}{R} - \tan^{-1} \frac{R \cos \theta}{X_4 - R \sin \theta}$
end	$-\cos^{-1} \frac{2R}{X_4} + \frac{\pi}{2} / 0$	1	Z - Rcos θ	w/Lano	$R^2 \cos^2 \theta + (X_4 - R \sin \theta)^2$
	$0/\cos^{-1} \frac{X_2}{R}$	2 HOR	Z - Rcos θ	w/Lano	same
	$\cos^{-1} \frac{X_2}{R}$	3 HOR	Z - Rcos θ	w/Lano	$X_3 + t + Z_2 - R \sin \theta$
	$\frac{\pi}{2}/\cos^{-1} \frac{X_2}{R} + \frac{\pi}{2}$	4	$X_3 + t + Z_2 - R \sin \theta$	$Z - R \cos \theta$	$\frac{(R \cos \theta - X_2) M}{X_3 + t - R \sin \theta}$
	$\cos^{-1} \frac{X_2}{R} + \frac{\pi}{2}$	5	$X_3 + t + Z_2 - R \cos(\theta - \frac{\pi}{2})$	$\frac{-M(X_2 - R \cos \theta) M}{X_3 - R \sin \theta}$	Smaller of: $X_3 + t + Z_2 - R \sin \theta$, $\frac{(X_3 - R \sin \theta) M}{X_2 - R \cos \theta}$
$X_2 + Y_2 = (X_3 + t) \tan \alpha + \frac{R}{\cos \alpha}$	$\theta_{\text{max}} = \pi + \alpha$				$\frac{M(Y_2 + X_2 - R \sin(\theta - \frac{\pi}{2}))}{t + X_3 - R \cos(\theta - \frac{\pi}{2})}$

CONFIGURATION FACTOR

Postion: End

Theta(Deg)	F12
0.	0. 1000E+01
5.	0. 9670E+00
10.	0. 9635E+00
15.	0. 9547E+00
20.	0. 9402E+00
25.	0. 9194E+00
30.	0. 8921E+00
35.	0. 8580E+00
40.	0. 8172E+00
45.	0. 8357E+00
50.	0. 7651E+00
55.	0. 6782E+00
60.	0. 5779E+00
65.	0. 4710E+00
70.	0. 3666E+00
75.	0. 2432E+00
80.	0. 1393E+00
85.	0. 6399E-01
90.	0. 8413E-02
95.	0. 1810E-01
100.	0. 3000E-01
105.	0. 4440E-01
110.	0. 6125E-01
115.	0. 7969E-01
120.	0. 9780E-01
125.	0. 1130E+00
130.	0. 1228E+00
135.	0. 1321E+00
140.	0. 1183E+00
145.	0. 1023E+00
150.	0. 8484E-01
155.	0. 6622E-01
160.	0. 4689E-01
165.	0. 2725E-01
170.	0. 0000E+00
175.	0. 0000E+00
180.	0. 0000E+00
185.	0. 0000E+00
191.	0. 0000E+00
196.	0. 0000E+00

CONFIGURATION FACTOR

Postion: Center

Theta(Deg)	F12
0.	0. 1000E+01
5.	0. 9980E+00
10.	0. 9917E+00
15.	0. 9806E+00
20.	0. 9641E+00
25.	0. 9414E+00
30.	0. 9121E+00
35.	0. 8752E+00
40.	0. 8302E+00
45.	0. 7766E+00
50.	0. 7141E+00
55.	0. 6430E+00
60.	0. 5643E+00
65.	0. 4801E+00
70.	0. 3935E+00
75.	0. 3087E+00
80.	0. 2303E+00
85.	0. 1625E+00
90.	0. 1076E+00
95.	0. 6616E-01
100.	0. 3690E-01
105.	0. 1770E-01
110.	0. 6344E-02
115.	0. 9701E-03

PROGRAM SHAPE

C
 C PROGRAM SHAPE CALCULATES THE CONFIGURATION FACTORS ON ROCKETS
 C LOCATED IN THE PALLET. THE FACTOR IS DETERMINED AS A FUNCTION
 C OF ANGULAR POSITION FOR A ROCKET ON THE TOP ROW OF THE PALLET,
 C IN EITHER A CENTERED OR END POSITION. PHYSICAL DIMENSIONS ARE
 C LISTED IN TERMS OF VARIABLES CORRESPONDING TO THE ATTACHED FIGURE.
 C THE CONFIGURATION FACTOR IS SYMMETRIC WITH RESPECT TO 0 ON THE
 C CENTERED ROCKET. THE END ROCKET IS DIVIDED INTO 6 SECTIONS, EACH
 C REQUIRING DIFFERENT EQUATIONS TO FIND F12.

C
 DIMENSION THETA(100), F12(100)
 REAL*8 POS(1)

C
 C-----DIMENSIONS IN INCHES

Z=4.5
 X4=5.563
 R=2.438
 X3=3.688
 T=1.625
 Z2=2.0
 Y2=2.625
 X2=1.813

C
 PI=3.141592654
 THETA(1)=0.
 DELT=.0875 ! RADIANS, 5 DEGREES

C
 TYPE*, 'INPUT POSITION'
 TYPE*, '..... (0)CENTER '
 TYPE*, '..... (1)END '
 ACCEPT*, IPOS
 IF(IPOS.EQ.0)THEN
 POS(1)='Center '
 ENDIF
 IF(IPOS.EQ.1)THEN
 POS(1)='End '
 ENDIF
 I=1

C
 C-----OPEN OUTPUT FILE
 OPEN(UNIT=2, NAME='SHAPE.DAT', TYPE='NEW')
 WRITE(2, 1000) POS(1)
 1000 FORMAT(1H1, ///, 5X, 'CONFIGURATION FACTOR', ///, 5X, 'Position: ', A8)
 WRITE(2, 1200)
 1200 FORMAT(///, 5X, 'Theta(Deg)', 5X, 'F12', /)

C
 TH1=ACOS(2.*R/X4)+PI/2.
 TH2=ACOS(X2/R)
 TH4=ACOS(X2/R)+PI/2.
 THMAX=3.48 ! RADIANS, 199 DEGREES

C
 100 IF(IPOS.EQ.0)THEN ! CENTER POSITION
 IF(THETA(I) LT (-1*TH1) .OR THETA(I).GT.TH1)THEN
 TYPE*, 'THETA OUT OF BOUNDS '
 CALL EXIT
 ENDIF
 IF(THETA(I) EQ 0)THEN
 F12(I)=1
 GO TO 500
 ENDIF
 W=Z-R*COS(THETA(I))
 E=W/TAN(THETA(I))

```

D = ((R*COS(THETA(I)))*2+(X4-R*SIN(THETA(I)))*2)*0.5
F=W/TAN(ASIN(R/D)-ATAN(R*COS(THETA(I))/(X4-R*SIN(THETA(I))))
CALL FCALC(THETA(I),W,E,F,F12(I))
WRITE(3,*)'ISECT,W,E,F,F12(I)',ISECT,W,E,F,F12(I)
ENDIF
IF(IPOS.EQ.1)THEN                                !END POSITION
****SECTION 1****
IF(THETA(I).LT.0 .AND. THETA(I).GE.(-1*TH1))THEN
ISECT=1
W=Z-R*COS(THETA(I))
E=W/TAN(THETA(I))
D = ((R*COS(THETA(I)))*2+(X4-R*SIN(THETA(I)))*2)*0.5
F=W/TAN(ASIN(R/D)-ATAN(R*COS(THETA(I))/(X4-R*SIN(THETA(I))))
CALL FCALC(THETA(I),W,E,F,F12(I))
WRITE(3,*)'ISECT,W,E,F,F12(I)',ISECT,W,E,F,F12(I)
****SECTION 2****
ELSEIF(THETA(I).LT.TH2 .AND. THETA(I).GE.0)THEN
ISECT=2
IF(THETA(I).EQ.0)THEN
F12(I)=1.
GO TO 500
ENDIF
WH=Z-R*COS(THETA(I))
WV=X3+T+Z2-R*SIN(THETA(I))
EH=WH/TAN(THETA(I))
EV=Z-R*COS(THETA(I))
FH=X3+T+Z2-R*SIN(THETA(I))
FV=(R*COS(THETA(I))-X2)*WV/(X3+T-R*SIN(THETA(I)))
CALL FCALC(THETA(I),WH,EH,FH,F12H)
ANGLE = PI/2. - THETA(I)
CALL FCALC(ANGLE,WV,EV,FV,F12V)
F12(I)=F12H+F12V
WRITE(3,*)'ISECT,WH,WV,EH,EV,FH,FV,F12(I)',ISECT,WH,
WV,EH,EV,FH,FV,F12(I)
****SECTION 3****
ELSEIF(THETA(I).GE.TH2 .AND. THETA(I).LT.(PI/2.))THEN
ISECT=3
WH=Z-R*COS(THETA(I))
WV=X3+T+Z2-R*SIN(THETA(I))
EH=WH/TAN(THETA(I))
EV=-1.*(X2-R*COS(THETA(I)))*WV/(X3-R*SIN(THETA(I)))
FH1=X3+T+Z2-R*SIN(THETA(I))
FH2=(X3-R*SIN(THETA(I)))*WH/(X2-R*COS(THETA(I)))
FH=AMIN1(FH1,FH2)
FV=Z-R*COS(THETA(I))
CALL FCALC(THETA(I),WH,EH,FH,F12H)
ANGLE = PI/2. - THETA(I)
CALL FCALC(ANGLE,WV,EV,FV,F12V)
F12(I)=F12H+F12V
WRITE(3,*)'ISECT,WH,WV,EH,EV,FH,FV,F12(I)',ISECT,
WH,WV,EH,EV,FH,FV,F12(I)
****SECTION 4****
ELSEIF(THETA(I).GE.(PI/2.) .AND. THETA(I).LT.TH4)THEN
ISECT=4
W=X3+T+Z2-R*COS(THETA(I)-PI/2.)
E=-1*W*(X2-R*SIN(THETA(I)-PI/2.))/
(X3-R*COS(THETA(I)-PI/2.))
F=W*(Y2+X2-R*SIN(THETA(I)-PI/2.))/
(T+X3-R*COS(THETA(I)-PI/2.))
ANGLE = PI/2. -THETA(I)
CALL FCALC(ANGLE,W,E,F,F12(I))
WRITE(3,*)'ISECT,W,E,F,F12(I)',ISECT,W,E,F,
F12(I)

```

```

C      ****SECTION 5****
      ELSEIF (THETA(I).GE. TH4 .AND. THETA(I).LT. THMAX) THEN
          ISECT=5
          W=X3+T+Z2-R*COS(THETA(I)-PI/2)
          E=-1.*W*(R*COS(THETA(I))+X2)/
1          (T+X3-R*SIN(THETA(I)))
          E1 = W*TAN(PI-THETA(I))
          IF (E1.LT.E) E= 0.0
          F=W*(Y2+R*COS(THETA(I))+X2)/(T+X3-R*SIN(THETA(I)))
          ANGLE = PI/2. -THETA(I)
          CALL FCALC(ANGLE,W,E,F,F12(I))
          IF (F12(I).LT.0.01) F12(I)=0.0
      TYPE*, 'THETA, E, E1, F12 = ', THETA(I), E, E1, F12(I), W, F
1          WRITE(3, *) 'SECT, W, E, F, F12(I)', ISECT, W, E, F,
          F12(I)
      ELSE
          GO TO 999
      ENDIF
  ENDIF
ENDIF
C
500 WRITE(2, 1500) THETA(I)*57.29578, F12(I)
1500 FORMAT(1X, 5X, F5.0, 5X, E12.4)
      TYPE*, 'THETA', THETA(I)*57.29578
C      TYPE*, 'W, E, F, F12', W, E, F, F12(I)
C      TYPE*, 'SECT ', ISECT
      THETA(I+1)=THETA(I)+DELT
      I=I+1
      GO TO 100
999 CONTINUE
      CALL EXIT
      END
C
C
      SUBROUTINE FCALC(THETA,W,E,F,F12)
C
C-----CALCULATE CONFIGURATION FACTOR
C
      F12=(((E*COS(THETA))+W*SIN(THETA))/(2*SQRT(E**2.+W**2.)))
1      +(((F*COS(THETA))-(W*SIN(THETA)))/(2.*SQRT(F**2.+W**2.)))
C
      RETURN
      END

```

APPENDIX E - NATURAL CONVECTION WITHIN THE SHIPPING TUBE

The burster section of the rocket contains an airgap between the fiberglass shipping case and the rocket. Heat from the fire warms the shipping tube and then passes through the air space to the rocket. As the temperature difference across the air space increases, natural convection within the space also increases. This process accelerates the heating of the rocket.

The natural convection between two concentric cylinders has been defined in nondimensional terms. The Nusselt number (Nu), the ratio of the effective thermal conductivity through a fluid with convection to the thermal conductivity with just conduction, is expressed as a function of Rayleigh Number which is the ratio of buoyant to viscous forces in the fluid. The Rayleigh number (Ra) is a function of the temperature across the airgap and the air properties. The following figure illustrates the increasing heat transfer with buoyancy.

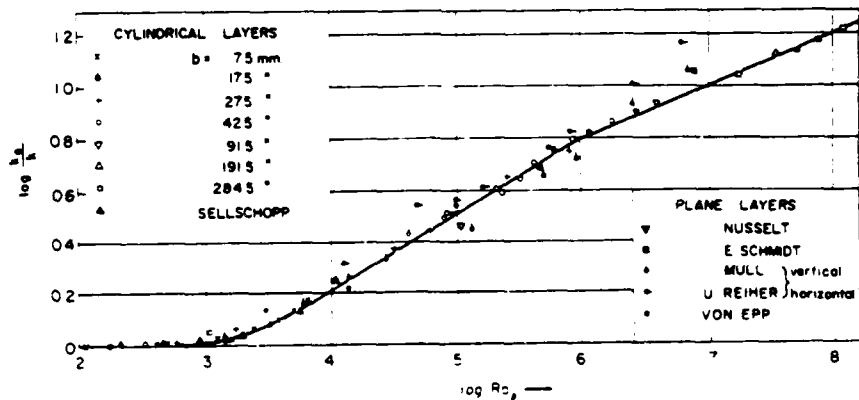


Figure E1. Equivalent heat conductivity for free convection through fluid layers. From H. Kraussold, Forsch. Gebiete Ingenieurw., 5:83 (1934). (Taken from Eckert and Drake [16]).

Enhanced heat transfer to the rocket by convection is accounted for by evaluating the Rayleigh number under the worst case loading, finding the corresponding Nusselt number from the figure, and then multiplying the thermal

conductivity of the gas by that factor. For the shipping tube air space the temperature differential producing the most convection is

$$\begin{aligned}\Delta T &= \text{Fire Temp} - \text{Ambient Temp} \\ &= 1850^{\circ}\text{F} - 70^{\circ}\text{F} = 1780^{\circ}\text{R}.\end{aligned}$$

Gas properties evaluated at the average of the temperature extremes (960°F) are

$$\begin{aligned}\beta &= \text{Thermal Expansion Coeff.} = \frac{1}{T} = 0.0007^{\circ}\text{R}^{-1} \\ g &= \text{Acc. Due to Gravity} = 32.2 \text{ ft/s}^2 \\ \alpha &= \text{Thermal Diffusivity} = 4.631 \text{ ft}^2/\text{hr} \\ \nu &= \text{Kinematic Viscosity} = 88.58 \times 10^{-5} \text{ ft}^2/\text{sec} \\ L &= \text{Air Gap Thickness} = 1.06 \text{ inches}\end{aligned}$$

$$Ra = \frac{\beta g \Delta T L^3}{\alpha \nu} = 2.42 \times 10^4$$

From the graph,

$$\log \frac{ke}{k} = 0.3$$

$$\frac{ke}{k} = 2.0$$

By increasing the thermal conductivity of the gas in the air space by a factor of two, the natural convection will conservatively be taken into account.

APPENDIX F - AGENT BURST ANALYSIS

The purpose of this analysis is to determine the agent temperature required to burst the casing. Thermal properties of the agent are assumed to be those of SAE 50 WT oil in the transient thermal analysis. Vapor pressure - temperature correlations for the agent are assumed to be those of steam. The aluminum casing is 0.058 inches thick and 2.16 inches in radius. The ultimate tensile strength is assumed to be 64000 psi initially and change with temperature as shown in the following figure.

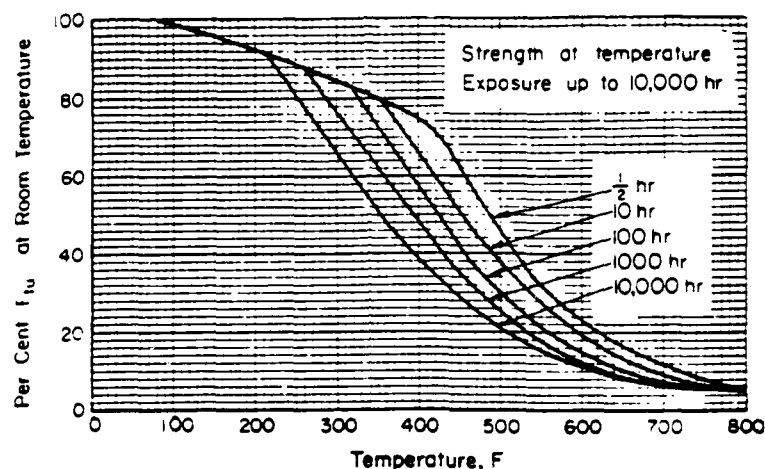


Figure F1. Effect of temperature on the ultimate tensile strength (F_{tU}) of 2024-T3 and 2024-T4 aluminum alloy (all products except extrusions).

When the agent is roughly 400°F, the aluminum temperature is about 600°F. From the figure (taken from Reference F1) the strength of the aluminum is between 12 and 22 percent of room temperature ultimate.

The maximum internal pressure in a thin walled cylinder is found in Reference F2 to be

$$P = \frac{tY}{R}$$

where

- P = Maximum Internal Pressure
- t = Cylinder Thickness
- Y_0 = Maximum Ultimate Tensile Strength
- R = Inner Radius of the Cylinder.

An iterative procedure was required to determine the temperature of the agent (saturated steam) which would have a vapor pressure sufficient to rupture the thermally-weakened cylinder. The stress at which wall failure would occur was determined from $\sigma_{fail} = tY_0/R$ and Figure F1. The vapor pressure for saturated steam was found from the temperature of the "agent" material. That pressure was compared to σ_{fail} to see if the internal pressure was sufficient to rupture the case. After several iterations, it was determined that an agent temperature of 439°F resulted in a [saturated steam] pressure of 378 psi, corresponding to a rupture stress of 378 psi for aluminum thermally weakened to 22% of ultimate. The critical bulk temperature of the agent is then taken to be approximately 439°F.

References:

- F1. 'Metallic Materials and Elements for Aerospace Vehicle Structures.' MIL-HDBK-5A, Department of Defense, 1966.
- F2. Shigley, J. E., Mechanical Engineering Design, McGraw-Hill Inc., 1977.
- F3. Baumeister, T., Mark's Standard Handbook for Mechanical Engineers, McGraw-Hill Book Co., 1978.

APPENDIX G
THERMAL PROPERTY DATA
(FIGURES p1 - p6)

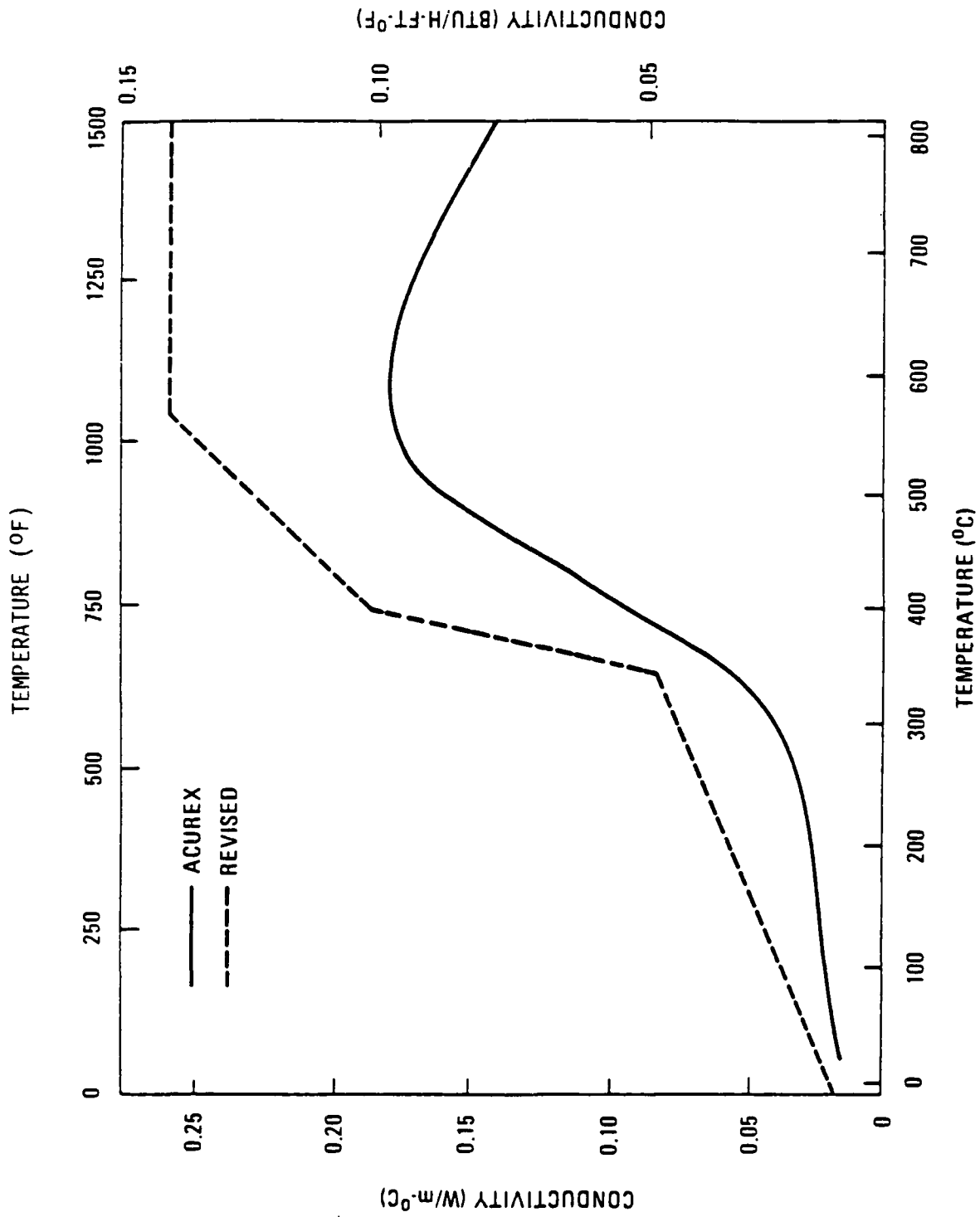


Figure p1. Thermal Conductivity of FR-9606 Foam

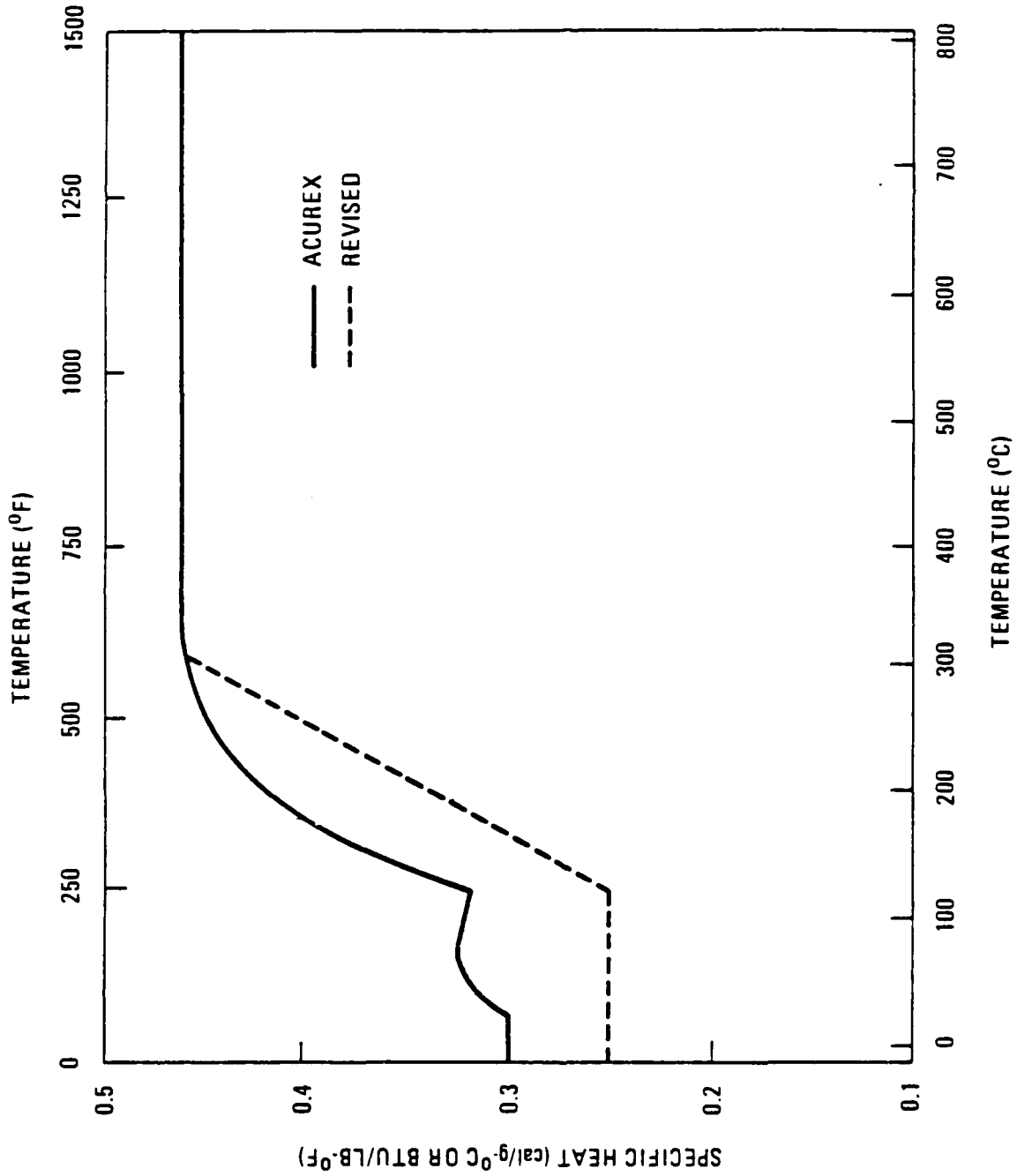


Figure p2. Specific Heat of FR-9606 Foam

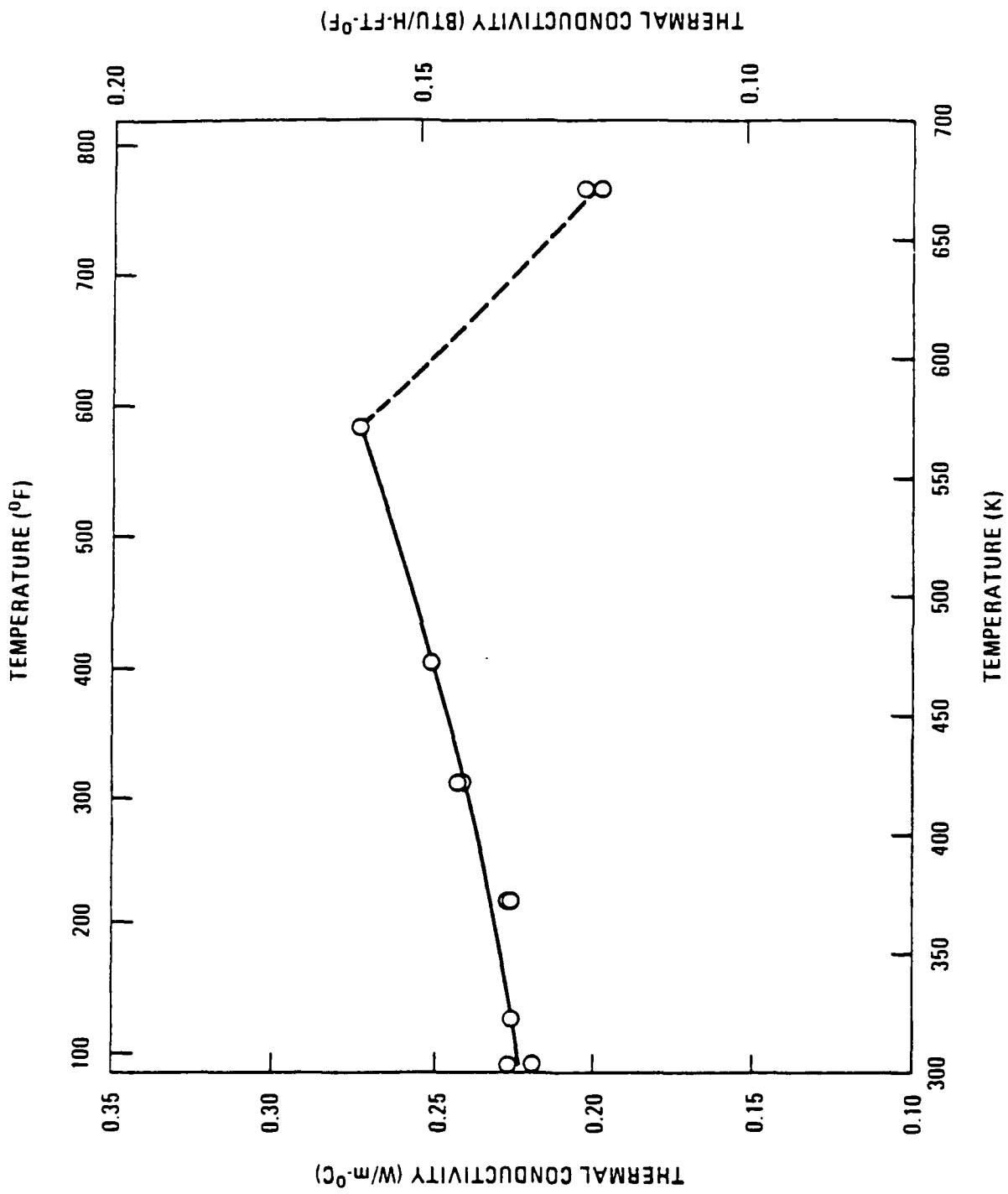


Figure p3. Thermal Conductivity of Kevlar-29/EVA Laminate

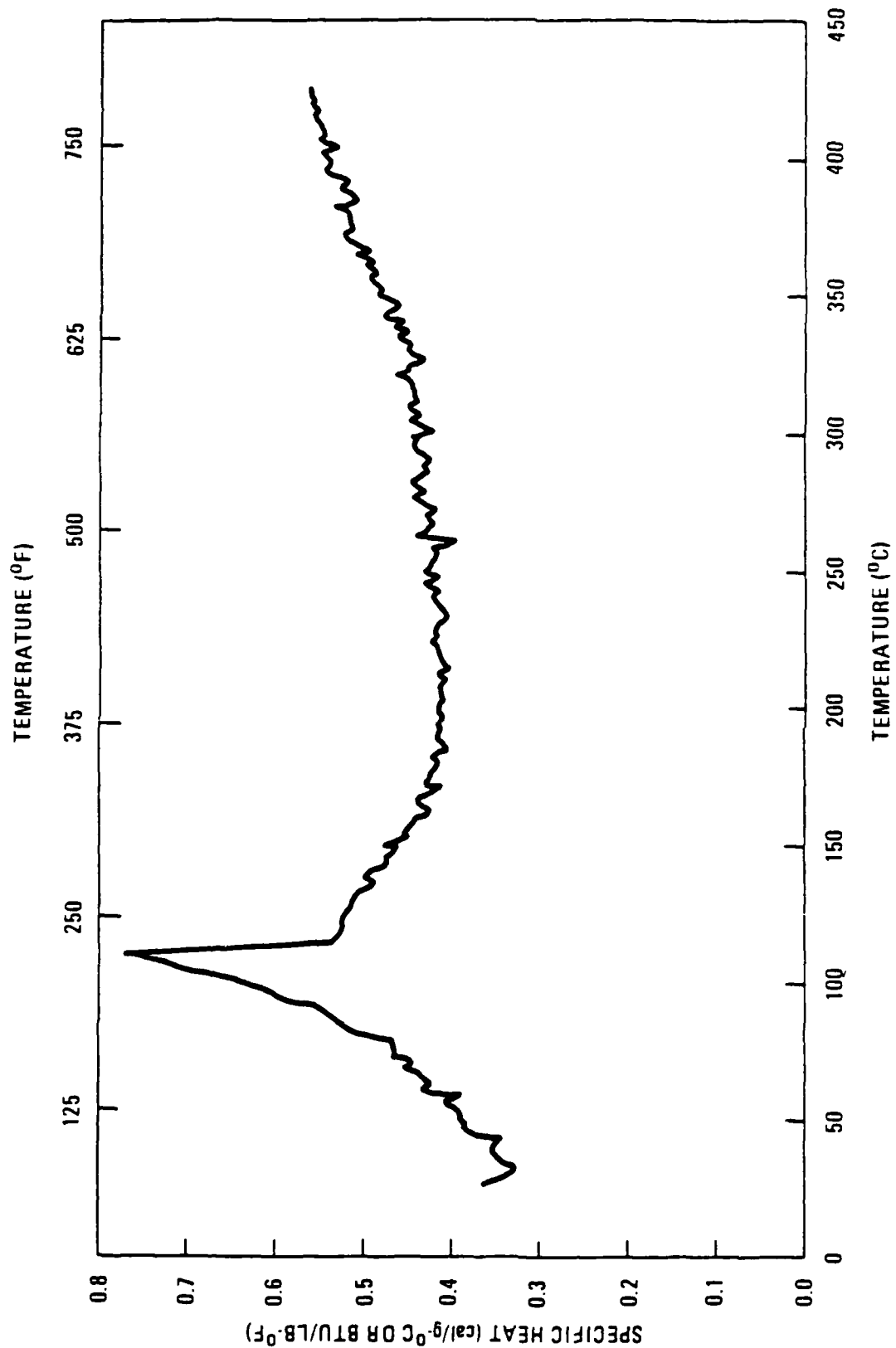


Figure p4. Specific Heat of a Woven Kevlar-29/EVA Laminate

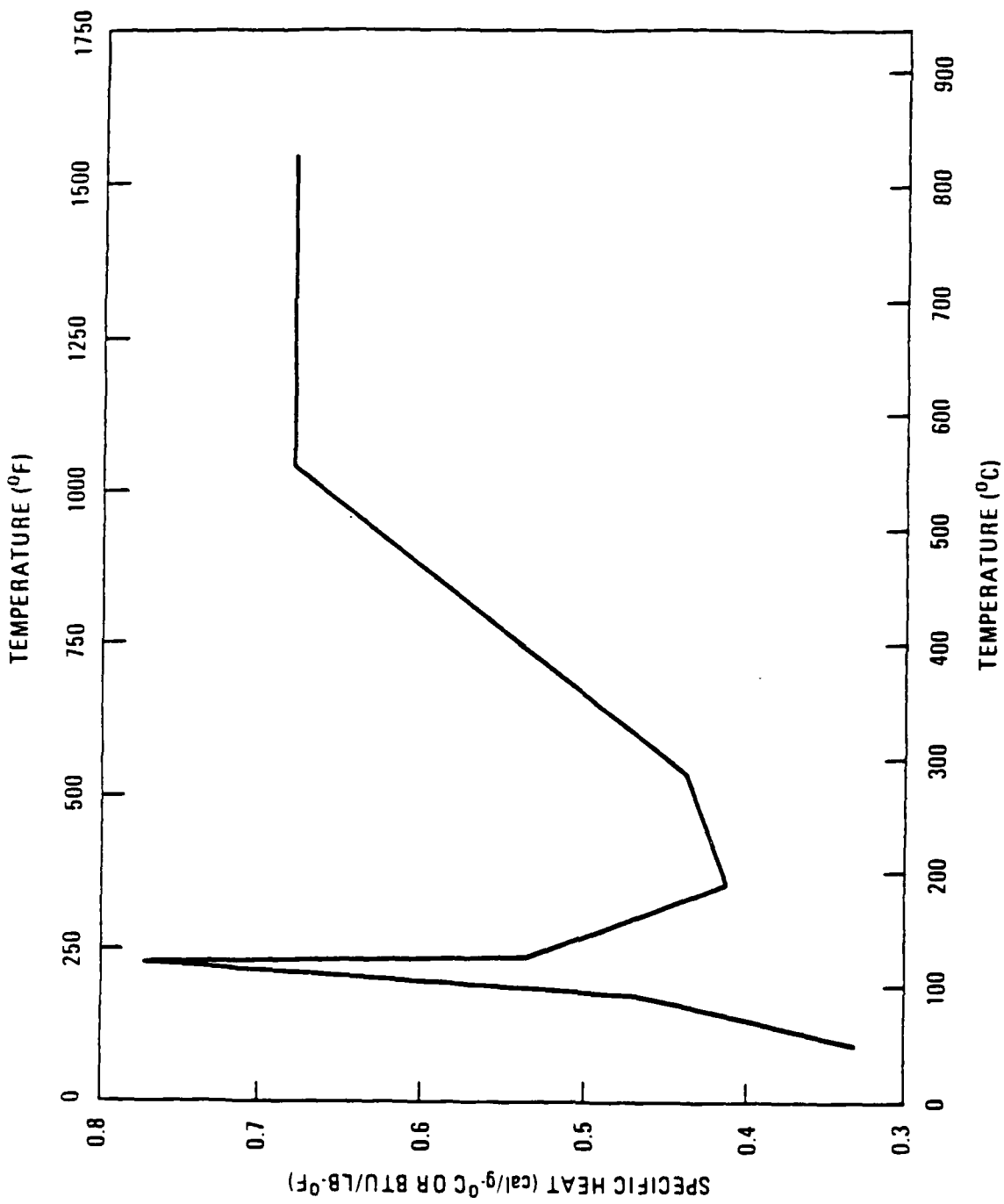


Figure p5. Specific Heat of Kevlar-29/EVA Laminate

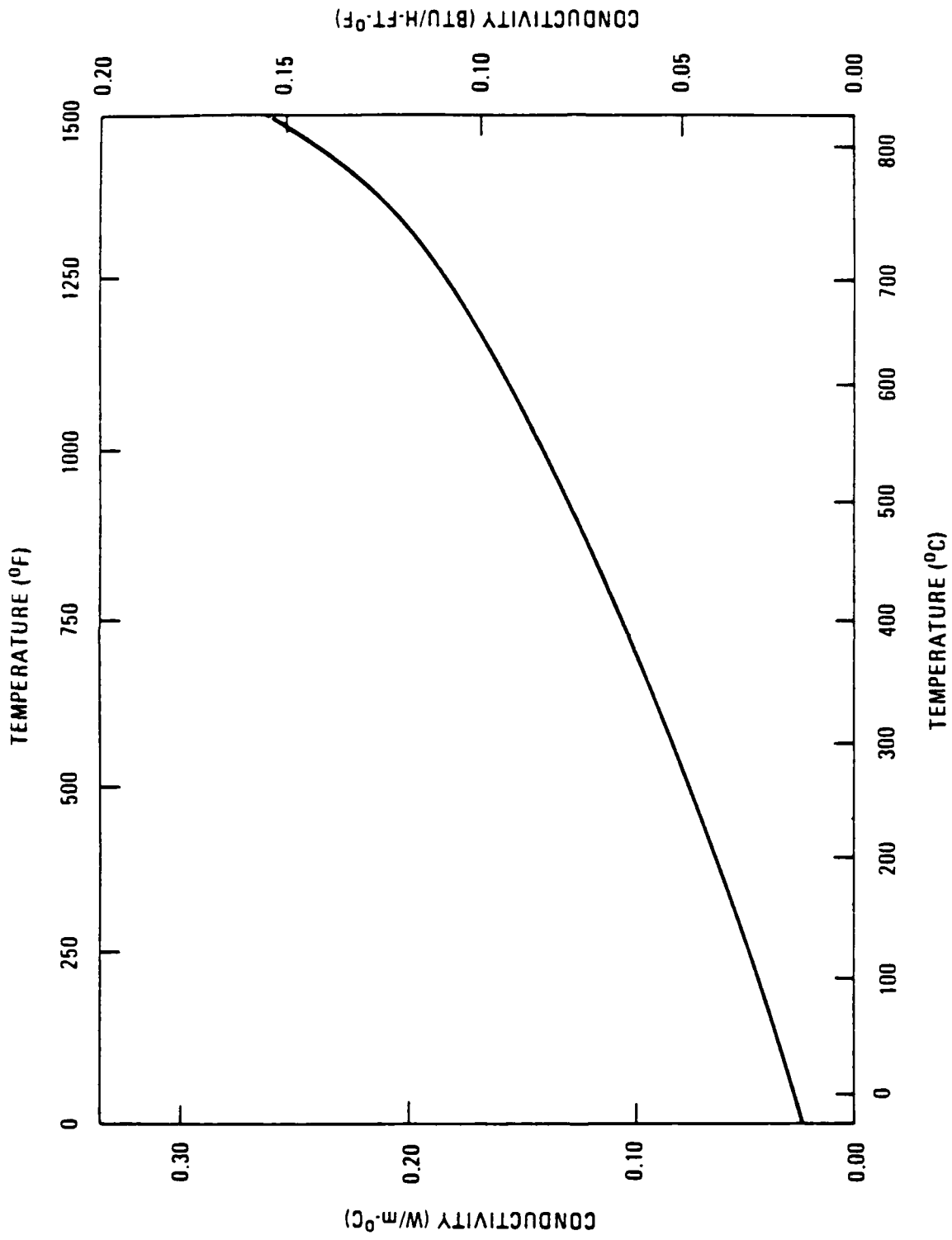


Figure p6. Thermal Conductivity of Insulation